Conformation of Human Microtubule Associated Protein-Tau

Thesis submitted to the University of Hamburg in partial fulfillment of the requirements for the degree of Ph.D.

Submitted by

Sadasivam Jeganathan

Born in India

September, 2007

Hamburg

Genehmigt vom Department Biologie
der Fakultät für Mathematik, Informatik und Naturwissenschaften
an der Universität Hamburg
auf Antrag von Herrn Professor Dr. E. MANDELKOW
Weiterer Gutachter der Dissertation:
Herr Priv.-Doz. Dr. H. QUADER
Tag der Disputation: 26. Oktober 2007

Hamburg, den 12. Oktober 2007

Professor Dr. Reinhard Lieberei
Leiter des Departments Biologie

1 Introduction

1.1 Protein misfolding diseases

Many human diseases are associated with aberrant aggregation of cellular proteins resulting in deposition of extracellular amyloid like structures or intracellular inclusions due to failure of the protein to remain in or adopt a functional conformational state. The diseases can be broadly grouped into (i) neurodegenerative; aggregation occurs in the brain, (ii) nonneuropathic localized; aggregation occurs in a single type of tissue other than the brain and (iii) nonneuropathic systemic; aggregation occurs in multiple tissues (Chiti and Dobson, 2006).

Neurodegenerative diseases include neuronal pathologies in which a progressive loss of structure or function of neurons is found, ultimately leading to the death of neurons. Some of the proteins that aggregate in neurodegenerative diseases are α-synuclein (in Parkinson disease), Aβ peptide and tau (in Alzheimer disease), huntingtin (in Huntington disease) and prion (in Prion disease).

In Alzheimer disease (AD), aggregates of microtubule-associated protein-tau are found in intracellular compartments together with extracellular aggregates of the Aβ peptide. The aggregates of tau alone occur in a group of neurodegenerative diseases such as progressive supranuclear palsy, corticobasal degeneration, Pick disease and frontotemporal dementia and parkinsonism linked to chromosome 17 (FTDP-17). These diseases, together with AD are collectively known as neurodegenerative tauopathies. The mechanisms of the formation of aggregates from soluble tau have been studied in great detail, particularly in AD and FTDP-17 (Lee et al., 2001).

1.1.1 Alzheimer disease (AD)

Alzheimer disease (AD) is the most common cause of dementia that is characterized by the persistent decline of cognitive function, alterations in judgment, perception and finally personality. The occurrence of dementia is age related because the prevalence of dementia is below 1 % in individuals aged 60-64 years, but increases almost exponentially in people aged 85 years or older. The prevalence of dementia was reported between 24 % and 33 % in the western countries (Ferri et al., 2005).

Major pathological hallmarks of AD are intracellular neurofibrillary tangles (NFT) and extracellular amyloid plaques (Fig. 1.1). NFTs are composed of microtubule associated protein-tau filaments, often referred to as paired helical filaments (PHFs) due to their appearance in electron microscope (EM). The extracellular plaques are composed of aggregated, fibrillar β-amyloid peptide (Aβ) (Lee et al., 2001). Aβ peptide is processed from the β-amyloid precursor protein (βAPP) by enzymes β-secretase (or β-amyloid cleaving enzyme, BACE) and γ-secretase

(Hardy and Selkoe, 2002; Cummings, 2004). Though tangles and plaques are found in conjunction, the appearance and distribution of Aβ deposits are difficult to correlate with the onset of disease whereas the appearance and distribution of tangles have been well correlated with the onset of disease (Braak and Braak, 1995).
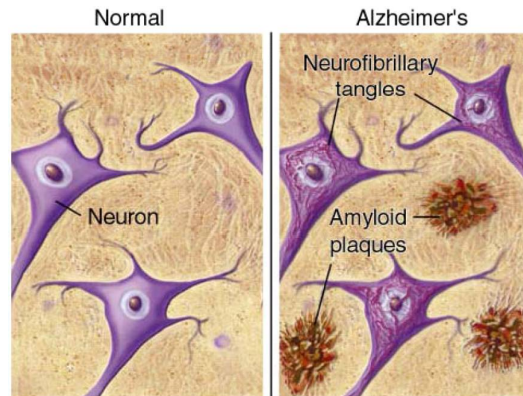
Figure 1.1: Pathological hallmarks of AD. Extracellular plaques which are deposits of Aβ peptide produced from APP and the intracellular tangles which are aggregates composed of microtubule associated protein-tau are found together in AD. The formation of amyloid plaques and tangles contribute to the dysfunction and ultimately the degradation of the neurons in the brain and the subsequent symptoms of AD. (This figure is reproduced from www.ahaf.org/alzdis/about/AmyloidPlaques.htm).

1.1.1.1 Tau hypothesis in AD

Tau belongs to a class of proteins called microtubule-associated proteins (MAPs) whose major function is to stabilize microtubules (MT) that serve as cytoskeleton. Thus microtubules are important for cell viability, particularly for neurons. In AD, tau is hyperphosphorylated at many sites (Gong et al., 2005) probably due to the disturbance in the regulation of tau phosphorylation which is achieved by the balanced activity of multiple kinases and phosphatases. Hyperphosphorylated tau can no longer bind to microtubules and fails to stabilize them causing disturbance of normal function in neurons (Fig. 1.2) (Mandelkow and Mandelkow, 1998). It is also reported that hyperphosphorylated tau might sequester normal functional tau and other MAPs (Alonso et al., 2001). In either way, the local concentration of tau is increased in the cytosol and this might favor the aggregation to PHFs and larger aggregates. In addition, both the loss of microtubule stabilization and the tangle formation could compromise neuronal and synaptic function (Thies and Mandelkow, 2007).
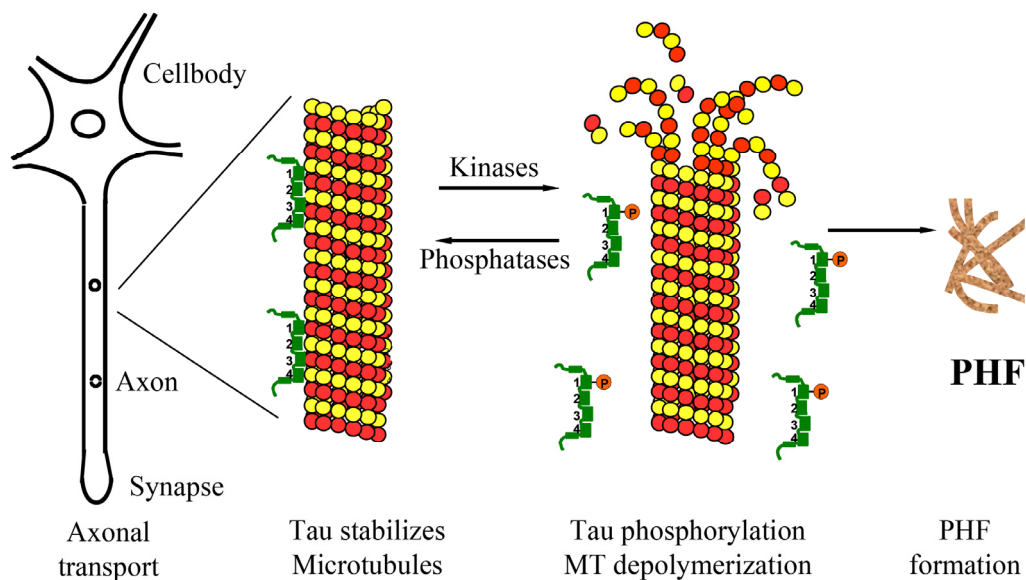
Figure 1.2: Tau hypothesis of AD. Hyperphosphorylation of tau due to the disturbances in the regulation of activity of kinases and phosphatases results in the detachment of tau from microtubules. Subsequent failure of microtubules stabilization causes disturbance in the axonal transport. Accumulation of hyperphosphorylated tau in cytosol might favor the aggregation into PHFs which can further augment the obstruction of axonal transport. Ultimately, normal neuronal functions are deceased leading to neurodegeneration (Mandelkow and Mandelkow, 1998).

1.1.2 Frontotemporal dementia and Parkinsonism linked to chromosome 17

Frontotemporal dementias are characterized by a confined atrophy of frontal and temporal lobes of the cerebral cortex. It occurs rarely as familial but more commonly as sporadic diseases. Almost all the forms of frontotemporal dementia with parkinsonism were linked to chromosome 17q21-22 resulting in the name as frontotemporal dementia and parkinsonism linked to chromosome-17 (FTDP-17) (Wilhelmsen et al., 1994; Hutton et al., 1998; Poorkaj et al., 1998; Spillantini et al., 1998). Tau gene is localized to chromosome 17q21-22 and all cases of FTDP-17 that have been characterized showed pathology caused by tau filaments. Presently, 32 different mutations in the tau gene are known to occur in FTDP-17. These mutations include either missense, deletion or silent mutation in the coding region (Fig. 1.3) or intronic mutations located close to the splice-donor site of intron following the alternatively spliced exon 10 (R2) (van Swieten and Spillantini, 2007).

Tau mutations in FDTP-17 fall largely into two categories: those that affect (i) the alternative splicing of pre-mRNA and (ii) the normal function of tau at the structural level (e.g. binding to microtubules or aggregation propensity). Most of the missense mutations that occur in repeat domains reduce the binding ability of tau to microtubules (Hasegawa et al., 1998; Hong et al., 1998; Barghorn et al., 2000). A number of other missense mutations may promote the aggregation of tau (Goedert et al., 1999; Barghorn et al., 2000; von Bergen et al., 2001). Mutations such as R5L, K257T, I260V, G272V, ΔK280, P301L, Q336R, V337M and R406W are shown to accelerate the tau aggregation relatively faster than the wild type in the presence of

heparin or arachidonic acid. Mutation ΔK280 can in fact drive self aggregation of tau into filaments (von Bergen et al., 2001; Barghorn and Mandelkow, 2002). The intronic mutations as well as most of the coding region mutations in exon 10 (N279K, L284L, ΔN296, N296N, N296H, S305N and S305S) increase the splicing of exon 10, thus decreasing the ratio of 3R to 4R isoforms (Hutton et al., 1998; D'Souza et al., 1999; Yoshida et al., 2002).
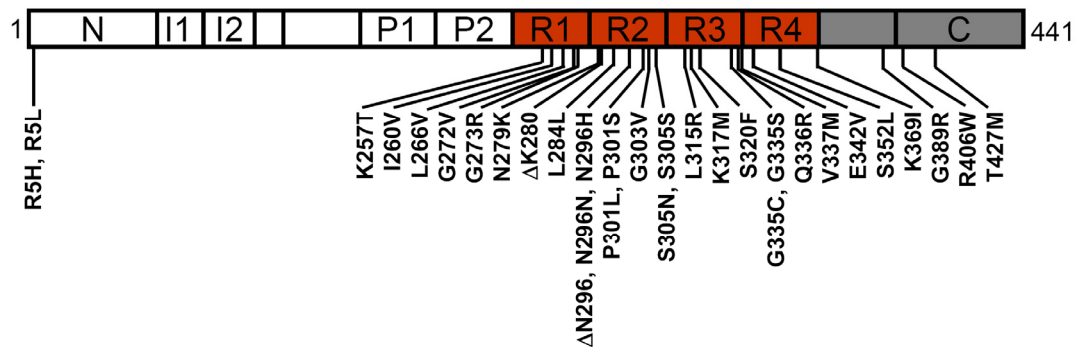
Figure 1.3: Mutations in the tau gene in FTDP-17. Tau mutations occur in FTDP-17 are shown. Mutations influence either the splicing of exon 10 (altering ration of 3R and 4R isoforms) or function of tau (mostly by increasing aggregation ability or reducing microtubules binding ability). The mutations are numbered according to the longest isoform-htau40 (441 amino acids) and are located in the coding region.

1.2 Tau: A microtubule associated protein

Tau was initially isolated from the brain as one of the microtubule associated proteins, named then as 'tau factor' (Weingarten et al., 1975). A single gene encodes tau, which generates six main isoforms of 352 to 441 amino acids, in the human central nervous system by alternative splicing, and several further variants in peripheral nerves (Goedert, 1996; Andreadis, 2005). Tau isoforms are categorized based on the basis of alternatively spliced domains near the N-terminus (insert domains denoted as I) and in the C-terminal half (second repeat domain denoted as R) (Table 1.1).

Tau isoform	Denotation	Number of amino acids	Molecular weight (Da)
htau23	0I/3R	352	36750
htau37	1I/3R	381	39720
htau39	2I/3R	410	42603
htau24	0I/4R	383	40007
htau34	1I/4R	412	42967
htau40	2I/4R	441	45850

Table 1.1: List of tau isoforms present in CNS. This table shows tau isoforms occurring in CNS listed by name, denotation based on the presence or absence of I and R domains, number of amino acids and the molecular weight (Goedert et al., 1989).

The domains of tau are broadly divided into an acidic N-terminal 'projection domain' (M1-Y197) and a C-terminal 'assembly domain' (S198-L441) based on limited proteolysis and microtubule binding ability (Gustke et al., 1994). Tau domains are further defined based on the

character of the primary sequence (Fig. 1.4). The part of N-terminus with amino acids M1-G120 constitutes the acidic domain. This domain includes two insert domains that are alternatively spliced (I1 and I2; E42-A103). The region G120-Q244 is basic in nature, but in addition proline is a prominent feature in the region (hence named proline rich region with further subdivision into P1 and P2 at Y197). The region T244-K368 is characterized by three or four imperfect repeats (R1-R4) of 31 or 32 residues. The region following the repeats (K369-L441) is the C-terminal tail and can be further subdivided into a domain with residues K369-S400 (R' or P3) that are weakly homologous to the repeats and the region with C-terminal residues (S400-L441).
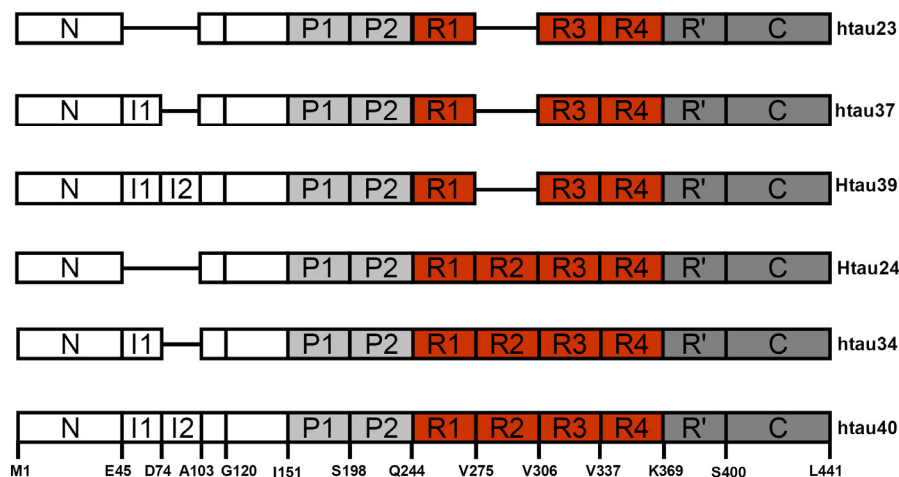
Figure 1.4: Domains of tau. Tau isoforms in the CNS are represented with the organization of domains. Tau domains are broadly divided into N-terminal 'projection domain' (amino acids M1-Y197) and C-terminal 'assembly domain' (amino acids S198-L441). The C-terminal assembly domain includes three or four pseudo-repeats (~31 residues each, R1-R4), which are together with their proline-rich flanking regions (P1 and P2) constitute the microtubule binding region. Repeat R2 and the two near N-terminal inserts (I1 and I2) may be absent due to alternative splicing.

1.2.1 Cellular functions of tau

Microtubule dynamics-assembly and disassembly of tubulin subunits-is influenced by the presence or absence of microtubule associated proteins (MAPs) on the microtubules. Microtubules that serve as the tracks for motor proteins are important for the intracellular transport of vesicles, organelles, and protein complexes by motor proteins (Hirokawa, 1993, 1994; Garcia and Cleveland, 2001). Tau is recognized as the important protein to stabilize microtubules. Over-expression of tau in chinese hamster ovary (CHO) cells causes a change in cell shape, retarded cell growth and dramatically altered the distribution of various organelles that are known to be transported via microtubule-dependent motor proteins (Ebneth et al., 1998). Particularly in axons, its expression is strongly up-regulated during neuronal development including the development of cell processes and establishment of cell polarity (Drubin and Kirschner, 1986). Neuronal polarity is also established by the transport of tau mRNA to the proximal axon where translation occurs (Litman et al., 1994).

The region of tau responsible for microtubule binding comprises of the repeat domains (R1-R4) and proline rich flanking regions (P2 and R' or P3). Tau which exhibits a basic character is complementary to the acidic surface of microtubules (Butner and Kirschner, 1991; Gustke et al., 1994; Goode et al., 1997), particularly to the glutamate rich C-terminus of tubulin (EGEGEEEGEE in α-tubulin and EFEEEGEEDE in β-tubulin; (Paschal et al., 1989). In the case of tau, clusters of positively charged amino acids in the repeats have been shown to be involved in microtubule binding by NMR analysis (Mukrasch et al., 2005; Mukrasch et al., 2007).

Tau can be phosphorylated by multiple kinases at multiple sites (Fig. 1.5) (Johnson and Stoothoff, 2004). The phosphorylation sites can be broadly subdivided into three classes: (i) several SP/TP motifs in the flanking regions of the repeats that are targets of proline-directed kinases such as glycogen synthase kinase3β (GSK3β) (Ishiguro et al., 1993), cyclin-dependent kinase5 (CDK5) (Baumann et al., 1993) or mitogen activated kinase (MAPK) (Drewes et al., 1992; Lu et al., 1993). (ii) KXGS motifs in repeats that are targets of non-proline directed kinases such as protein kinaseA (PKA), microtubule affinity regulating kinase (MARK) (Drewes et al., 1997) and synapses of amphids defective family kinases (SADK) (Kishi et al., 2005). (iii) Tyrosine residues at Y18 and Y394 that are targets of src family kinases (SFK) such as fyn (Lee et al., 1998; Lee, 2005) and c-Abl (Derkinderen et al., 2005).
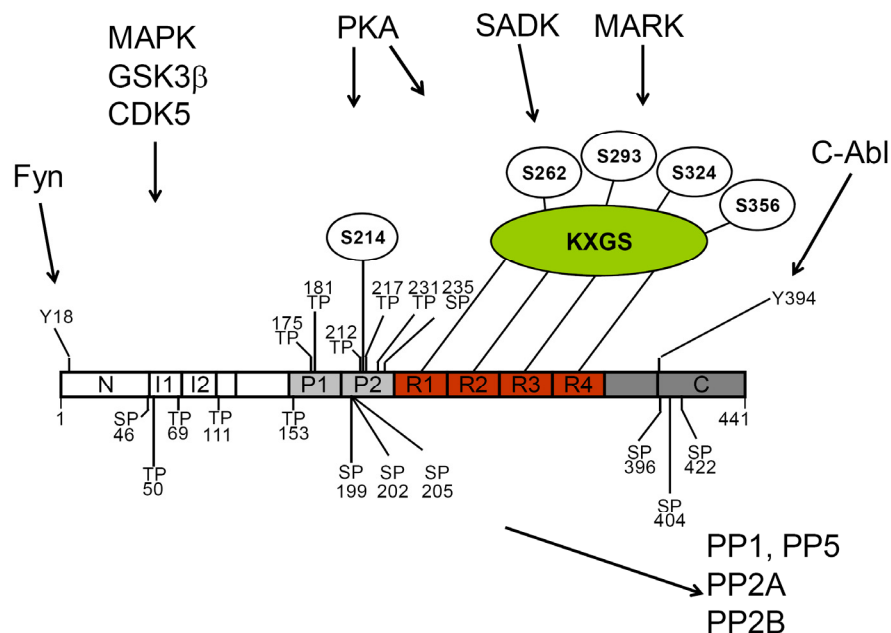
Figure 1.5: Phosphorylation sites of tau. Full length isoform htau40 is shown with phosphorylation targets of many different kinases. The SP/TP motifs are the main targets for proline directed kinases such as GSK3β, CDK5 and MAPK. S214 and KXGS motifs are targets of non-proline directed kinases such as PKA, MARK and SADK. Tyrosine residues at position 18 and 394 are target of src family kinases such as fyn and c-AbI. The phosphorylated tau can be dephophorylated by phosphatases such as PP2A and PP2B.

Tau is readily dephosphorylated by several protein phosphatases, most notably PP1, PP2A, PP2B and PP5 (Tian and Wang, 2002; Gong et al., 2004). Nonetheless, PP2A is believed to be a major tau phosphatases (Sontag et al., 1999).

The SP/TP phosphorylation has only a moderate influence on tau-MT interaction but is strongly up-regulated in AD and other tauopathies and is therefore used for post-mortem diagnosis (Mandelkow et al., 2007).

Other phosphorylation sites include targets of non-proline directed kinases-PKA (S214), MARK (KXGS motifs including S262, S356), SADK (S262) or Ca2+/calmodulin-dependent protein kinase II (S416). Phosphorylation at S262 or S214 result in the strong reduction of tau's ability to bind microtubules (Brandt et al., 1994; Drewes et al., 1997; Ebneth et al., 1999) and the phosphorylations at these sites are feature of AD (Gustke et al., 1992; Mandelkow et al., 1995; Mandelkow and Mandelkow, 1998). Enhanced phosphorylation at several SP/TP motifs and at S214 has been shown in mitotic cells (Illenberger et al., 1996) establishing the role of tau and its phosphorylation in the regulation of microtubule dynamics. Phosphorylation of tau or related MAPs by MARK appears to be important for the establishment of cell polarity and for the outgrowth of neurites (Kosik and McConlogue, 1994; Biernat and Mandelkow, 1999), but overactivity of MARK leads to cell death due to microtubule destabilization caused by phosphorylation of tau at the KXGS motifs in the repeat domain (Drewes et al., 1998). SADK which can phosphorylate tau at S262 has been shown to be required for neuronal polarity as well (Kishi et al., 2005).

Tyrosine residues of tau have been shown to be phospohorylated by src family kinases such as fyn (Y18) (Lee et al., 1998; Lee, 2005), lck (Y29) (Williamson et al., 2002) and c-Abl (Y394) (Derkinderen et al., 2005). In addition, the upregulation of fyn was shown to occur in AD brain (Shirazi and Wood, 1993). It is believed that the phosphorylation of tyrosine residues in tau may play an important role in both physiological (e.g. cell signaling) and pathological conditions (e.g. AD).

The N-terminal projection domain of tau (~200 residues) was found to project away from the microtubule surface (Chen et al., 1992). It may contribute to the spacing of microtubules but *in vitro* analysis shows that tau probably does not function as a spacer between microtubules (Marx et al., 2000). Another hypothesis is that this domain acts as an anchor for other cell components such as kinases, phosphatases, or the plasma membrane (Brandt et al., 1995; Mandelkow and Mandelkow, 1998; Sontag et al., 1999).

1.2.2 Pathological modifications of tau

In AD, the properties of tau change in several ways leading to loss of its normal cellular function followed by its aggregation. The modifications of tau in AD and their consequences are the following:

• Tau undergoes an abnormal 'hyperphosphorylation' at many sites, mostly at SP/TP motifs. Analysis of brain tissue and cell models of AD revealed that abnormal phosphorylation occurs before aggregation (Mandelkow et al., 1995; Trojanowski and Lee, 1995).

• Tau shows a loss of microtubule binding which is probably due to hyperphosphorylation at sites (e.g. S262 or S214) that detach tau from microtubules (Drewes et al., 1997). This could account for the disappearance of microtubules causing the breakdown of intracellular traffic which would result in the death of neuron.

• Tau aggregates into 'paired helical filaments' (PHFs) which shows a two-stranded appearance, with width of 10-20 nm (Crowther, 1991). The PHFs in turn bundle into neurofibrillary tangles. Elevated cytosolic concentration of tau due to detachment from microtubules can drive tau into aggregation in AD brain.

• Proteolysis and ubiquitination are posttranslational modifications of tau that probably represent cellular attempts to degrade the aberrant protein (via the proteasome or calpain pathway (Litersky and Johnson, 1995)). The truncations of tau at the C-terminus (E391) by unidentified proteases (Novak et al., 1993) and at D421 by members of the caspase family (Gamblin et al., 2003b; Rissman et al., 2004) have been shown to increase the rate of polymerization. This could be due to nucleation of the aggregation by some proteolytic fragments and exposure of certain residues with increased seeding capacity.

• Nitration and glycation are the other posttranslational modifications of tau in AD. Nitration of tau is shown to be a salient feature of diverse tauopathies (Horiguchi et al., 2003) and antibodies against site specific nitration in tau stains AD brain but not the normal brain (Reynolds et al., 2005). Glycation is a consequence of oxidative damage and crosslinking, which accumulates once tangles are formed (Yan et al., 1994).

• There is an increase of tau in the cerebrospinal fluid (from ~200 to ~600 pg/ml), which probably arises from dying neurons (Vigo-Pelfrey et al., 1995).

• Tau acquires pathological conformation before its aggregation in AD brain that was evidenced from the reactivities of certain antibodies that detect an early conformational change of tau in AD (e.g. Alz-50, MC1, Tau-66) (Carmel et al., 1996; Jicha et al., 1997a).

1.2.3 Structural properties of tau

1.2.3.1 Structure of soluble tau

Tau when first isolated from brain showed surprising heat stability (Weingarten et al., 1975). Later analysis by sedimentation and CD showed tau to be a highly asymmetric molecule with very little secondary structure (Cleveland et al., 1977). Analysis by proton NMR revealed that tau had a flexibility reminiscent of denatured and unfolded proteins (Woody et al., 1983). Efforts to visualize tau in EM suffered from its low contrast due to its hydrophilic nature (Zingsheim et al., 1979), but the glycerol-spray technique revealed the structure of tau to be an elongated and flexible rod, about 35 nm in length (Wille et al., 1992).

The heat stability of tau was exploited for its purification from *E.coli* and the purified tau surprisingly retained its ability to assemble microtubules (Fellous et al., 1977; Biernat et al., 1992). A detailed investigation of tau structure in solution using solution X-ray scattering and CD revealed that tau behaves as a random Gaussian coil with persistence length of ~2 nm (Schweers et al., 1994). Intrinsic fluorescence analysis of tryptophan mutants of tau confirmed that residues along the polypeptide chain were indeed completely solvent exposed, supporting the lack of structure (Li et al., 2002). All these observations proved that tau in solution does not contain any secondary structure and can be regarded as 'natively denatured'(Schweers et al., 1994; Barghorn et al., 2004).

Analysis of repeat domain constructs by NMR spectroscopy confirmed the paucity of secondary structural elements, but there are hexapeptide motifs in R2 and R3 showing inherent β-structure propensity (Mukrasch et al., 2005). Tau construct-K32 (Repeats domains plus its flanking regions; S198-Y394) showed a lack of well ordered structure by NMR analysis. However, the presence of some more structural elements was revealed particularly in flanking regions. The residues V256-S262 (in the centre of R1) and Q351-L357 (in the centre of R4) as well as residues in the flanking regions of repeat domains (K224-R230 in P2 and V363-E372 in R4 and R') also showed preferential β-structure (Mukrasch et al., 2007). The short stretches of amino acids showing β-structure in the beginning of R2 and R3 coincide with the sequences PHF6 (VQIVYK in R3) and PHF6* (VQIINK in R2, boxed residues in Fig. 1.6), involved in PHF formation (von Bergen et al., 2000; von Bergen et al., 2001).

As tau mainly binds to and stabilizes microtubules, it was expected that the binding to microtubules can induce some structure. Some reports stated that tau becomes more compact upon binding with microtubules (Butner and Kirschner, 1991) whereas other studies indicated that even when bound to microtubules, tau retains much of its disordered state (Al-Bassam et al., 2002; Santarella et al., 2004). Nonetheless, NMR analysis of tau-microtubule interactions

highlighted binding of several stretches of positively charged amino acids present in the repeat domains and the flanking regions to microtubules. The residues [275]VQIINKKLDLS[285] strongly contribute to the interaction with microtubules along with clusters of positively charged residues upstream of the PGGG motifs (Mukrasch et al., 2005; Mukrasch et al., 2007). In the flanking regions, the residues [225]KVAVVRT[231] and [240]KSRLQTAPV[248] (both in P2) and [370]KIETHKLTFREN[381] (in R') are potential binding sites of microtubules (Mukrasch et al., 2007).

In support of the experimental evidences on the unfolded nature of tau, algorithms that predict protein disorder from the primary sequence also reveal the disordered structure (von Bergen et al., 2006a). These algorithms predict the presence of the structural elements in R2 and R3 which is in good agreement with experimental data that show nascent β-structure for hexapeptides PHF6 and PHF6* (von Bergen et al., 2000; von Bergen et al., 2001; Mukrasch et al., 2005). In addition, algorithms that predict the aggregation prone regions of a protein point to the residual structure present in repeats of tau (PHF6 and PHF6*) (Fernandez-Escamilla et al., 2004; Pawar et al., 2005; Li and Lee, 2006).

Figure 1.6: Primary structure of tau. Domains of htau40 and the corresponding sequences of amino acids are identically colored. SP/TP phosphorylation sites (●), non-proline directed sites (KXGS sites and S214) (●) are shown. Amino acid residues constituting the two hexapeptides motifs (PHF6* and PHF6) in R2 and R3 are boxed. Residues forming the discontinuous epitope recognized by the Alz-50 antibody are underlined (For tau sequences see Lee et al., 1988; Goedert et al., 1989).

Lack of structure in natively unfolded proteins is hypothesized to be due to their low content of hydrophobicity and a high net charge near physiological pH (Uversky et al., 2001; Uversky, 2002a). It was shown that natively unfolded proteins are characterized by a high mean net charge (the net charge at pH 7.0 divided by the total number of residues) and low mean hydrophobicity (the sum of the hydrophobicities of all residues divided by the number of residues in the polypeptide) (Uversky et al., 2000). Indeed, the primary sequence of tau (Fig. 1.6; (Lee et al., 1988; Goedert et al., 1989) has a low hydrophobic content (mean hydrophobicity = 0.404) but a net charge of only +2 (mean net charge = 0.005) (Uversky et al., 2000). However, this value of net charge disguises the fact that tau is a multidomain protein with each domain carrying a different high net charge (Seitz et al., 2002). This holds particularly true for the repeat domains (Q244-N368) that aggregate faster than full length tau. The repeat domains exhibit a mean hydrophobicity of 0.43 and a high net charge of +9 (mean net charge = 0.072) that are consistent with values predicted for natively unfolded protein. Hence, the failure of tau to adopt a defined structure correlates well with the scarcity of hydrophobic amino acids (Note that folding of a protein is driven by hydrophobic amino acids by mediating hydrophobic collapse (Daggett and Fersht, 2003a; Daggett and Fersht, 2003b)) and the high net charge at physiological pH (resulting in repulsive force). For some of the natively unfolded proteins, it has been shown that either the minimization of net charge by manipulating the pH of the solvent or elevated temperature can induce partial folding by permitting hydrophobic-driven collapse to a partially folded intermediate (Uversky et al., 2001; Uversky, 2002a).

Evidence for folding within tau

Some indirect observations suggest that tau can not simply be a total random coil in the strict sense. Analysis by size exclusion chromatography shows that hydrodynamic radii of tau isoforms do not correspond to fully denatured state, but rather to a state intermediate between molten-globule and denatured (Barghorn et al., 2004; von Bergen et al., 2005). Perhaps the most compelling hints for distinct conformational states come from the reactivities of antibodies with discontinuous epitopes (listed in Table 1.2), which often recognize tau at an early stage of neurodegeneration.

Antibody	Recongition sites	References
Alz50 and MC1	residues near the N-terminus (7-9) and in the third repeat (313-322)	Carmel et al., 1996; Jicha et al., 1997a; Jicha et al., 1997b
Tau-66	elements upstream of the repeat domain and residues in repeat R3	Ghoshal et al., 2001; Garcia-Sierra et al., 2003
MN423	a truncation site downstream of the repeats (at E391) and residues within the repeat domain	Skrabana et al., 2004
SMI34	repeat domain and one of the KSP motifs upstream or downstream from the repeats	Lichtenberg-Kraag et al., 1992

Table 1.2: Tau antibodies with discontinuous epitopes. They are often used in the analysis of an early stage of neurodegeneration.

1.2.3.2 Structure of paired helical filaments

PHFs were identified as basic elements of neurofibrillary tangles (Kidd, 1963; Terry, 1963) and the subsequent isolation of PHFs from AD brain (Ihara et al., 1983; Wisniewski et al., 1984) enabled the analysis of the basic parameters of PHFs. It was shown that PHFs are ~ 8 nm x 20 nm in dimension using negatively stained electron micrographs (Crowther and Wischik, 1985). Analysis of the protein compositions of PHFs revealed tau as major component (Delacourte and Defossez, 1986; Kosik et al., 1986; Nukina and Ihara, 1986; Wood et al., 1986; Wischik et al., 1988b).

The assembly of PHFs *in vitro* was initially hampered by the high solubility of the protein. Assembly conditions were found in several steps by testing different tau constructs and optimizing assembly conditions including oxidation (Wille et al., 1992; Schweers et al., 1995; Barghorn and Mandelkow, 2002). In addition, aggregation of tau into PHFs *in vitro* was achieved by addition of polyanionic cofactors such as heparin (Goedert et al., 1996), RNA (Kampers et al., 1996) or arachidonic acid micelles (Wilson and Binder, 1997). Further analysis showed that filaments from *in vitro* aggregation resembled filaments from AD brain such that the core of PHFs contains the repeat domains while the N- and C-terminal domains contribute to the "fuzzy coat"(Wischik et al., 1988a; von Bergen et al., 2006b).

Cross β-structure was proposed as a typical feature of aggregates of amyloidogenic proteins (Kirschner et al., 1986; Sunde et al., 1997; Goux et al., 2004). Consistent with other amyloid proteins, the aggregation of tau is driven by a transition from random coil to β-structure in the repeat domain wherein hexapeptide motifs (PHF6 in R3 and PHF6* in R2) are important for aggregation (Barghorn et al., 2000; von Bergen et al., 2001). Further, cross β-structure of PHFs obtained *in vitro* and from AD brain was confirmed by X-ray diffraction (Sunde et al., 1997; Berriman et al., 2003; Goux et al., 2004) and the β-structural transition upon aggregation is

supported by data from CD and FTIR spectroscopy analysis (von Bergen et al., 2000; von Bergen et al., 2001; Barghorn et al., 2004). Consistent with cross β-structure, inhibition of aggregation can be achieved by proline scanning mutagenesis in these motifs which prevents β-structure. Conversely, aggregation is enhanced by mutations that strengthen β-structure propensity such as ΔK280 and P301L (Barghorn et al., 2000; von Bergen et al., 2001).
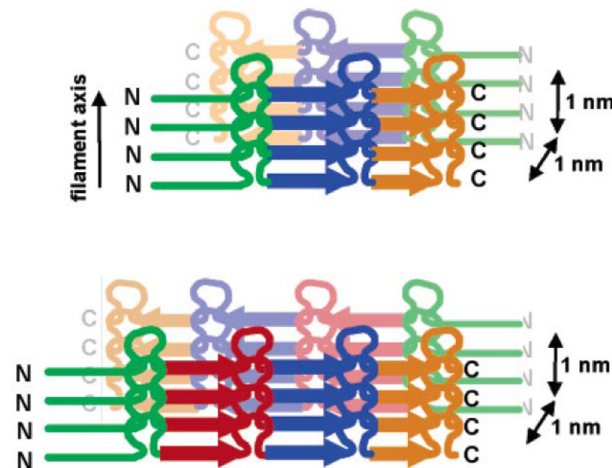
Figure 1.7: Possible models of the arrangement of tau molecules within the PHFs. Possible arrangements of tau molecules, deduced from limited proteolysis of PHFs and scanning transmission electron microscopy are shown for the construct K19 (A) and K18 (B). The four repeats are color coded (R1, R2, R3 and R4 in green, red, blue and orange respectively). The filament axis is vertical in the plane of the paper. The front four molecules form a β-sheet whose strands run perpendicular to the filament axis; behind it a second sheet in faded colors is shown. Figure reproduced from von Bergen et al., 2006b.

Even though the exact molecular details of interactions of tau within PHF are still unknown, recent studies have attempted to resolve the molecular architecture of PHF. One model of PHF was the β-helix model based on studies using site-directed electron paramagnetic resonance (EPR). The data suggest that residues of R2 (272-289) and R3 (301-320) are arranged in a way that identical amino acids are stacked in register along the fiber axis (Margittai and Langen, 2004, 2006). Other constraints for the arrangement of tau in PHF comes from scanning transmission electron microscopy (STEM) analysis where it was shown that the mass per-length of the PHF core is about 60-70 kDa/nm, equivalent to roughly 3.5-4.5 tau molecule per nm (von Bergen et al., 2006b). This data can be fitted to a model in which there are ~2 molecules per nm and ~ 2 protofibrils constitute the PHF as successive molecules in a cross β-structure that are spaced 0.47 nm apart (Figure 1.7).

Analysis by intrinsic tryptophan fluorescence showed that PHFs can be dissolved by relatively low concentrations of denaturants, e.g. by half maximal concentrations of ~1-1.8 M GdnHCl, depending on tau construct (Li et al., 2002). Though the relatively hydrophobic hexapeptides (VQIINK in R2 and VQIVYK in R3) are involved in formation of β-structure, the role of hydrophobic interactions and salt bridges for the stability of PHFs are not well understood.

1.3 Aim of this study

The microtubule associated protein-tau stabilizes microtubules in its physiological role whereas it aggregates into pathological paired helical filaments (PHFs) in AD, in spite of its high solubility. The presence of long range interactions within tau in the soluble form have not been previously reported in detail. Likewise, the molecular details of the interactions of tau within PHFs (i.e. interactions between strands and protofilaments) are still unknown.

The aim of the present study was to improve our understanding of the structural and biophysical properties of tau in solution and of tau aggregates (PHFs). The experiments were aimed at the following: (i) to identify the determinants of the unfolded nature of tau, (ii) to analyze the long range interactions within the tau molecule, (iii) to define factors that contribute to the conversion of soluble tau to the aggregated state and (iv) to analyze the factors that stabilize tau within PHFs.

2 Materials and Methods

2.1 Materials

2.1.1 Laboratory equipment

Analytical HPLC:

SMART-system with the following gel filtration columns:

Fast Desalting PC (3.2 mm x 100 mm)	Amersham Biosciences, Freiburg
Superose PC12 (3.2 mm x 300 mm)	Amersham Biosciences, Freiburg

Preparative FPLC:

Äkta Explorer-system with the following gel filtration columns:

Superdex G200 HR 16/60 (120 ml)	Amersham Biosciences, Freiburg
Superdex G75 HR 16/60 (120 ml)	Amersham Biosciences, Freiburg

Äkta Explorer-system with the following anion exchange columns:

SP Sepharose 16/10 (20 ml)	Amersham Biosciences, Freiburg

Spectrophotometers:

Kontron spectrophotometer	Kontron Instruments, Neufahrn
Tecan spectrophotometer	Labsystems, Frankfurt
Spex Fluoromax spectrophotometer	Polytec, Waldbronn
Jasco J-810 CD spectrometer	Jasco, Gross-Umstadt
Jasco J-410 FTIR spectrometer	Jasco, Gross-Umstadt

Centrifuges:

Eppendorf centrifuge type 5415C and 5402	Eppendorf, Hamburg
Table ultracentrifuge TL-100	Beckmann, München
Ulracentrifuge L8-70M	Beckmann, München

Miscellaneous:

Transmission electron microscope	CM-12 Phillips (Tecnai)
PCR machine	Eppendorf, Hamburg
Analytic balances type BP 310 S and PT 1200	Sartorius, Göttingen
BTX electroporation system	Cole-Parmer Instrument, UK
Intelligent dark box II, Las-1000+	Fuji, Japan

2.1.2 Chemicals

Chemicals of highest quality were obtained from the following suppliers:

Sigma, Merck, Fluka, Serva, Gerbu, AppliChem, Amersham Pharmacia Biotech, New England Biolabs, Qiagen, Molecular Probes

2.1.3 Software

Vector NTI   Invitrogen, Karlsruhe

EMBOSS   http://emboss.sourceforge.net/

2.1.4 Molecular biology reagents

2.1.4.1 Kits, spin columns and reagents for DNA

Invisorb spin plasmid mini kit   Invitek, Berlin

Nucleospin gel extraction kit   Macherey-Nagel, Düren

Zero Blunt TOPO PCR cloning kit   Invitrogen, Karlsruhe

Agarose for DNA electrophoresis   Serva, Heidelberg

2.1.4.2 Vectors and DNA standards

pNG2 (a derivative of pET-3a)   Merck-Novagen, Darmstadt

Small ladder   MBI Fermentas, St.Leon-Rot

2.1.4.3 Antibiotics and media

Ampicillin   Gerbu, Gaiberg

Carbenicillin   Applichem, Darmstadt

LB medium   Carl Roth GmBH, Karlsruhe

2.1.4.4 Bacterial strains

Cloning strains:

XL2-Blue and XL10-Gold   Stratagene, Netherlands

DH5α library efficiency   Invitrogen, Karlsruhe

Expression strain:

BL21 (DE3)   Invitrogen, Karlsruhe

2.1.4.5 Enzymes, substrates and nucleotides

All restriction endonucleases   New England Biolabs, Frankfurt

DNA ligase   New England Biolabs, Frankfurt

Pfu Ultra DNA polymerase   Stratagene, Netherlands

Pwo master mix   Roche diagnostic, Mahnheim

50X dNTPs master mix   Invitek, Berlin

$MgCl_2$ Merck-Novagen, Darmstadt

2.1.5 Stock and working buffer solutions

PBS (1X): 137 mM NaCl, 3 mM KCl, 10 mM Na_2HPO_4, 2 mM KH_2PO_4.

To make 20X PBS, 160 g NaCl, 4 g KCl, 28.8 g Na_2HPO_4 and 4.8 g KH_2PO_4 were dissolved and adjusted to 1000 ml with water, filtered and stored at room temperature.

1X TAE: 40 mM Tris-acetate, 1mM EDTA (pH 8.0).

To make 50X TAE, 242 g Tris base, 57.1 g glacial acetic acid and 100 ml of 0.5 M EDTA (pH 8.0) were dissolved in water and adjusted to 1000 ml.

6X DNA loading buffer: 10 mM Tris-HCl (pH 7.6); 0.03 % bromophenol blue; 0.03 % xylene cyanol FF; 60 mM EDTA; 60 % glycerol.

TE Buffer: 10 mM Tris HCl pH 7.5; 1 mM EDTA.

1X SDS running buffer: 25 mM Tris base; 192 mM Glycine; 0.1% SDS.

To make 10X SDS running buffer (Laemmli buffer), 30.3 g Tris base, 144 g Glycine and 10 g SDS were dissolved and made up to 1000 ml with water.

4X SDS loading buffer: 200 mM Tris-HCl (pH 6.8), 400 mM DTT, 8 % SDS, 0.4 % Bromophenol blue, 50 % glycerol.

2.2 Methods

2.2.1 Molecular biology methods

2.2.1.1 Cultivation of *E.coli*

2.2.1.1.1 Culture medium

Luria Bertani (LB) medium: 10 g Bacto-Tryptone, 5 g Bacto-yeast extract and 5 g NaCl in 1000 ml, sterilized by autoclaving and stored at 4°C.

LB-agar plates: LB medium containing 1.5 % of agar was autoclaved and stored at 4°C. When needed, it was melted in micro oven. After letting it to cool down to 55°C, an appropriate antibiotic was added and poured into petri plates with a diameter of 10 cm in the clean bench, allowed to solidify and stored at 4°C for further use.

SOC medium: 0.5 % Yeast extracts; 2 % Bacto-tryptone; 10 mM NaCl; 2.5 mM KCl; 10 mM $MgSO_4$; 10 mM $MgCl_2$; 20 mM Glucose.

2.2.1.1.2 Transformation of *E. coli* strains

E. coli cells competent for transformation were either purchased from commercial sources (see section 2.1.4.4) or prepared manually in the laboratory. The vector pNG2 in which all the tau constructs and mutants were created has ampicillin resistance.

Transformation by heat-shock method

XL2-Blue, XL10-Gold and DH5α cells were transformed with a plasmid of interest by the heat-shock method. For the transformation, 20-100 ng of DNA was added to 20-50 μl aliquots of competent cells and allowed to stand on ice for 30 minutes. Cells were then given heat shock at 42°C for 45 seconds and placed again on ice for 1-2 minutes. 200-300 μl of SOC medium were added to the cells and were incubated at 37°C with shaking for 1 hour. Finally, 100-200 μl of cells was plated on a LB agar plate containing ampicillin and were incubated overnight at 37°C.

Transformation by electroporation

BL21-DE3 electrocompetent cells used for expression of proteins were transformed by electroporation in which the electrocompetent cells plus DNA placed in a plastic cuvette containing electrodes are subjected to a short electric pulse, about 2400 volts/cm causing small holes in the membrane through which the DNA enters. For the transformation by electroporation, 0.5-1.0 ng of DNA was added to 20 μl of the electrocompetent cells and the contents were transferred into a pre-chilled electroporation cuvette. The cuvette was placed in the electroporater (BTX electroporation system, Cole-Parmer Instrument, UK) and then electric pulse was applied. Precooled SOC medium was immediately added to the cells and was transferred to new sterile eppendorf tube. The cells were incubated at 37°C for 30 minutes with shaking and were plated on a LB agar plate containing ampicillin followed by overnight incubation of the plate at 37°C.

2.2.1.1.3 Inoculation and glycerol stocks of *E.coli*

A single colony of *E.coli* from LB agar plate was picked and inoculated into 5 ml LB medium containing ampicillin. This was incubated at 37°C with shaking to allow growth of *E.coli*. For long term storage, 0.7 ml of grown culture was gently mixed with 0.3 ml of sterile 100 % glycerol, shock frozen in liquid N_2 and stored at -80°C.

2.2.1.2 Mini preparation of plasmid DNA

Plasmid DNA was isolated from *E.coli* cultures using the Invisorb Spin plasmid mini kit. Isolation of plasmid was done according to the protocol provided by the manufacturer. All plasmids were eluted and stored at -20°C in TE buffer.

2.2.1.3 Determination of DNA concentration and purity

The concentration and the degree of purity of purified plasmid DNA was determined based on the Beer-Lambert law by measuring the absorbance at 260 nm and 280 nm:

$$A_{260} = \varepsilon_{260}\, c\, l \text{ and } A_{260} \times 50 = \mu g/ml \text{ (when } l = 1 \text{ cm)} \qquad \text{Equation 1}$$

A_{260} is the absorbance at 260 nm, ε_{260} is the molar absorption coefficient, c is the molar concentration and l is the optical path length (usually 1 cm). For a protein-free and RNA-free solution of DNA the ratio of A_{260}/A_{280} should be 1.5-2.0. Any proteinaceous contamination present in the preparation would decrease the ratio to < 1.5 whereas RNA contamination would increase the ratio to > 2.0. DNA preparations having the A_{260}/A_{280} ratio of 1.5–2.0 were used after further analysis of DNA in agarose gel electrophoresis for the concentration and purity.

2.2.1.4 Agarose gel electrophoresis of DNA

The size and purity of DNA was analyzed by agarose gel electrophoresis. For optimal resolution, the concentration of agarose was adapted to the size of the DNA of interest as listed in Table 2.1.

Agarose concentration (%)	DNA size (kb)
0.7	20-1
0.9	7-0.5
1.2	6-0.4
1.5	4-0.2
2.0	3-0.1

Table 2.1: Concentration of agarose used depending on DNA size. The table shows concentration of agarose to be used depending on the size of DNA to be analyzed (Sambrook and Maniatis, 1989).

The required amount of agarose was taken in 1X TAE buffer and melted by boiling it in a microwave oven. The agarose solution was poured into a cassette and allowed to solidify. Then agarose gel was immersed in a chamber with TAE buffer and DNA samples in gel loading buffer were loaded onto the gel. The electrophoresis was carried out at 100 V after that the gel was stained in Ethidium bromide (EtBr) bath (0.5 µg/ml). Binding of EtBr by intercalation of its planar group between the stacked bases of the DNA increases its fluorescent yield compared to that of the dye in free solution. During ultraviolet irradiation, DNA absorbs at 254 nm and transmits energy to the dye and the bound dye itself absorbs radiation at 302 nm, as well as 366 nm. As a result, the energy is reemitted at 590 nm in the red orange region of the visible spectrum, which was used to visualize DNA under a UV transilluminator. The gel was photographed using a gel documentation system.

2.2.1.5 Site directed mutagenesis of DNA

Most of the mutations were created either using site-directed mutagenesis using the Quick Change site-directed mutagenesis kit (Stratagene, Netherlands) or using mega primer which is a short PCR product amplified with mutational primers.

Site directed mutagenesis by complementary primers

The complementary primers, designed based on the template plasmid, carrying desired mutation were used to amplify the template plasmid using PCR.

The mixture of PCR reaction for site directed mutagenesis was as following:

10X *Pfu* ultra buffer	2.0 µl	PCR program used:
dsDNA template (25 ng/µl)	2.0 µl	
dNTPs (2.5 mM)	2.0 µl	
Forward primer (10 pmoles/µl)	1.0 µl	
Reverse primer (10 pmoles/µl)	1.0 µl	
Pfu ultra polymerase (2.5 U/µl)	0.5 µl	
H₂O to a final volume of	20 µl	

PCR program used:

96°C 2 min | 96°C 45 sec | 50°C 45 sec | 68°C 6 min | 68°C 12 min → 17 cycles
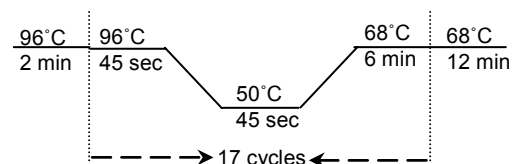
In a PCR cycle, initial denaturation is done for few minutes at 96°C to unwind the plasmid DNA. The actual cycle involves continuous temperature shifts such that DNA is melted at higher temperature, primers are able to anneal to template at lower temperature and finally polymerase can exhibit its action at extension temperature. Annealing temperature depends on the primer content whereas the extension time varies with length of the template used.

Site directed mutagenesis by mega primer method

By this method, it was possible to introduce two or more mutations in a single PCR amplification of template by using initially created short PCR product with primers either one or both of them having desired mutations.

Generation of short fragment (mega primer)

PCR reaction mixture for the generation of short product was as following:

dsDNA template (25 ng/µl)	1.0 µl	PCR program used:
Forward primer	2.5 µl	
Reverse primer	2.5 µl	
H₂O to volume of	18.0 µl	
PWO master mix	25.0 µl	

PCR program used:

96°C 2 min | 96°C 45 sec | 50°C 45 sec | 68°C 1 min | 68°C 5 min → 27 cycles
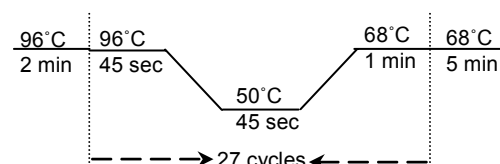
The short product (mega primer) obtained was gel purified and used for setting up long PCR.

Generation of long fragment by using mega primer

Since the mega primers created are usually between 50-300 nucleotides, annealing step in PCR cycle was not needed for next PCR for creating long product:

PCR reaction mixture as following:

Template (25 ng/μl)	2.0 μl	PCR program used:
dNTP (2.5mM)	2.0 μl	
10X P*fu* ultra buffer	2.5 μl	
Mega primer (100 ng/μl)	7.0 μl	
Pfu ultra polymerase	0.2 μl	
H$_2$O to volume of	25.0 μl	
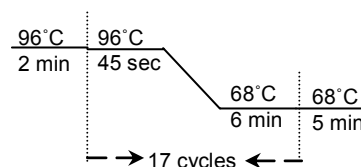
With all PCR for mutations, a negative control was set up with all the components without one of the primers. The amplifications were checked in 0.8 % agarose gel by loading 5 μl of PCR product.

DpnI digestion

The amplified PCR products were subjected to *DpnI* digestion resulting in the disruption of methylated template DNA (template) but not the amplified DNA which would carry mutation.

0.1-0.5 μl of *DpnI* was added directly to PCR products (both negative and positive controls) and incubated at 37°C for 2-3 hours. After the digestion, the digested products were again checked in 0.8 % agarose gel. Transformation of PCR products was done by heat shock method followed by plasmid preparation from few isolated colonies. The presence of mutation in the purified plasmid was confirmed by DNA sequencing.

2.2.1.6 DNA sequencing

The sequencing reactions were performed in 96 PCR machine using fluorescent dye labeling based on the Sanger method (Sanger et al., 1977)

Sequencing reaction mixture contained:

Terminator ready reaction mix	8 μl	The running cycles for sequencing in PCR:
DNA of interest (100 ng/μl)	5-7 μl	
Primer (10 pmol/μl)	1 μl	
H$_2$O to a final volume of	20 μl	
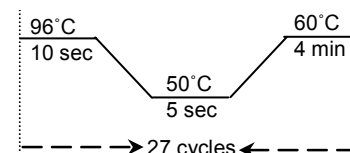
After PCR sequencing reaction, the DNA was pelleted by ethanol precipitation: To 20 μl of sequencing reaction, 16 μl of water and 64 μl of 95 % ethanol were added, mixed and centrifuged at 13000 rpm for 10 minutes at room temperature. The pellet from the centrifugation was washed with 250 μl of 70 % ethanol to remove any trace of salts by centrifugation at 13000 rpm for 10 minutes at room temperature. The pellet was then air dried at 90°C for 5 minutes, resuspended in 30 μl of HPLC-grade H$_2$O and was ready for sequencing.

The ABI PRISM 310 Genetic Analyzer (Applied Biosystems, Darmstadt) was used to sequence the DNA. The sequencing results were analyzed with the VectorNTI software (Invitrogen, Karlsruhe).

2.2.2 Biochemical and biophysical methods

2.2.2.1 SDS-PAGE

SDS-PAGE (sodium dodecyl sulfate polyacrylamide gel electrophoresis) was performed for the electrophoretic separation of the protein (Laemmli, 1970; Matsudaira and Burgess, 1978). By mixing the solution of proteins with SDS, the protein is denatured and gets a negative charge in proportion to its mass due to binding of SDS to the protein, yielding an approximately uniform mass to charge ratio. This enables the proteins to be separated strictly by their molecular weight. With the addition of SDS, proteins are briefly heated to 95°C in the presence of a reducing agent (DTT or β-BME) to promote denaturation. The denatured proteins are subsequently applied to one end of a layer of polyacrylamide gel submerged in a suitable buffer and an electric current is applied across the gel causing the negatively-charged proteins to migrate depending on their size. In SDS PAGE, the protein separation is performed using a discontinuous buffer system. In early stage of electrophoresis, an ion gradient is formed in the stacking gel that causes all of the proteins to focus into a single sharp band. A change of pH and the subsequent elimination of the ion gradient in the resolving gel causes the proteins to separate by the molecular size sieving.

A system with vertically oriented glass plates with 1 mm spacer in between was used for casting gels. The SDS-PAGE gels were cast as following: First the resolving gel (Table 2.2) poured between assembled glass plates and a layer of isopropanol was applied on it. After polymerization of the gel, the layer of isopropanol was removed. Then the stacking gel (Table 2.2) was put on top of the polymerized resolving gel and the combs were inserted.

Components	Separating gel		Stacking gel (4 %) (ml)
	10 % (ml)	17 % (ml)	
40 % Acrylamide/ Bis acrylamide (37.5:1)	15.00	25.60	5.40
Tris HCl (1.0 M, pH 8.8)	22.00	22.00	-
Tris HCl (0.25 M, pH 6.8)	-	-	27.00
10 % SDS	0.60	0.60	0.54
TEMED	0.12	0.12	0.108
10 % APS	0.065	0.065	0.065
H_2O	22.00	11.50	20.90

Table 2.2: Solutions for preparing SDS-PAGE gel. This table shows the compositions of solution used for making 10 % and 17 % SDS-PAGE gel.

To perform electrophoresis, the gel was placed in an electrophoresis chamber covered with 1X SDS-running buffer and combs were removed. The protein samples were mixed with Laemmli loading buffer and were denatured by heating at 95°C for 5 minutes. Then samples were loaded along with molecular weight marker proteins (Table 2.3) on to the wells and electrophoresis was performed at a constant current of 35 mA.

Protein name	Molecular weight (kDa)
β-Galactosidease	116.0
Bovine serum albumin	66.2
Lactate-dehydrogenase	45.0
Restriction endonuclease Bsp981	35.0
Lactoglobulin	18.0
Lysozyme	14.4

Table 2.3: Marker proteins for SDS-PAGE gel. The details of molecular weight marker proteins used for running the SDS gel are shown.

After the electrophoresis, the gel was transferred to the Coomassie staining solution (0.1 % Coomassie brilliant blue R-250, 45 % methanol and 9 % acetic acid) and stained for 20 minutes on an orbital shaking platform. To visualize protein bands on the gel, the gel was placed in the intensive destaining solution (50 % methanol, 10 % acetic acid) for 20 minutes and then in the normal destaining solution (5 % methanol, 7.5 % acetic acid).

2.2.2.2 Protein purification methods

2.2.2.2.1 Bacterial culture and harvesting

The cultivation of bacterial cells for the protein expression was done as following: either a single colony of the plasmid transformed into BL21-DE3 cells or from glycerol stocks was inoculated into 5 ml LB medium containing the ampicillin from LB agar plates and the culture was grown overnight at 37°C. 1 ml of this culture was used for inoculating 100 ml LB medium. This pre-culture was then used for inoculating a fresh 1 liter LB medium supplemented with ampicillin and grown at 37°C with shaking until the optical density at 600 nm (OD_{600}) reached 0.6. At this stage, 1 ml of this culture was collected and treated as uninduced control. The rest of the culture was induced with 0.5 mM IPTG and was let to grow at 37°C for 4-6 hours. The grown cells were then harvested by centrifugation at 8 krpm for 15 minutes (JLA rotor, Ultracentrifuge Coulter-Avanti J-26 XP,Beckmann) and resuspended in cell lysis buffer (20 mM Na-MES pH 6.8, 1 mM EGTA, 0.2 mM $MgCl_2$, 5 mM DTT, 1 mM PMSF, 10 µg/ml leupeptin, 2 mM benzamindin and 10 µg/ml pepstatin A).

2.2.2.2.2 Cell lysis and initial protein purification

The resuspended cells were subjected to mechanical cell disruption by high shear force using French press (A valve-type processor, SLM Instruments, UK). The cells were disrupted by forcing the cell suspension through a narrow valve under high pressure (20000-30000 psi or 140-210 MPa). The cell lysate was centrifuged at 40 krpm (Ti45 rotor, Ultracentrifuge Coulter-Optima LE-80K, Beckman) for 45 minutes at 4°C and the supernatant was collected. The further purification of tau was followed as described previously (Biernat et al., 1992). In brief, the supernatant was added with NaCl to final concentration of 0.5 M and DTT to final concentration of 5 mM and was boiled at 95°C for 20 minutes. The sample after heating was again centrifuged at 40 krpm for 45 minutes at 4°C and the supernatant collected was dialyzed against suitable buffer required for further purification (SP-Sepharose buffer A, see section 2.2.2.2.3.1).

The purification of tryptophan containing tau mutant proteins used for fluorescence experiments was slightly modified because of the influence of high temperature on tryptophan fluorescence. To the supernatant of cell lysate, 25 % ammonium sulphate (14.4 g/100 ml) was added in stepwise manner in order to avoid unequal local concentration at 4°C. The solution was centrifuged at 40 krpm (Ti45 rotor, Ultracentrifuge Coulter-Optima LE-80K, Beckman) for 45 minutes at 4°C and the supernatant was collected. To the supernatant, ammonium sulphate was added to the final concentration of 55 % (19.1 g/100 ml) in a stepwise manner at 4°C. This solution was again centrifuged at 40 krpm for 45 minutes at 4°C and the pellet was collected. The pellet was resuspended and dialyzed against suitable buffer required for further purification (SP-Sepharose buffer A, see below). The dialyzed sample was centrifuged at 40 krpm for 45 minutes at 4°C and was ready for further purification.

2.2.2.2.3 Purification by Chromatography

Further purification of tau was performed by fast performance liquid chromatography (FPLC) using Äkta purifier and Äkta explorer FPLC- devices (Amersham Biosciences, Freiburg).

2.2.2.2.3.1 Cation exchange chromatography

Ion exchange chromatography relies on charge-charge interactions between the proteins and the charges immobilized on the ion exchange resin. After the proteins are bound, elution of protein is carried out using a gradient of buffer, which steadily increases the ionic strength of the eluting solution. Alternatively, the pH of the elution buffer can be modified in order to give the protein or the matrix a charge at which they will not interact and proteins of interest elutes from the resin.

Since tau contains positive charges around pH 7.0, cationic exchangers were used and protein was eluted with a gradient of NaCl (varying ionic strength). The column used for cation

exchange chromatography was SP-Sepharose 16/10 (Amersham Biosciences, Freiburg). After equilibration with 5 column volumes of the SP-Sepharose buffer A (20 mM Na-MES pH 6.8, 50 mM NaCl, 1 mM EGTA, 1 mM $MgSO_4$, 2 mM DTT, 0.1 mM PMSF), the dialyzed protein sample obtained either by heating or ammonium sulphate precipitation was loaded on the column using a super loop (Amersham Biosciences, Freiburg) and the column was washed with 5-7 column volumes of SP-Sepharose buffer A to remove unbound proteins.
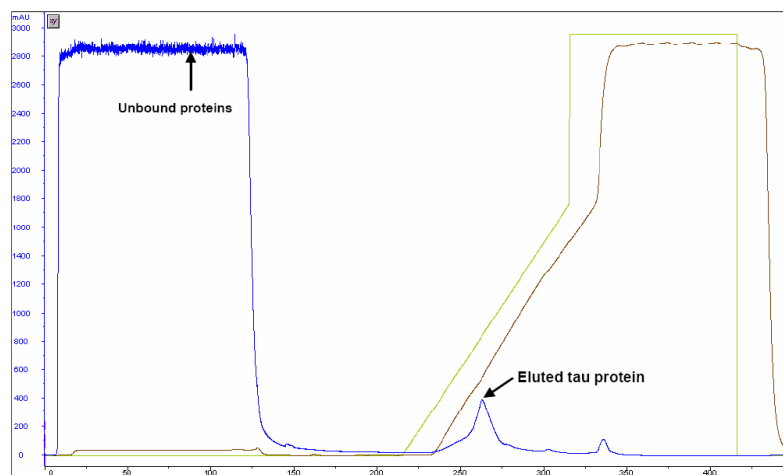
Figure 2.1: Elution profile of tau protein in SP-Sepharose 16/10 column. The protein sample obtained either by heating or ammonium sulphate precipitation was loaded on the SP sepharose column and eluted with linear gradient of ionic strength. The peaks corresponding to unbound proteins and eluted protein were shown by arrows.

The elution was carried out with a linear gradient of SP-Sepharose buffer B (20 mM Na-MES pH 6.8, 1 M NaCl, 1 mM EGTA, 1 mM $MgSO_4$, 2 mM DTT, 0.1 mM PMSF) in two steps: first from 0 to 60 % in 5-8 column volumes and then to 100 % in 1-2 column volumes. An elution profile of a tau mutant protein from SP-sepharose 16/10 is shown in Figure 2.1. The eluted fractions were checked on SDS-PAGE and fractions containing the protein of interest were pooled together and concentrated using Amicon centrifugal filter devices (Millipore, UK).

2.2.2.2.3.2 Gel filtration chromatography

Gel filtration (or size exclusion) chromatography achieves separation of the analytes based on their differences in size and shape. The gel filtration column is tightly packed with porous polymer beads with different pore size. When the protein is made to pass through the beads using a single buffer solution, the larger molecules, which can not be accommodated into the pores of beads, elutes first and smaller molecules trapped into the pores elute later.

The concentrated protein solution from SP Sepharose column was injected onto pre-equilibrated gel filtration column (HiLoad 16/60 Superdex G200 or HiLoad Superdex G75, prep grade, Amersham Biosciences, Freiburg) using a 1 ml loop with an injection needle. Isocratic elution was performed with PBS buffer containing 1-2 mM DTT at a flow rate of 0.5 ml/min. The

elution profile of a tau mutant protein is shown in Figure 2.2. The eluted fractions were analyzed on SDS-PAGE and pure protein fractions were used for further experiments.
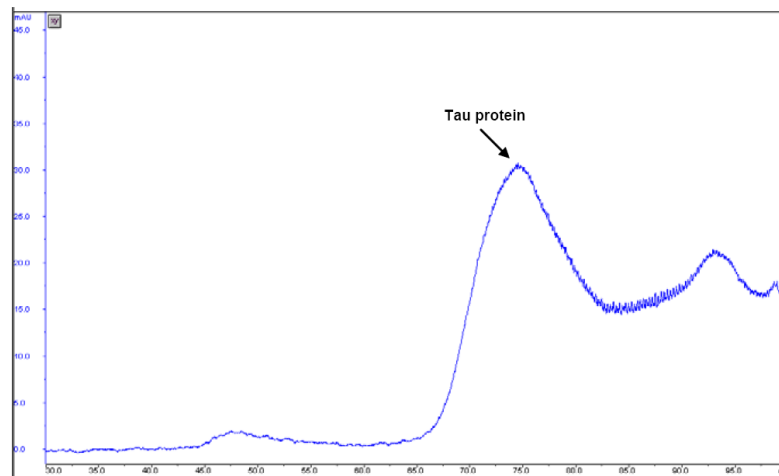
Figure 2.2: Elution profile of tau protein in a gel filtration column. The concentrated protein solution from the SP Sepharose column was loaded on a Superdex G200 column and isocratic elution was performed with PBS buffer. The eluted fractions were analyzed on SDS-PAGE and pure protein fractions were used for further experiments.

2.2.2.3 Microtubule polymerization assay

The ability of tau and its mutants to promote microtubule assembly was monitored by UV light scattering at an angle of 90° and a wavelength of 350 nm in a quartz cuvette (path length-0.15 cm) in a Kontron spectrophotometer (Kontron Instruments, Germany) in the presence and absence of tau. A typical experiment was set as following: 5 µM tau was mixed with 30 µM tubulin dimer at 4°C in microtubule assembly buffer (100 mM Na-PIPES, pH 6.9, 1 mM EGTA, 1 mM $MgSO_4$, 1 mM GTP, 1 mM DTT) in a final volume of 20 µl. The reaction was started by raising the temperature to 37°C. The control experiment was conducted without tau. Typical microtubule assembly curves stimulated by tau are shown in Figure 2.3.
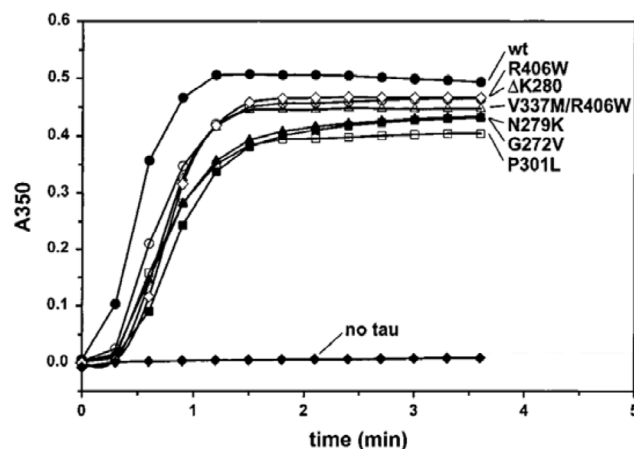
Figure 2.3: Microtubule assembly by tau mutants. Assembly of microtubules is observed by the optical density at 350 nm after a mixture of 30 µM tubulin and 5 µM tau at 4 °C was warmed to 37 °C. Tubulin alone is unable to polymerize because its concentration is below the critical concentration (bottom curve). Wild-type compared with the mutants of htau40 show a slightly increased ability to promote MT assembly. Figure reproduced from Barghorn et al., 2000.

2.2.2.4 Analytical size exclusion chromatography

Elution profiles of tau isoforms and constructs were obtained by size exclusion chromatography using a Superose PC12 column (Amersham Biosciences, Freiburg) connected to a SMART-HPLC system (Amersham Biosciences, Freiburg). A set of standard proteins and tau isoforms and constructs were subjected to isocratic elution in PBS or PBS containing 2 M GdnHCl with a flow rate of 20 µl/min and the elution was monitored by UV absorbance at 214, 256 and 280 nm. The elution volume of tau isoforms and constructs in the presence and absence of GdnHCl was then used to calculate the apparent Stokes radius of tau with reference to Stokes radii of standard proteins

2.2.2.5 Fluorescence resonance energy transfer (FRET) studies

Fluorescence resonance energy transfer (FRET) is the transfer of excited-state energy from a donor (D) which is initially excited to an acceptor (A) and is a result of long range dipole-dipole interactions between them. The rate of energy transfer depends upon the extent of spectral overlap of the emission spectrum of the donor with the excitation spectrum of the acceptor, the quantum yield (which is defined as the ratio of the number of photons emitted to the number of photons absorbed) of the donor, the relative orientation of the donor and the acceptor transition dipoles and the distance between them. The efficiency of energy transfer is the fraction of photons absorbed by the donor that are transferred to acceptor which is given by the equation,

$$\mathbf{E_{FRET}} = [1+(R/R_0)^6]^{-1} \qquad \text{Equation 2,}$$

where the Förster distance R_0 is the distance at which energy transfer is 50 % (Fig 2.4) and R is the distance between the donor and acceptor.
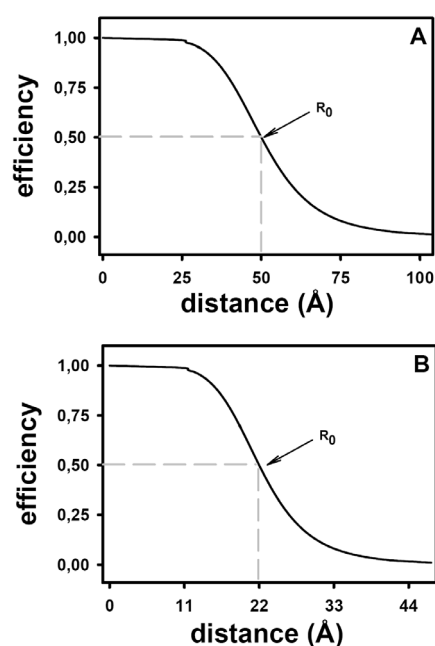
Figure 2.4: Dependence of distance on FRET efficiency. (A) Distance as function of efficiency for a theoretical FRET pair of donor and acceptor. Note the 50 % efficiency would result in 50 Å distance. (B) Distance dependence of the tryptophan-IAEDANS pair as function of efficiency with $R_0 = 22$ Å.

Typically, a protein is modified with covalent linkage of a donor and an acceptor. Because tryptophan residue has intrinsic fluorescence, it is often used as donor. If a protein contains a single donor and acceptor, then distance between donor and acceptor can be estimated from the efficiency of energy transfer. The transfer efficiency can be determined by steady-state measurements of donor emission in the presence (D_A) and absence of acceptor (D) from the following equation,

$$E_{FRET} = (1-D_A/D) \ (1/f_A) \qquad \text{Equation 3,}$$

where, f_A is fraction labeling ratio of the acceptor. Using the efficiency calculated from equation 3 and the knowledge of R_o for the given donor and acceptor pair, the distance between donor and acceptor can be calculated using equation 2.

For example, if one assumes R_o = 50 Å for given donor-acceptor pair and the measured efficiency is 0.5 (assuming 100 % labeling efficiency), then the equation 2 can rearranged as

$$R = R_o \ [(1-E)/E)]^{1/6} \qquad \text{Equation 4}$$

Substituting all the values would result,

$$R = 50 \ [(1-0.5)/0.5)]^{1/6}$$
$$R = 50 \ [1]^{1/6}$$
$$R = 50 \ \text{Å}$$

If one assumes R_o = 50 Å for a given donor-acceptor pair and the measured efficiency is 0.5 with only 80 % labeling efficiency, then the resulting distance without the correction for the unlabeled fraction could be larger than the actual distance. Substituting all the values without correction factor would result in R = 50 Å. But 20 % of the donor could not transfer its energy to donor due to incomplete labeling efficiency (Lakowicz., 1999). So the actual distance can be calculated using equation 3 with the correction factor (Li et al., 2005),

$$E_{FRET} = 0.5/0.8$$
$$E_{FRET} = 0.625$$

Now substituting all the values in equation,

$$R = 50 \ [(1-0.625)/0.625)]^{1/6}$$
$$R = 50 \ [0.6]^{1/6}$$
$$R = 50 * 0.918$$
$$R = 45.9 \ \text{Å}$$

In the case of the tryptophan-IAEDANS pair (R_o = 22 Å), a small error in labeling ratio would give distance values that are within acceptable error range even without a correction factor. If the measured efficiencies are 0.7, 0.5 and 0.3 with 100 % labeling, then

E = 0.7	E = 0.5	E = 0.3
$R = 22 [(1-0.7)/0.7)]^{1/6}$	$R = 22 [(1-0.5)/0.5)]^{1/6}$	$R = 22 [(1-0.3)/0.3)]^{1/6}$
$R = 22 [0.428]^{1/6}$	$R = 22 [0.5]^{1/6}$	$R = 22 [2.33]^{1/6}$
$R = 22 * 0.87$	$R = 22 * 1$	$R = 22 * 1.15$
$R = 19.1$ Å	$R = 22.0$ Å	$R = 25.33$ Å

If the measured efficiencies are 0.7, 0.5 and 0.3 with only 80 % labeling efficiency and correcting the measured efficiencies for fractional labeling ratio, then

E = 0.7	E = 0.5	E = 0.3
$R = 22 [(1-0.875)/0.875)]^{1/6}$	$R = 22 [(1-0.625)/0.625)]^{1/6}$	$R = 22 [(1-0.375)/0.375)]^{1/6}$
$R = 22 [0.142]^{1/6}$	$R = 22 [0.6]^{1/6}$	$R = 22 [2.33]^{1/6}$
$R = 22 * 0.72$	$R = 22 * 0.92$	$R = 22 * 1.09$
$R = 15.89$ Å	$R = 20.2$ Å	$R = 23.95$ Å

Thus, the distances calculated with or without correction for the fractional labeling ratio are within a difference of 10-15 %.

Full length tau does not contain a single tryptophan residue but has five tyrosine residues (Y18, Y29, Y197, Y310 and Y394, numbered according to htau40) and two naturally occurring cysteines (C291 and C322). This feature of tau enables conservative exchange of tyrosine to tryptophan (intrinsic fluorophore with quantum yield ~ 0.3) and chemical modification of cysteine to link to a fluorophore without much perturbation of structure. A series of tau constructs with a single tryptophan (acts as donor) and a single cysteine (acts as acceptor) was created for FRET analysis. The cysteine residue of tau mutant protein was labeled with IAEDANS (quantum yield ~ 0.8), a sulhydryl reactive dye obtained from Molecular Probes, Karlsruhe. Typically, tryptophan excited at 290 nm transfers its emission intensity (~ 350 nm) to IAEDANS which emits at longer wavelength (~ 490 nm) as the excitation spectrum of IAEDANS overlaps with the emission spectrum of tryptophan. The energy transfer is calculated according to the equation 3 and subsequently the distance between tryptophan and IAEDANS is calculated from equation 2 given the Förster radius (R_o) of 22 Å for the Tryptophan-IAEDANS pair (Matsumoto and Hammes, 1975; Wu and Brand, 1994).

2.2.2.5.1 Labeling of proteins with IAEDANS

Tau mutant protein in PBS buffer (~100 μM) was incubated with a 10 molar excess of DTT for 10 minutes at 37°C. The protein was subjected to size exclusion chromatography (Fast Desalting column, Amersham Bioscience, Freiburg) to remove DTT and the eluted protein was immediately supplemented with a ~ 20 molar excess of IAEDANS (dissolved in DMF). The labeling reaction was allowed to proceed overnight at 4°C. The reaction was dialyzed against

PBS and residual IAEDANS was then removed by size exclusion chromatography (Fast Desalting column, Amersham Bioscience, Freiburg). The concentration of protein was determined by absorption at 280 nm using the molar extinction coefficient ϵ_{tau} = 10800 to 12100 $M^{-1}cm^{-1}$ depending on the different contents of aromatic residues in the isoforms and mutants of tau that were derived using the ProtParam tool (Gasteiger E. et al., 2005). The amount of bound IAEDANS was determined by the absorption at 336 nm using the molar extinction coefficient $\epsilon_{IAEDANS}$ = 6100 $M^{-1}cm^{-1}$ (Hudson and Weber, 1973). The protein concentration was corrected for the contribution of the IAEDANS at 280 nm and the calculated stoichiometry was usually 0.8-0.9.

2.2.2.5.2 Fluorescence measurements

All the steady-state fluorescence measurements were performed in a Spex Fluoromax spectrophotometer (Polytec, Waldbronn) using 3 x 3 mm quartz microcuvettes from Hellma (Mühlheim, Germany) with 20 μl sample volume at room temperature. The protein sample was excited at 290 nm to avoid the contribution of tyrosine emission and in all cases, the experimental parameters were as follows: scan range = 300-550 nm, excitation slit width = 4 nm, emission slit width = 6 nm, integration time = 0.25 s and photomultiplier voltage = 950 V.

2.2.2.6 Polymerization of tau *in vitro*
2.2.2.6.1 PHF assembly

Aggregation of tau protein was started by incubating soluble tau protein, typically in the concentration range of 50-500 μM and in the volume range of 20-100 μl, in the presence of the anionic cofactor heparin (MW ~ 3000 or ~ 6000 Da, Sigma, Munich) at 37°C with the protein to heparin ratio 4:1. For experiments of aggregation optimizing conditions, tau protein was taken either in various buffers and pH (of 20 mM concentration) or in a buffer (of 20 mM concentration) with incubation at various temperatures or in a buffer (of 20 mM concentration) containing increasing salt concentration. Aggregation reactions of tau constructs with 4 repeats were supplemented with 1 mM DTT and the typical incubation was ~ 3 days for tau constructs and ~ 5 days for full-length tau isoforms. The formation of aggregates was assayed by ThS fluorescence and the morphology of filaments was analyzed electron microscopy.

The pelleting of PHFs were done at 61 krpm (= 160000g) for 45 minutes at 4°C (TLA 100.3 rotor, TL-100 centrifuge, Beckmann). When needed, PHFs were resuspended with a buffer of choice and pelleted again by centrifugation to minimize the concentration of unpolymerized protein.

2.2.2.6.2 Thioflavin S (ThS) assay

PHF formation was monitored by ThS fluorescence assay (Friedhoff et al., 1998). It is well established that the binding and subsequent increase in ThS fluorescence is specific for the cross-β-structure that is typical of amyloid fibers.

5 μl of PHF reaction mixture was mixed with 45 μl of 50 mM NH_4Ac containing 20 μM ThS and transferred into a 384-well plate (black microtiter 384 plate round well, ThermoLabsystems, Dreieich). After 15-30 minutes incubation to allow ThS to bind, fluorescence intensity was measured in a Tecan instrument (Ascent, Labsystems, Frankfurt). The experimental parameters were as follows: excitation wavelength = 440 nm, emission wavelength = 521 nm, excitation slit width = 7.5 nm, emission slit width = 7.5 nm and the temperature = 25°C. Background fluorescence from ThS alone was subtracted when needed and the measurements were carried out in triplicates.

2.2.2.6.3 ANS fluorescence measurement

Aggregation of tau was also monitored by ANS fluorescence. The increase of ANS fluorescence is observed when it binds to solvent exposed hydrophobic patches (Slavik, 1982).

5 μl of PHF reaction mixture was mixed with 45 μl of 50 mM sodium phosphate pH 7.0 containing 100 μM ANS and transferred into a 384-well plate (black microtiter 384 plate round well, ThermoLabsystems, Dreieich). The measurements were carried out at 25°C in a TECAN spectrofluorimeter (Ascent, Labsystems, Frankfurt) using an excitation wavelength of 390 nm, an emission wavelength of 475 nm and spectral bandwidths of 7.5 and 7.5 nm for emission and excitation respectively. ANS fluorescence measurements in the presence of GdnHCl were carried out in the same conditions. The effect of GdnHCl on ANS fluorescence was eventually subtracted.

2.2.2.6.4 Transmission electron microscopy

Electron microscopy is an imaging technique in which a beam of electrons passes through a specimen and the transmitted beam is visualized on a photographic film or CCD camera. To enhance the structural details of a sample, staining with heavy metals such as osmium, lead or uranium can be used because the heavy atoms, having dense nuclei, scatter the electrons out of the optical path and hence areas where electrons are scattered appear dark on the screen or on a positive image.

The protein samples were diluted to 1-10 μM and placed on 600 mesh carbon coated copper grids for 45 seconds, washed twice with H_2O and negatively stained with 2 % uranyl acetate for 45 seconds. The specimens were examined with a Philips CM12 electron microscope at 100 kV.

Images of PHFs were collected at magnification of 45000 either in the electron image films (SO-163, Eastman Kodak Co., 8.3 x 10.2 cm) and then developed, fixed and dried or captured with CCD camera (TVIPS, Gauting, Germany) using EMMENU 4 software.

2.2.2.7 Circular dichroism spectroscopy

Circular dichroism (CD) spectroscopy measures differences in the absorption of left-handed polarized light versus right-handed polarized light which arise due to structural asymmetry. A typical CD spectrum contains both positive and negative signals. Information about the secondary structure of a protein can be obtained from the Far-UV spectral region (190-250 nm). At these wavelengths, the chromophore is the peptide bond and the signal arises depending on whether it is located in a regular, folded environment. Secondary structures of protein, α-helix, β-sheet, turn and random coil structures, each give rise to spectra with characteristic shape and magnitude (Fig. 2.5). The CD spectrum for a protein is in turn an average of the entire secondary structure populated in the protein.
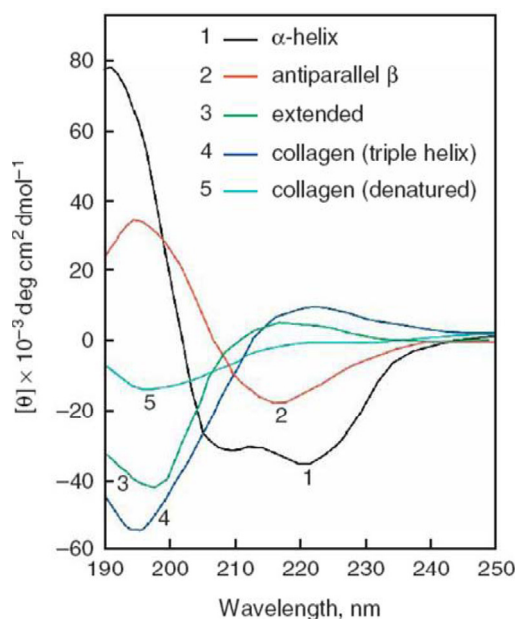
Figure 2.5: Reference CD spectra. Representative CD spectra of polypeptides and proteins are shown. (1) CD spectra of poly-L-lysine in the α-helical conformation (black), (2) in the antiparallel β-sheet (red) at pH 11.1, (3) extended conformation at pH 5.7 (green), (4) collagen in its native triple-helical (blue) and (5) collagen in denatured forms (cyan). Note that the extended conformation of poly-L-lysine is similar to the conformation of poly-L-proline II helix Figure Picture reproduced from Greenfield, 2006.

All CD measurements were carried out with a Jasco J-810 CD spectrometer (Jasco, Groß-Umstadt) in a cuvette with a path length of 0.1 and 0.01 cm. The spectra were recorded at 20°C between 190-260 nm at a scanning speed of 100 nm/min with a bandwidth of 0.1 nm and a response time of 4 s. In each experiment, three spectra were summed and averaged.

3 Results

3.1 The structure of soluble tau under varying conditions

Tau exhibits mostly random coil in solution, but aggregates to PHFs which has partial β-structure. It is classified to be a natively unfolded protein. Full length tau-htau40 has low hydrophobicity (mean hydrophobicity = 0.428) but a net charge of only +2 (mean net charge = 0.005) at physiological pH. It was reported for some natively unfolded proteins that the minimization of the net charge by manipulating the pH of the solvent or incubation at higher temperatures can induce partial folding by permitting hydrophobicity-driven collapse (Uversky et al., 2001). To understand more of the parameters defining the unfolded nature of soluble tau isoform and constructs were subjected to structure inducing environments and subsequently monitored for any structural transition.

Full length isoform htau40wt and tau constructs-K19, K18 and K18ΔK280 which comprise either three or four repeats (Fig. 3.1A) were used for analyzing the structural properties in the soluble state by CD under various pH, elevated temperatures, high salt and in structure affecting solvents. The net charge of tau isoforms and constructs with respect to pH was predicted by the "EMBOSS iep" program (Rice et al., 2000). The isoelectric points (pI) for K19, K18 and htau40wt were found to be 10.49 and 10.46 and 8.46, respectively (Fig. 3.1B).
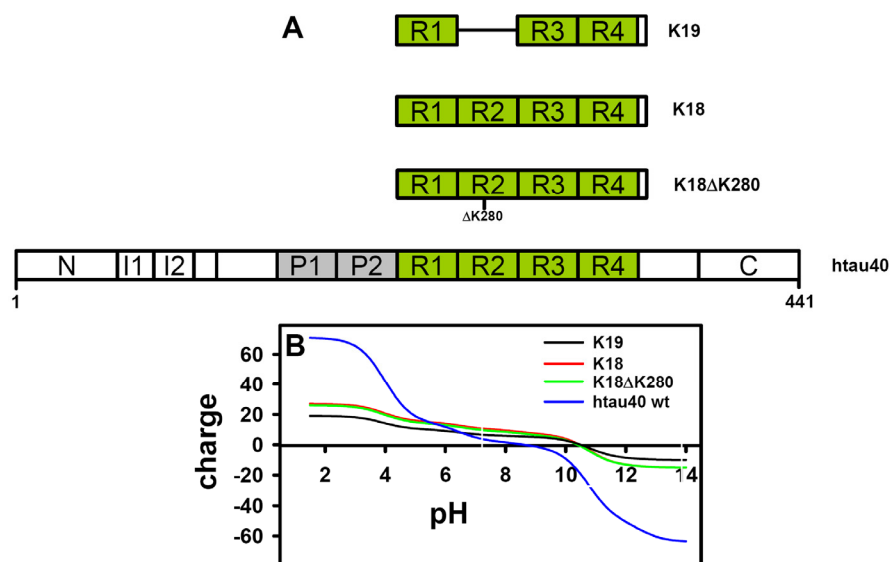
Figure 3.1: Tau constructs and pH dependent net charge. (A) Full length isoform htau40wt and tau constructs-K19, K18 and K18ΔK280 are shown. (B) The change of net charge of tau constructs and isoform with respect to pH was predicted by the EMBOSS IEP program (Rice et al., 2000).

3.1.1 Influence of pH on the structure of soluble tau

To test whether the minimization of net charge might induce partial folding of tau, soluble tau incubated at different pH was analyzed by circular dichroism (CD) spectroscopy. The CD spectrum of K19 at pH 7.0 showed a minimum at ~ 200 nm (Fig 3.2A) indicating a mostly random coil conformation (Greenfield and Fasman, 1969). Surprisingly, the spectra of K19

remained the same when incubated at pH 2.0 and pH 12.0 indicating no structural change (Fig 3.2A). For better interpretation, the ratio between the negative intensity at 200 nm (indicative of random coil) and 217 nm (marker for β-structure) of spectra obtained at other pH values was plotted against pH. It was found that the structure of K19 did not change significantly at any pH though charge neutralization occurs at pH > 10.0 (Fig 3.2B). A similar lack of change of the 200/217 nm ratio at varying pH was also observed for other tau constructs such as K18 and K18ΔK280 (Fig. 3.2B). This indicates that the second repeat did not alter the conformation. For the full length isoform htau40wt, the 200/217 nm ratio was also nearly unchanged reflecting that full length tau as well as tau constructs did not undergo any significant structural transition upon pH variation (Fig. 3.2B). We conclude that the failure of tau to become folded even when the charge is neutralised can be attributed to its very low hydrophobic content.
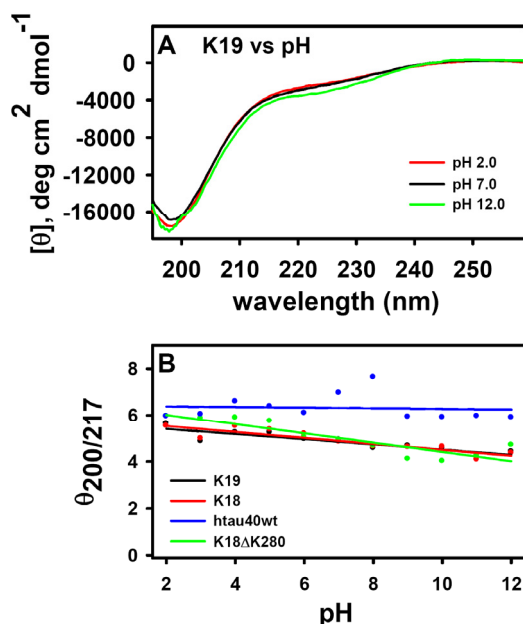
Figure 3.2: CD spectra of tau upon as a function of pH. (A) Representative CD spectra of K19 at pH 2.0 (black), pH 7.0 (red) and pH12.0 (green) are shown. (B) 200/217 nm ratio of CD spectra obtained at each pH for K19 (black), K18 (red), htau40wt (blue) and K18ΔK280 (green) are plotted against pH. Note that spectra do not indicate any structural change in tau with change of pH. The measurements were obtained at 20°C with a 0.1 cm cuvette. Parameters were: scanning speed 100 nm/min; band width 0.1 nm; response time 4 s.

3.1.2 Influence of elevated temperature on the tau structure

Elevated temperature is known to increase hydrophobic interactions due to thermodynamic properties associated with changes in water structure (Baldwin, 1986; Lesk, 2003). To test if elevated temperature could cause a structural transition of soluble tau, the secondary structure of soluble tau was determined by CD at various temperatures (from 5-90°C). Upon stepwise elevation of temperature, the CD spectra of K19 underwent a shift with a decrease of the intensity at 200 nm and an increase of the intensity at 217 nm (Fig. 3.3A) indicating a structural transition from a random coil to β-structure. This may be due to strengthening of hydrophobic interactions as shown for other natively unfolded proteins (Uversky, 2002a). For a better

interpretation, the 200/217 nm ratio was plotted as a function of temperature for K19 (Fig. 3.3B). The fitting of this 200/217 nm ratio for a simple two-state model did not point to any cooperative folding. The same behavior was observed for K18, K18ΔK280 and htau40wt (Fig. 3.3B). The absence of cooperative folding of tau points to the insufficient amount of the hydrophobic residues to drive tau into a well-ordered structure upon temperature elevation. Moreover, a red shift of only ~ 2 nm from ~ 196 nm was observed upon temperature elevation. This suggests that the transition observed with temperature rise is minimal, because any transition from random coil to α-helix or β-structure would result in a large red shift (from ~200 nm to ~ 217 nm).
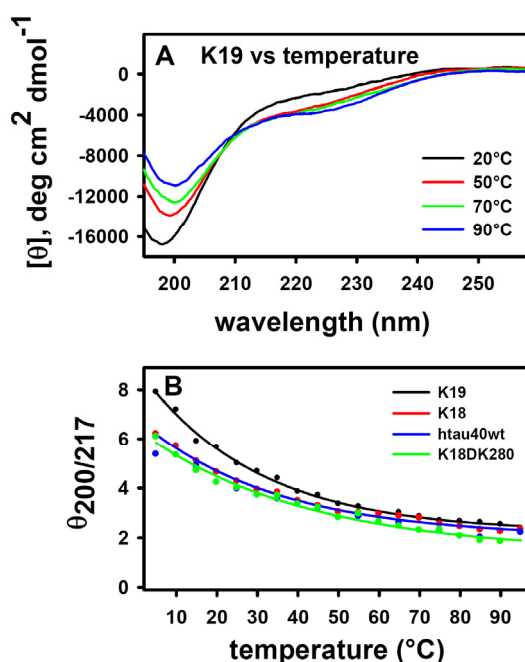
Figure 3.3: CD spectra of soluble tau in elevated temperature. (A) CD spectra of K19 at different temperatures: 20°C (black), 50°C (red), 70°C (green) and 90°C (blue). (B): 200/217 ratio of K19 (black), K18 (red), ht40 (blue) and K18ΔK280 (green) at various temperatures. Note that the spectral change indicate tau adopts β-structure, but the transition is not cooperative fashion pointing to lack of sufficient hydrophobic residues. The conditions for the measurements were as described in Fig 3.1.

3.1.3 Influence of high salt and organic solvent on the structure of soluble tau

Salt ions are thought to associate with oppositely charged side chains of amino acids in the protein. The increasing salt concentration can shield the charged residues allowing the protein to fold corresponding to its hydrophobic content without charge repulsion. To check if any changes take place in the structure of tau upon increased salt concentrations, tau constructs were investigated by CD at various salt concentrations (0-750 mM Na_2SO_4). There was no indication of structural changes (Fig. 3.4A and 3.4B). Hence, the inability of salt to induce any ordered structure speaks for the low hydrophobic content of tau as primary reason for the unfolded nature.

In general, the effect of alcohols such as TFE, HFIP, ethanol, methanol, isopropanol is considered to arise from the low polarity of the solvent (Thomas and Dill, 1993; Liu and Bolen, 1995). As an example, TFE interacts with carbonyl oxygen atoms of the protein backbone and

hydrophobic side chains and thus disrupts the stability of hydrophobic core by minimizing water-protein interactions. This in turn favors the formation of intramolecular hydrogen bonding leading to the formation of secondary structure, in particular α-helix (Shiraki et al., 1995; Povey et al., 2007). The structure of tau was investigated by CD at various concentrations of isopropanol (0-25 %). A slight effect on the structure of tau was observed in the presence of isopropanol. It seemed to induce α-helix to a small extent in full-length tau and the repeat domain tau constructs (Fig. 3.4C and 3.4D). The transition of the mutant K18ΔK280 was relatively more pronounced in 25% isopropanol than other tau constructs. Note that the formation of α-helix for the region ^{315}LSKVTSKC^{322} in R3 peptide was reported in the presence of TFE (Minoura et al., 2002; Minoura et al., 2004). In addition, the aggregation of tau in the presence of moderate concentrations of TFE was shown (Hiraoka et al., 2004; Kunjithapatham et al., 2005; Minoura et al., 2005; Mizushima et al., 2006). The presence of α-helix in the repeats region (^{253}Leu-Gly^{261}, ^{315}Leu-Gly^{323}, and ^{346}Leu-Gly^{355}) was also reported in presence of SDS micelles (Barre and Eliezer, 2006).
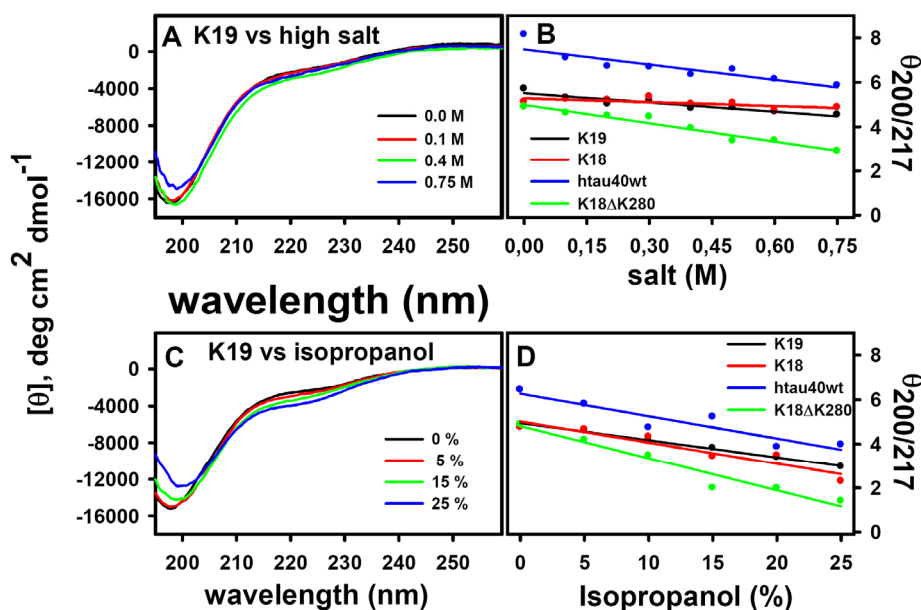
Figure 3.4: CD spectra of soluble tau in high salt and alcohol. (A) CD spectra of K19 at different salt concentration: 0 mM (black), 100 mM (red), 400 mM (green) and 750 mM (blue). (B) 200/217 ratio of K19 (black), K18 (red), ht40 (blue) and K18ΔK280 (green) at various salt concentrations. (C) CD spectra of K19 at different isopropanol concentration: 0 % (black), 5 % (red), 15 % (green) and 25 % (blue). (D) 200/217 ratio of K19 (black), K18 (red), ht40 (blue) and K18ΔK280 (green) at various isopropanol concentrations. Tau secondary structure is not altered by high salt concentration but alcohol induces a slight shift from random coil to α-helix. The conditions for the measurements were as described in Fig 3.1.

3.2 FRET study of conformation of tau in solution

3.2.1 Proteins and mutations

Tau behaves as a natively unfolded protein over wide range of conditions, as evidenced from the above experiments where no significant amount of secondary structure was detected by CD. However, even unfolded proteins are likely to contain residual secondary structure elements (Fitzkee and Rose, 2004). Thus there might be some global conformation defined by interactions between the different domains of tau that would not be detectable by the usual spectroscopic methods such as CD and FTIR.

To examine such interactions, Fluorescence resonance energy transfer (FRET) analysis between different domains of tau was performed. In FRET, if donor and acceptor are within a certain distance, the emission energy of donor is transferred by resonance to the acceptor giving rise to quenching of donor emission and appearance of acceptor emission. The efficiency of the energy transfer which depends on the distance between donor and acceptor is given in equation 2. The efficiency of transfer (E_{FRET}) is measured using the relative fluorescence intensity of the donor, in the absence of (D) and presence of acceptor (D_A) and is given in equation 3.
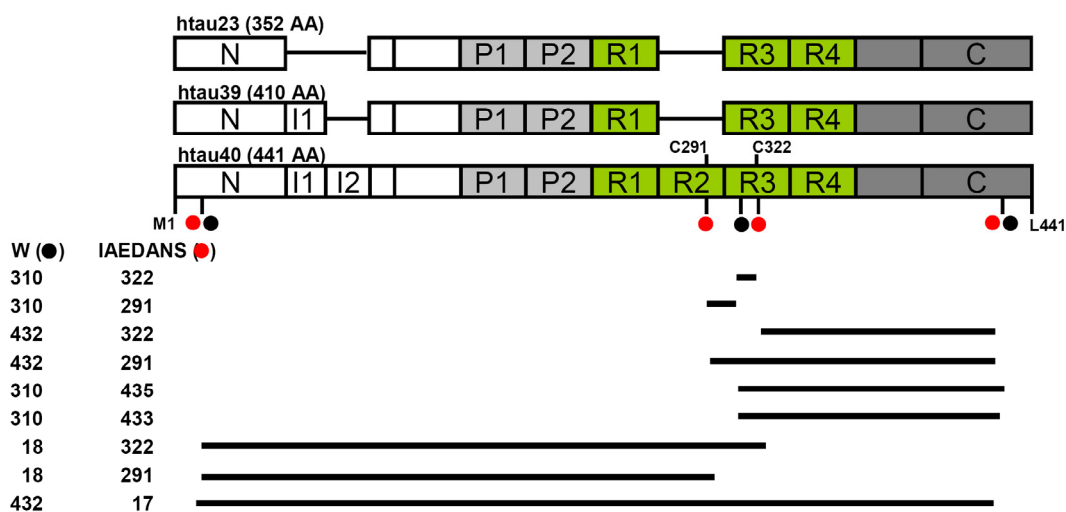
Figure 3.5: Proteins and mutations. A set of single tryptophan/cysteine tau mutants were created on the basis of three different isoforms: htau40, htau39, and htau23. The positions of the tryptophan and IAEDANS (labeled to cysteine) are indicated by black and red circles respectively. The FRET pairs within each mutant are shown by black solid lines.

A series of recombinant tau mutants containing a single tryptophan (donor) and a single cysteine labeled with IAEDANS (acceptor) was created and thus allowed FRET analysis between different domains of tau (W-IAEDANS pairs, Fig. 3.5). The mutants were created based mostly on htau40 or htau39 and htau23. As tau contains no intrinsic tryptophan, conservative exchanges at hydrophobic amino acids for inserting tryptophan (Y18W, Y310W and V432W) and at polar amino acids for cysteine mutation (T17C, S433C and S435C) were made with the aim of minimizing perturbations of the protein structure. In some mutants, the naturally occurring

cysteines in tau (either C291 in R2 or C322 in R3, the other one being exchanged to Ala) were used for IAEDANS labeling.

Based on the position of tryptophan and cysteine, FRET mutants were grouped into four categories:

i.   R-R$_{FRET}$ mutants used for measurement of energy transfer within the repeats of tau include htau40-310$_W$322$_{DANS}$, htau40-310$_W$291$_{DANS}$, and htau39-310$_W$322$_{DANS}$.

ii. R-C$_{FRET}$ mutants used for measurement of energy transfer between the repeats and the C-terminus of tau include htau40-432$_W$322$_{DANS}$, htau40-432$_W$291$_{DANS}$, htau40-310$_W$433$_{DANS}$, htau40-310$_W$435$_{DANS}$, htau39-432$_W$322$_{DANS}$ and htau23-432$_W$322$_{DANS}$.

iii. R-N$_{FRET}$ mutants used for measurement of energy transfer between the repeats and the N-terminus of tau include htau40-18$_W$322$_{DANS}$, htau40-18$_W$291$_{DANS}$, htau40-310$_W$17$_{DANS}$, htau39-18$_W$322$_{DANS}$ and htau23-18$_W$322$_{DANS}$.

iv. N-C$_{FRET}$ mutants used for measurement of energy transfer between N-terminus and C-terminus of tau include htau40-432$_W$17$_{DANS}$ and htau23-432$_W$17$_{DANS}$.

3.2.2 CD spectroscopy of FRET mutants of tau

To confirm that neither the mutations nor the labeling with IAEDANS caused a change in the overall structure of tau, all mutants were analyzed by CD spectroscopy.
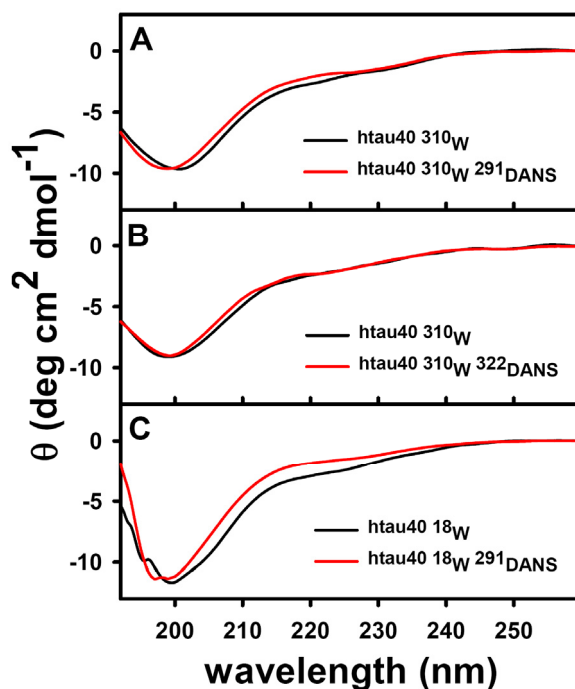
Figure 3.6: **Circular dichroism spectroscopy of unlabeled and labeled proteins.** The ellipticities of unlabeled and labeled FRET mutants measured by CD are shown (A-C). The unlabeled protein is represented by the black line, the labeled protein by the red line. All spectra exhibit a minimum at ~ 200 nm similar to htau40wt, indicating a mostly random coil structure.

The CD spectra of all the unlabeled mutants exhibited a minimum at ~ 200 nm (Fig. 3.6) which indicates a mostly random coil structure and was similar to the spectra obtained from wild type protein (Barghorn et al., 2000). The same was true for the labeled proteins. Thus neither the insertion of tryptophan nor the labeling with IAEDANS had an impact on the overall secondary structure of the protein as seen by CD (Fig. 3.6). However, it should be noted that CD is more sensitive to ordered structures (α-helix, β-sheet) and does not report on long range interactions present in protein.

3.2.3 Microtubule assembly ability of FRET mutants of tau

To test the effect of mutations and labeling on the physiological function of tau, microtubule assembly experiments in the presence of tau mutants were performed. Tubulin below the critical concentration (~ 30 μM) remained unpolymerized, but in the presence of htau40wt (5 μM) it polymerized rapidly. Unlabeled and labeled FRET mutant proteins promoted microtubule assembly but with slightly varying efficiencies (Fig. 3.7). These results confirmed that tau mutants retained their structural and functional properties like wild type tau, in good agreement with earlier studies (Li et al., 2002; Makrides et al., 2004).
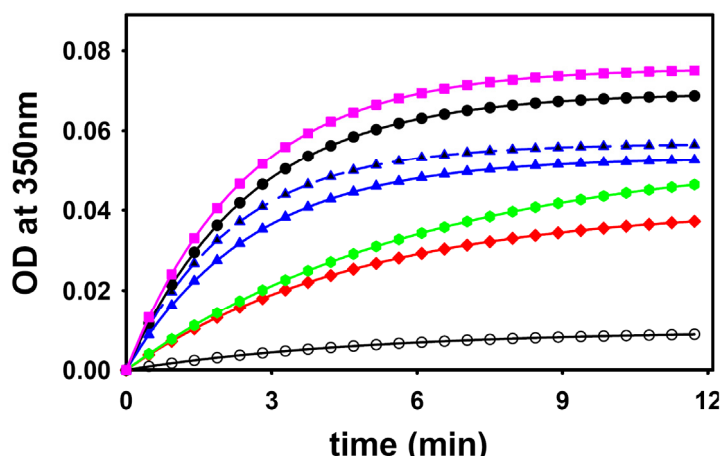
Figure 3.7: Microtubule assembly by unlabeled and labeled FRET mutants. The polymerization of tubulin in the absence of tau (empty black circles) showed almost no increase in the absorbance whereas it increased rapidly as the microtubules polymerized in the presence of htau40wt (filled black circles). Unlabeled and labeled mutants showed a similar effect on microtubule assembly and comparable to that of htau40wt: (htau40-310$_W$ 433$_C$ = blue triangles up, htau40-310$_W$ 433$_{DANS}$ = blue triangles up, htau40-310$_W$322$_{DANS}$ = green hexagons, htau40-18$_W$322$_{DANS}$ = red diamonds and htau40-432$_W$17$_{DANS}$ = pink squares).

3.2.4 FRET analysis of R-R$_{FRET}$ mutants

To measure the distance within the repeat domain, tau mutants of htau40 and htau39 with FRET pairs of tryptophan at 310 and IAEDANS either labeled at C291 or C322 were used. When the unlabeled mutant with single tryptophan at position 310 and single cysteine at position 322 (referred as htau40-310$_W$322$_C$) was excited at 290 nm, it exhibited the typical tryptophan fluorescence with an emission maximum at 352 nm (Fig. 3.8A) suggesting that residue 310 is almost completely solvent exposed (Eftink, 1991), in agreement with our earlier study (Li et al.,

2002). After IAEDANS labeling at C322 (referred as htau40-310$_W$322$_{DANS}$), excitation at 290 nm resulted in an additional emission peak at 490 nm (Fig. 3.8A) and concomitantly a decrease of tryptophan emission fluorescence, although the protein concentration (2 µM) was the same in both the cases. The transfer efficiency (E) of this mutant was calculated to be 0.67 using equation 3 and the donor-acceptor distance (R) to be 19.5 Å using equation 2 described in the Methods (Section 2.2.2.5), assuming a Förster radius for the FRET pair of tryptophan and IAEDANS of 22 Å (Matsumoto and Hammes, 1975; Wu and Brand, 1994).
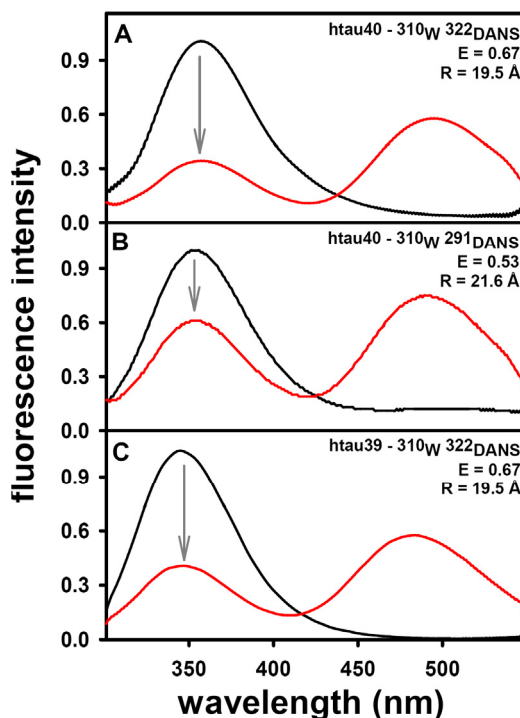
Figure 3.8: FRET analysis within the repeat domain. The fluorescence emission spectra for the following proteins are shown (A) htau40-310$_W$322$_C$ (unlabeled, black line) and htau40-310$_W$322$_{DANS}$ (labeled, red line), (B) htau40-310$_W$291$_C$ (black) and htau40-310$_W$291$_{DANS}$ (red) and (C) htau39-310$_W$322c (black) and htau39-310$_W$322$_{DANS}$ (red). The protein (2 µM) was excited at 290 nm and the emission was recorded from 300-550 nm. The emission peak around 350 nm stems from tryptophan and the peak around 490 nm is due to IAEDANS emission. The strong decrease in tryptophan emission due to FRET is indicated by arrows.

In the case of htau40-310$_W$291$_{DANS}$, FRET was less pronounced (E = 0.53, Fig. 3.8B) compared to htau40-310$_W$322$_{DANS}$ that resulted in a distance of 21.6 Å. The mutant htau39-310$_W$322$_{DANS}$, based on the three-repeat isoform htau39, exhibited the same FRET efficiency (E = 0.67, Fig. 3.8C) as that of the mutant based on a four-repeat isoform-htau40-310$_W$322$_{DANS}$. These results show that a strong or medium FRET can be measured between W310 near the beginning of the third repeat and C322 or C291 near the middle of repeats R2 and R3, which holds true for both three and four repeat tau isoforms.

These observed distances were compared to the expectations based on a Gaussian coil model of a polypeptide. The mean end to end distance 'L$_m$' within a Gaussian coil of 'N' amino acids can be estimated as L$_m$ = L$_0$ x √N, where the prefactor 'L$_0$' (~ 8.3 Å) accounts for the stiffness of the molecule for the case of unfolded proteins (Fitzkee and Rose, 2004). For N = 12 and 19 the mean

distance in a random coil structure was calculated to be 28 Å and 36 Å respectively. Thus, the observed smaller FRET-distances of ~ 20 Å illustrates that the assumption of a pure random coil for tau is not applicable and a residual structure is adopted by the repeat domains, at least in the second and third repeat.

3.2.5 FRET analysis of R-C$_{FRET}$ mutants

The distance between the repeat region and the C-terminal tail was analyzed by FRET using the mutants carrying tryptophan at position 310 and IAEDANS at position 435 or 433 in the htau40 isoform as well as using a "dye swap" mutant (inverted position of donor and acceptor) with tryptophan at position 432 and IAEDANS at position 291 or 322 in htau40, htau39 and htau23 isoforms. The FRET analysis of htau40-432$_W$322$_{DANS}$ (Fig. 3.9A) and htau40-432$_W$291$_{DANS}$ (Fig. 3.9B) yielded efficiencies of 0.29 and 0.37 corresponding to distances of 25.6 Å and 24 Å respectively. These distances are surprisingly shorter than theoretical distances for a random coil model which are 99.3 Å and 87.7 Å between the pairs 291-432 and 322-432 respectively.
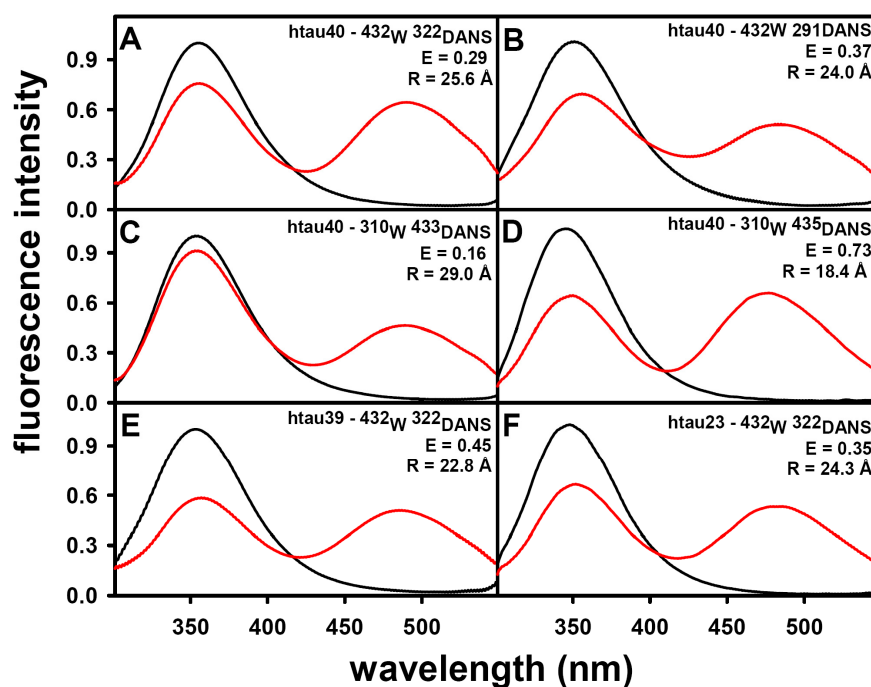
Figure 3.9: FRET between the repeat domain and the C-terminal tail. The fluorescence emission spectra for: (A) htau40-432$_W$322$_{DANS}$, (B) htau40-432$_W$291$_{DANS}$, (C) htau40-310$_W$435$_{DANS}$, (D) htau40-310$_W$433$_{DANS}$, (E) htau39-432$_W$322$_{DANS}$ and (F) htau23-432$_W$322$_{DANS}$. The experimental conditions were the same as in Fig. 3.8.

The dye-swapped FRET pair in the mutant htau40-310$_W$435$_{DANS}$ (Fig. 3.9C) exhibited an even higher efficiency (E = 0.73) and a resulting a distance of only 18.4 Å. In contrast, another mutant with the IAEDANS labeled at residue 433, only two residues upstream of the previous position (htau40-310$_W$433$_{DANS}$, Fig. 3.9D) yielded a very low efficiency of 0.16 corresponding to a distance of 29 Å. This remarkable difference in the FRET efficiency within two residues (from the 435-310 pair to the 433-310 pair) cannot be explained simply by distance considerations

alone. A more likely interpretation is a conformational change in the C-terminal tail which may fold over the repeat domain in one labeled mutant but not in the other. It should be noted that the C-terminal tail (residues 422-441) may adopt an α-helical structure and it is likely that positioning IAEDANS at 433 might destabilize the α-helical structure.

The mutant htau39-432$_W$322$_{DANS}$ based on the isoform htau39 exhibited a similar efficiency (E = 0.45) with a calculated distance of 22.8 Å (Fig. 3.9E). Thus, the missing second repeat (upstream of the reporter W310) in htau39 does not affect FRET between the C-terminus and the third repeat. The same was observed for the mutant of three repeat tau-htau23-432$_W$322$_{DANS}$ (Fig. 3.9F), which showed an efficiency of 0.35 and a resulting distance of 24.3 Å. Therefore, the absence of the N-terminal inserts had no impact on the interaction between the C-terminal end of tau and the center of the repeat domain.

3.2.6 FRET analysis of R-N$_{FRET}$ mutants

The interaction between the repeat region and the N-terminal end of tau was analyzed with mutants of htau40, htau39 and htau23 isoforms containing tryptophan at position 18 and IAEDANS at position 291 or 322 and also htau40 mutant with tryptophan at position 310 and IAEDANS at position17. In all cases the FRET efficiency was low compared to other mutants used (Fig. 3.10A-E). For htau40-18$_W$322$_{DANS}$ and htau40-18$_W$291$_{DANS}$ the observed FRET efficiencies were 0.14 and 0.08 resulting in distances of 30.1 Å and 33.5 Å respectively (Fig. 3.10A, B).

Similarly, for the dye-swapped mutant htau40-310$_W$17$_{DANS}$, the efficiency was 0.19 with the corresponding distance 28 Å (Fig. 3.10C). The efficiency for htau39-18$_W$322$_{DANS}$ (Fig. 3.10D) was 0.18 corresponding to distance of 28.8 Å. For the shortest isoform htau23 mutant (htau23-18$_W$322$_{DANS}$) the FRET efficiency was 0.19 resulting in R = 27.8 Å (Fig. 3.10E). Thus the FRET efficiencies between N-terminus and repeats were much lower than those between the C-terminus and repeats. In fact, the efficiencies below 0.2 were too small to give reliable distances because the efficiency depends on the 6th power of the distance (Equation 3 and Fig. 2.4).
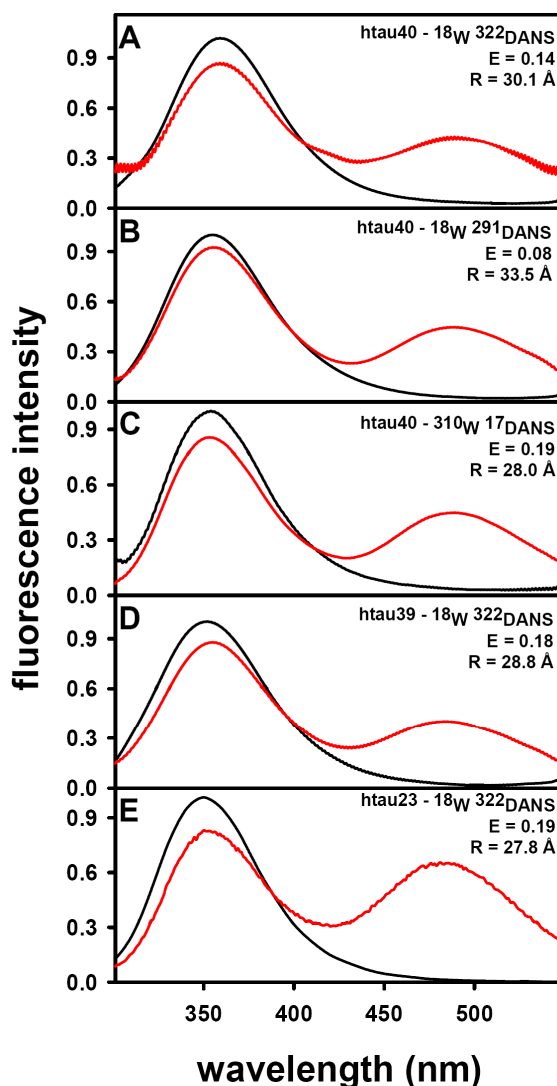
Figure 3.10: FRET between the repeat domain and the N-terminus. The fluorescence emission spectra of the FRET mutant proteins: (A) htau40-18$_W$322$_{DANS}$, (B) htau40-18$_W$291$_{DANS}$, (C) htau40-310$_W$17$_{DANS}$, (D) htau39-18$_W$322$_{DANS}$ and (E) htau23-18$_W$322$_{DANS}$. The experimental conditions were the same as in Fig. 3.8.

3.2.7 FRET analysis of N-C$_{FRET}$ mutants

To cover the largest possible distance within tau, FRET between the N- and C-terminal domains was analyzed using the mutant htau40-432$_W$17$_{DANS}$ (Fig. 3.11A). Interestingly, the observed efficiency was relatively high (0.59) resulting in a distance of 20.8 Å. This distance is much shorter than the theoretical value of 170 Å as expected for a random coil. A similar result was obtained with the mutant htau23-432$_W$17$_{DANS}$ yielding an efficiency of 0.36 and a distance of 24.2 Å (Fig. 3.11B).

Given the previous results that the N-terminus does not show FRET with the second or third repeat while the C-terminus does and the observation that the ends of tau seem to approach each other, the data suggested a complex of both termini and the repeats mediated by the C-terminus of tau (as illustrated in the discussion section; Fig. 4.3D and 4.4).
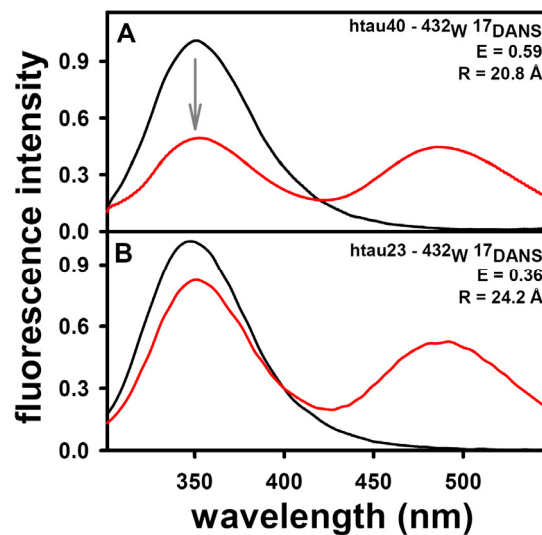
Figure 3.11: FRET between the N-terminal and the C-terminal domain. The fluorescence emission spectra are shown for (A) htau40-432$_W$17$_{DANS}$ and (B) htau23-432$_W$17$_{DANS}$. The experimental conditions were the same as in Fig. 3.8.

3.2.8 Competition experiments with FRET mutants

In all the experiments, it was important to verify that the observed FRET was due to intramolecular interactions within one tau molecule rather than to intermolecular between different molecules. This was ascertained by titration experiments (Fig. 3.12). Theoretically, if the FRET were intramolecular, the emission intensity of tryptophan and IAEDANS would increase linearly for a series of protein concentrations (example shown in Fig. 2.12A, B). By contrast, if the FRET were intermolecular, the emission intensity would not be linear (Fig. 2.12C, D).

Therefore, first a labeled FRET protein (htau40-310$_W$ 291$_{DANS}$) was measured in a series of concentrations. The emission intensity of protein increased linearly (Fig. 3.12E, F) showing that the FRET signal was intramolecular. To support further, labeled protein was titrated with an excess of htau40wt which contains only Tyr and Phe residues. The emission of IAEDANS was unaltered though a slight increase of emission around 350 nm was observed with addition htau40wt proving that energy transfer is intramolecular (Fig. 3.12G, H). To rule out the possibility that interaction observed between both termini of tau is intramolecular, labeled protein-htau40-310$_W$ 17$_{DANS}$ was added with excess of unlabeled protein-htau40-432$_W$. The result was that tryptophan emission increased with addition of unlabeled protein but not the emission of IAEDANS proving that the interaction between both termini of tau was also intramolecular. (Fig. 3.12I, J).
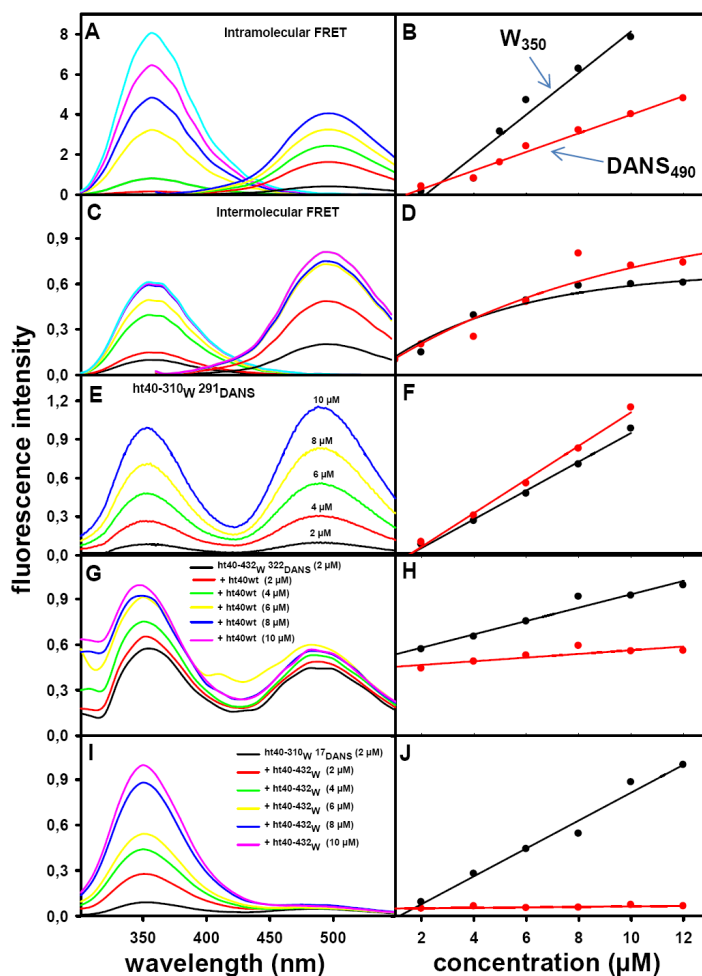
Figure 3.12: Competition experiments of FRET mutants. The fluorescence emission spectra are shown in the left panel of the above figure while the emission intensity of tryptophan and IAEDANS as function of concentration are shown in the right panel. (A) Theoretical emission of tryptophan and IAEDANS for an intramolecular interaction. Note that intensity increases linearly with concentration. (B) Emission intensity of tryptophan and IAEDANS against concentration for an assumed intramolecular situation. (C) Theoretical emission of tryptophan and IAEDANS for an intermolecular interaction. (D) Emission intensity of tryptophan and IAEDANS against concentration for an assumed intermolecular situation. (E) Emission intensity of htau40-310$_W$ 291$_{DANS}$ for a series of concentrations. (F) Emission intensity of htau40-310$_W$ 291$_{DANS}$ as function of concentration. (G) Emission intensity of htau40-432$_W$ 322$_{DANS}$ after addition of a series of concentrations of htau40wt. (H) Emission intensity of htau40-310$_W$ 322$_{DANS}$ + htau40wt as function of concentration. (I) Emission intensity of htau40-310$_W$ 17$_{DANS}$ after addition of a series of concentrations of htau40-432$_W$. (J) Emission intensity of htau40-310$_W$ 17$_{DANS}$ + htau40 432$_W$ as function of concentration. The experimental conditions were the same as in Fig. 3.8.

3.2.9 Electron paramagnetic resonance (EPR) spectroscopic analysis of tau mutants

If the polypeptide chain of tau were internally folded one might expect partial immobilization of residues. This question was addressed by EPR (collaboration with H. Brutlach and H. J. Steinhoff, Univ. Osnabrück). Mutants of htau40-310$_W$ with Cys at positions 17, 291, 322 and 431 were labeled with iodoacetamide spin labels (JAA6) with a six-membered nitroxide ring (TEMPO, 2,2,6,6-tetramethyl-1-piperidine-n-oxyl). The EPR spectra provide information on the local secondary and tertiary structure and on the mobility of the spin label. For example, highly mobile spin label side chains yield three sharp lines of similar height and small line widths, but the width, shape and height ratios of the absorption lines change when the motion becomes

restricted (Hubbell et al., 2000; Steinhoff, 2002). A quantitative measure of spin label dynamics is the effective reorientational correlation time (τ_R) of the nitroxide which is determined by simulated spectra. Approximate values of τ_R can be calculated from the line width of the center line, ΔB_0, and the line height ratios hi/hj of the three lines (Lund and Dalton, 1985).

The shape of the EPR spectra of htau40-17$_{JAA6}$, htau40-431$_{JAA6}$, htau40-322$_{JAA6}$ and htau40-291$_{JAA6}$ were similar (Fig. 3.13A) and were indicative of a high flexibility, similar to that observed in flexible termini, flexible loop regions or unstructured proteins (Steinhoff, 2002). This agrees well with recent observations on the mobility of residues in the third repeat (Margittai and Langen, 2004). Detailed comparison of the high field lines (Fig. 3.13B) revealed small differences between the spectra of labeled mutants, indicating that the C-terminal domain (JAA6 at residue 431) has the highest mobility, followed by the repeat (JAA6 at residues 291, 322) and the N-terminal domain (JAA6 at residues 17).
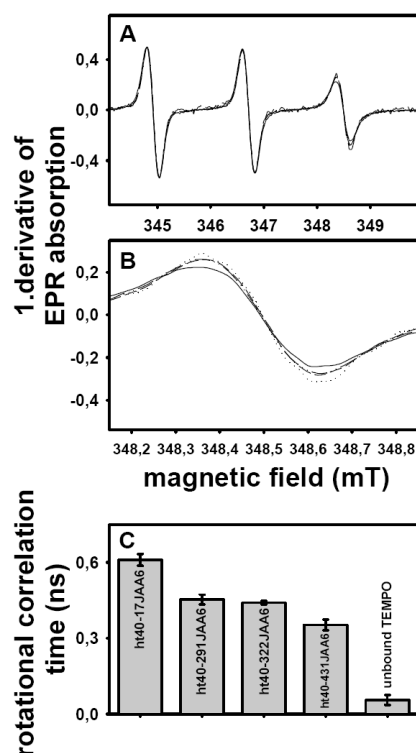
Figure 3.13: Electron paramagnetic resonance spectroscopy of tau mutants. (A) The EPR spectra are shown for htau40-17$_{JAA6}$ (solid line), htau40-431$_{JAA6}$ (long dashed line), htau40-322$_{JAA6}$ (short dashed line) and htau40-291$_{JAA6}$ (dotted line). (B) The differences in the EPR spectra of the mutant proteins are shown and a significant difference in label mobility at the C- and N-terminus are observed whereas the mobilities in the repeat region are almost identical. (C) The corresponding rotational correlation time (c) which is a measure for the immobility of the TEMPO label is shown for the protein in comparison with that of the unbound TEMPO. Error bars indicate doubled standard error.

The spin label mobility was expressed in terms of the effective rotational correlation times of the four investigated mutants and an unbound spin label for comparison (Fig 3.13C). The rotational correlation time of htau40-17$_{JAA6}$ was the highest (about 0.6 ns), whereas the mutants with the spin label within the repeat region (htau40-291$_{JAA6}$ and htau40-322$_{JAA6}$) showed rotational

correlation time of about 0.4 ns. The lowest correlation time and therefore the highest mobility was found for htau40-431$_{JAA6}$ (~0.2 ns). For comparison, the correlation time of an unbound TEMPO-label (2,2,6,6-tetramethyl-1-piperidine-n-oxyl) was about 0.05 ns, whereas that of a label immobilized inside a well folded protein is typically two orders of magnitude higher (Steinhoff, 1990)

3.2.10 Measuring the change of FRET upon denaturation

The distances between the C-terminus and the repeat domain and between the two ends of tau pointed to a residual interaction within a mostly unfolded protein. To test the stability of such interaction, FRET mutants were measured in the presence of the denaturant GdnHCl. When the unlabeled mutant-htau40-310$_W$291$_C$ was measured with increasing GdnHCl concentration, the tryptophan emission intensity was largely unaltered. However, the labeled mutant-htau40-310$_W$291$_{DANS}$ showed a gradual increase of tryptophan emission and concomitant decrease of IAEDANS emission against increasing concentrations of GdnHCl (0-5 M), consistent with a decreasing FRET efficiency (Fig. 3.14A).

Similar experiments were performed with htau40-432$_W$291$_{DANS}$ and htau40-18$_W$322$_{DANS}$ and the FRET efficiencies were plotted against GdnHCl concentration (Fig. 3.14B). In the case of htau40-310$_W$291$_{DANS}$, the FRET efficiency dropped from 0.53 to 0.32. Thus, the FRET pair undergoes a significant change, but retains a reasonable FRET efficiency that allows a reliable determination of distance which changes from 21.6 Å to 25.5 Å at 5 M GdnHCl. This distance is much lower than the theoretical distance of 36.5 Å. However, taking into account the uncertainty of theoretical distances in random coil structures it is within a acceptable range. For the distance between the repeats and the C-terminus (htau40-432$_W$291$_{DANS}$) the FRET efficiency dropped from ~ 0.3 to ~ 0.1, which made it difficult to calculate reliable distances. But in the case of htau40-18$_W$322$_{DANS}$ there was very low FRET in the soluble state (~ 0.14) and this decreases even further to 0.1. In summary, FRET within the repeats can be decreased by GdnHCl but remains measurable whereas FRET between the two termini and the repeats disappears almost completely (Jeganathan et al., 2006).
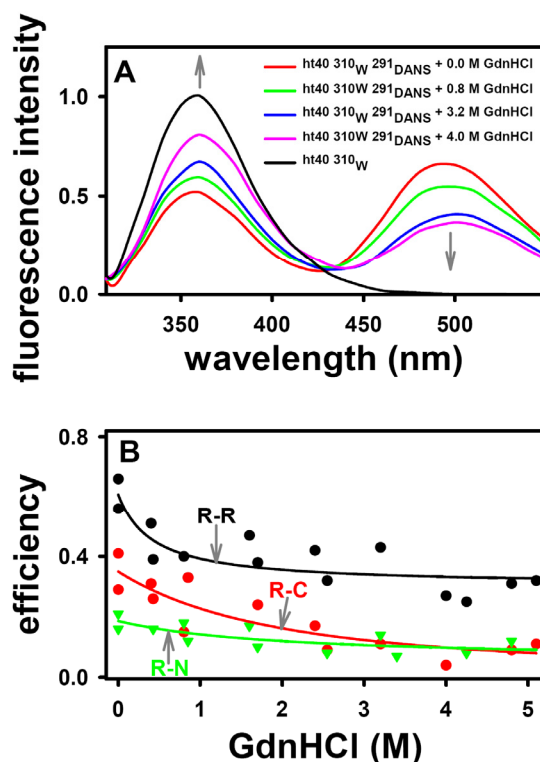
Figure 3.14: Denaturation of tau destroys folding and reduces FRET. (A) Fluorescence emission spectra of htau40-310$_W$291$_{DANS}$ with increasing concentrations of GdnHCl showed increasing tryptophan emission and decreasing IAEDANS emission (arrows). (B) Summary of efficiency of other FRET pairs against increasing GdnHCl concentration. FRET mutants were measured in the presence of increasing GdnHCl concentrations. The FRET efficiencies are plotted versus the GdnHCl concentrations (R-R: htau40-310$_W$291$_{DANS}$, R-C: htau40-432$_W$291$_{DANS}$ and R-N: htau40-18$_W$322$_{DANS}$).

3.2.11 Analysis of Stokes radius of tau by size exclusion chromatography

To analyze the effect of GdnHCl on the overall size of tau by an independent method, Stokes radii of tau isoforms and constructs were analyzed by size-exclusion chromatography in native as well as denaturing condition. All six tau isoforms and the constructs K19 and K18 comprising 3 or 4 repeats were analyzed in PBS and PBS containing 2 M GdnHCl (Fig. 3.15). Without denaturant, the correlation between Stokes radius and molecular weight corresponded to that expected for natively unfolded proteins (Tcherkasskaya and Uversky, 2003; Barghorn et al., 2004). After incubation with 2 M GdnHCl, the Stokes radii increased to values expected for fully denatured proteins (Uversky, 2002b). Thus, even though tau behaves as a natively unfolded protein in physiological buffers, the polypeptide chain could be further expanded by denaturation, consistent with the results obtained by FRET.
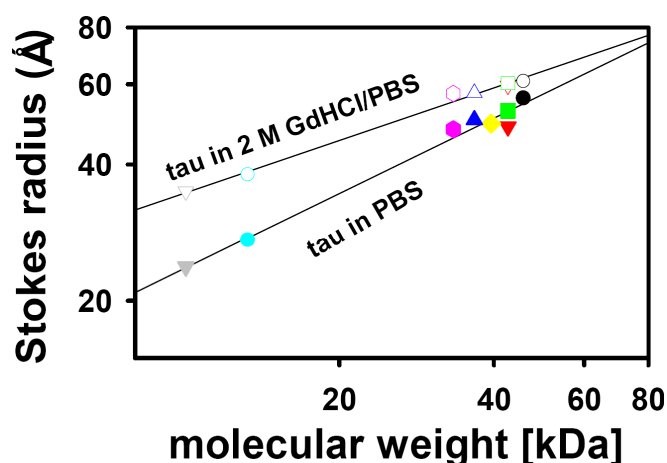
Figure 3.15: Size exclusion chromatography of tau upon denaturation. Tau isoforms and constructs comprising three or four repeats were analyzed by size exclusion chromatography in the absence (filled circles) and in the presence of 2 M GdnHCl (unfilled circles). Tau isoforms and constructs are represented as follows: htau40 (black), htau39 (red), htau39-310$_W$322$_{DANS}$ (green), htau24 (blue), htau23 (pink), K18 (cyan) and K19 (grey). Stokes radii of natively unfolded tau were calculated by reference to a standard of globular proteins and plotted versus their molecular weights. The increase in Stokes radius of tau isoforms and constructs were observed upon treatment with the denaturant.

3.2.12 Summary of FRET efficiencies

The FRET efficiencies of all mutants are summarized in Fig 3.16. The efficiencies of FRET pairs within the repeats are between 0.53 and 0.67 (Fig. 3.16, column R-R) resulting in distances of ~20 Å. FRET between the C-terminus and the repeat domain exhibited a higher variability in efficiency, for example, when the IAEDANS label was located in the C-terminal tail, showing efficiencies between 0.16 (htau40-310$_W$433$_{DANS}$) and 0.73 (htau40-310$_W$435$_{DANS}$) (Fig. 3.16, column R-C). This inconsistency points to a sequence dependence of the FRET efficiency in the C-terminal tail, which may be caused by an effect of the IAEDANS label on the local secondary structure. In the dye swap mutant containing tryptophan in the C-terminus and IAEDANS in the repeat domain, this effect was not found. Overall, the efficiencies were ~0.4, with a noticeable similarity between all isoforms, corresponding to distances of 23-25 Å between the C-terminus and the repeats. A similar pattern of FRET efficiencies between the N-terminus and the repeats was observed for the mutants based on the different isoforms (Fig. 3.16, column R-N). All the mutants showed a low FRET signal with transfer efficiencies between 0.1 htau40-18$_W$291$_{DANS}$) and 0.19 (htau40-310$_W$17$_{DANS}$) resulting in distances of 28-34 Å. The FRET efficiencies between the two ends of tau lay between 0.36-0.5 and are noticeably higher corresponding to distances of 21-24 Å (Fig. 3.16; column N-C) which is much lower than the theoretical distance of 170 Å.
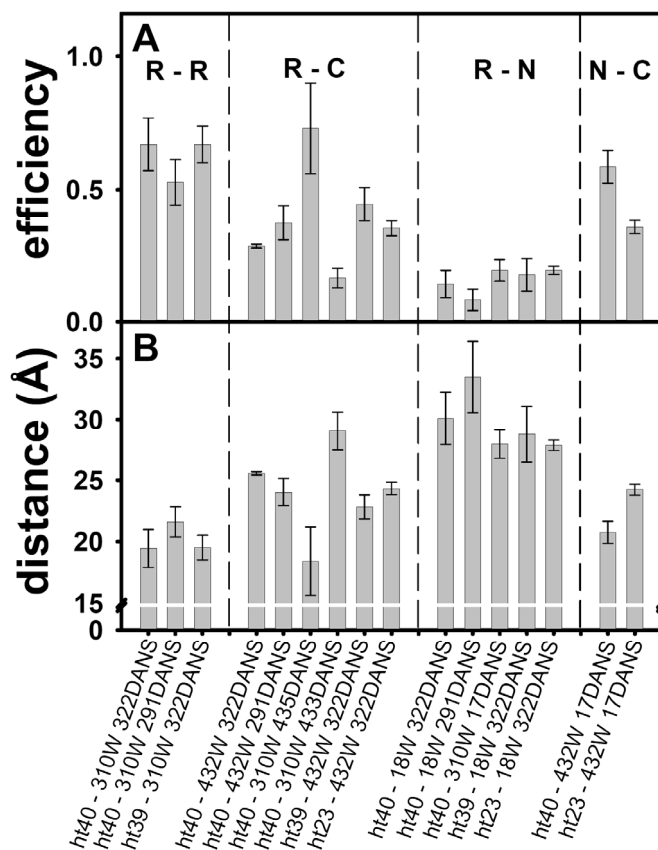
Figure 3.16: Summary of FRET efficiencies and calculated distances. (A) The FRET efficiencies of the mutants are summarized and (B) the corresponding distances are given in Å. The different mutants are indicated below the diagram and are divided into four groups: R-R (FRET within the repeat region), R-C (FRET between the repeats and the C-terminus), R-N (FRET between the N-terminus and the repeat domain) and N-C (FRET between N- and C-terminus).

3.3 Optimization of aggregation conditions for tau constructs K19 and K18

The aggregation of soluble tau into filaments *in vitro* can be enhanced by the addition of polyanions (Wilson and Binder, 1995; Goedert et al., 1996; Kampers et al., 1996; Friedhoff et al., 1998) and it is believed that polyanions favor aggregation by neutralizing the positive net charge in the repeat region of tau. Optimizing conditions for the aggregation of tau was earlier done in different pH and temperature (Friedhoff et al., 1998). We further extended the optimization of aggregation by incubating tau with various buffer components and pH as well as wide range of salt concentration and temperature. Tau constructs-K19 and K18 were used for optimizing the conditions and the aggregation was monitored by a fluorescent dye (Thioflavin S) for any structural transition upon aggregation.

3.3.1 Effect of buffer salt and pH on the aggregation of K19 and K18

To analyze the conditions suitable for the aggregation of tau constructs, polymerization reactions were set up with 50 µM of K19 and K18 in the presence or absence of heparin 3000 (heparin:protein = 1:4) in various buffers in the pH range 2.0-12.0. The extent of polymerization was determined by ThS fluorescence and the presence of PHFs was ascertained by EM. The aggregation efficiency of K19 with different buffer components and various pH showed that the aggregation efficiency was low at pH values < 5.0; moderate aggregation efficiency was found between pH 6.0 and 7.0 and the highest efficiency was detected between pH 8.0-10.0 (Fig. 3.17).
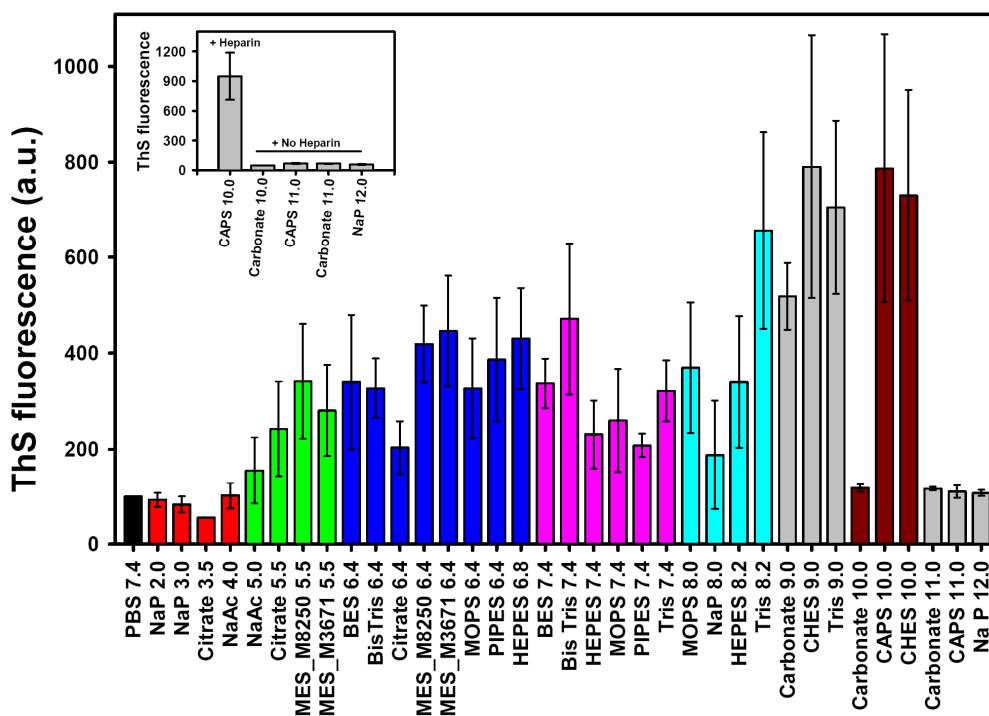
Figure 3.17: Profile of K19 aggregation efficiency in different buffers and pH. Aggregation of K19 was set up by taking 50 µM concentration of protein in 20 mM buffer of different components and various pH in the presence or absence of heparin 3000 (protein:heparin = 4:1). The reactions were incubated at 37°C for 3 days and the extent of aggregation was measured by ThS fluorescence in 384 well plate in a Tecan fluorescence instrument with excitation wavelength 441 nm and emission wavelength 521 nm with slit width of 7.5 nm for excitation and emission wavelengths.

Based on the highest efficiency of aggregation of K19 near the isoelectric point (= 10.49), it may be concluded that the minimization of net charge favors the aggregation. However, for the aggregation at pH near pI, the presence of the cofactor heparin was found to be necessary (Insert figure in Fig. 3.17). Moreover, the aggregation propensity of K19 at pH > pI was less even in the presence of heparin. This pointed to the fact that heparin is not only important for shielding the repulsive charge but might have an additional effect. It is notable that even at pH 10.0, lysine residues (pKa = 10.53) are still partially charged and are known to interact with heparin (312K in PHF6 and 331K) (Mukrasch et al., 2005). The morphology of filaments was checked by EM and showed that the filaments formed at pH 10.0 closely resemble the morphology of bonafide PHFs (Fig. 3.18).
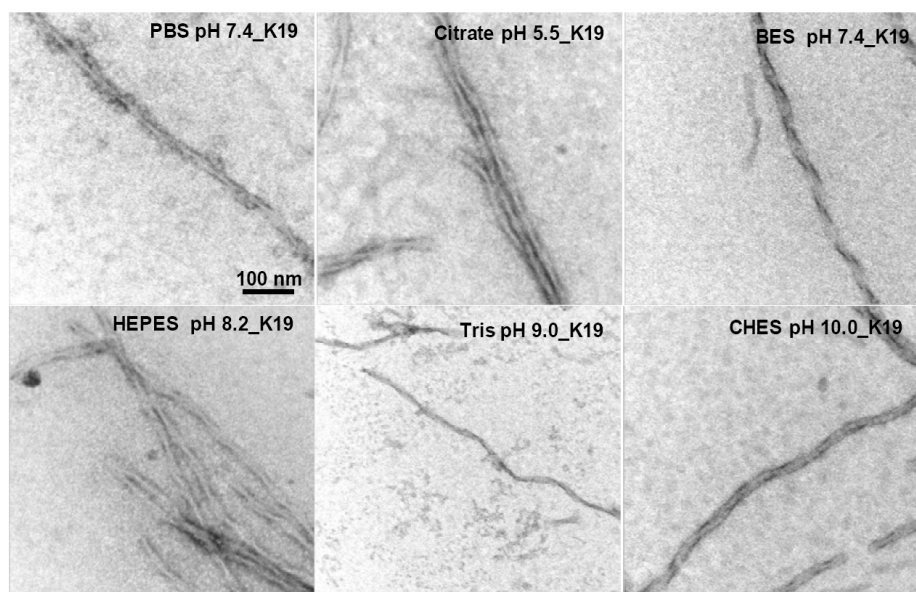
Figure 3.18: Electron micrographs of K19 filaments. EM pictures of the filaments of K19 obtained in different buffer conditions and pH are shown. An aliquot of a K19 aggregation sample was loaded on 600 mesh copper grid, washed twice with water and then stained with 2 % uranyl acetate. The grids were checked for presence of filaments in Phillips CM transmission microscope. The scale bar represents 100 nm and is the same for all the pictures.

A similar pattern of aggregation efficiency was observed for the construct K18, also exhibiting better aggregation efficiency around pH 10.0 (Fig. 3.19). The aggregation reactions were analyzed for the presence of PHFs by EM, revealing that the morphology of filaments was similar to that of filaments formed at pH 7.4 (Fig. 3.20).
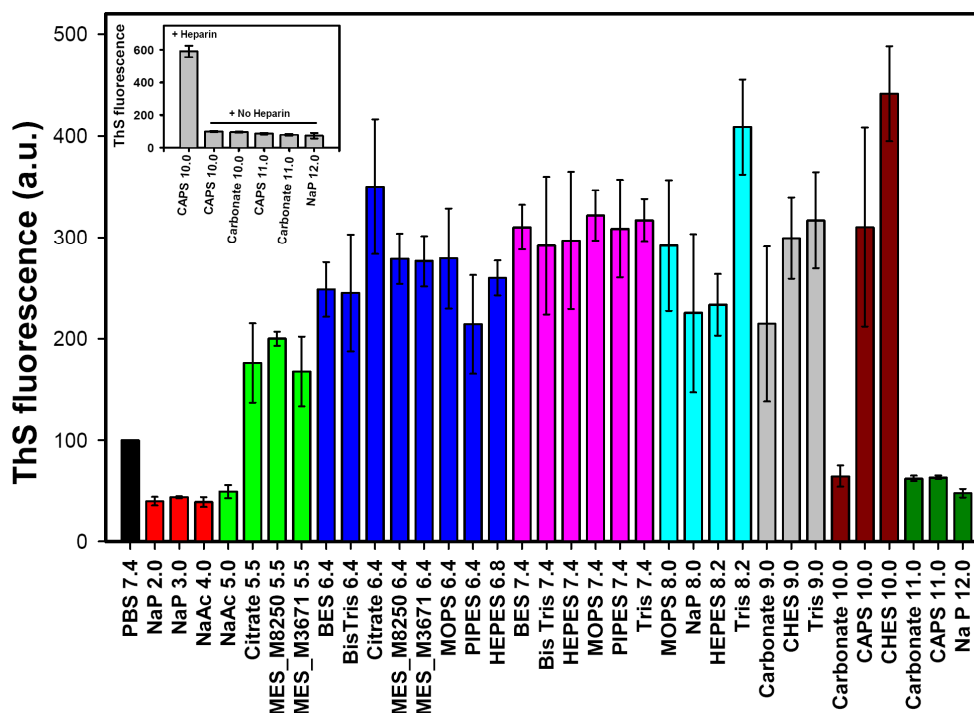
Figure 3.19: Profile of K18 aggregation efficiency in different buffers and pH. Aggregation of K18 was set up by taking 50 µM concentration of protein in the 20 mM buffer of different components and various pH values in the presence or absence of heparin 3000 (protein:heparin = 4:1). The reactions were incubated at 37°C for 3 days. The extent of aggregation was measured by ThS fluorescence as described in Fig. 3.17.
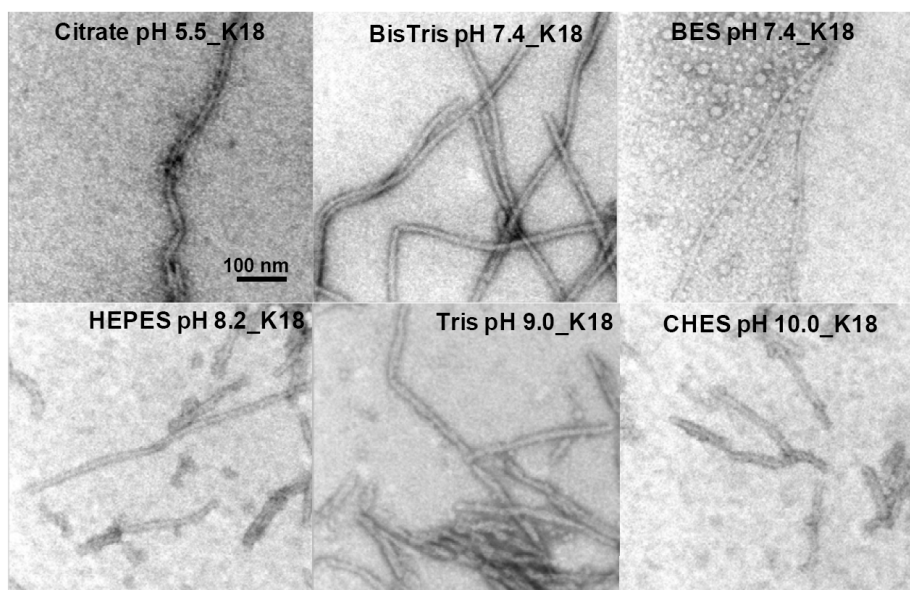
Figure 3.20: Electron micrographs of K18 filaments. EM pictures of filaments of K18 obtained in different buffer conditions and pH are shown. An aliquot of a K18 aggregation sample was loaded on 600 mesh copper grid, washed twice with water and then stained with 2 % uranyl acetate. The grids were checked for the presence of filaments analyzed in Phillips CM transmission microscope. The scale bar represents 100 nm and is the same for all the pictures.

3.3.2 Effects of salt concentration on the aggregation of K19 and K18

Salts can shield the charged side chains of amino acids. At increasing concentration, salt might cause the loss of hydrogen bonding between the oppositely charged residues or water molecules. To analyze the effect of high salt concentration on the aggregation of K19, polymerization reactions were set up with equal concentration of tau protein in the buffer containing increasing

salt concentration (0-500mM NaCl) in the presence of heparin 3000. The extent of polymerization was assayed by ThS fluorescence. The aggregation efficiency of K19 was strongly attenuated with increasing salt concentration (Fig. 3.21A). A similar pattern was observed for aggregation of K18 (Fig. 3.21B), in good agreement with an earlier study except that a drop at 0 mM salt (Friedhoff et al., 1998). The suppression of tau aggregation in the presence of salt might be due to abolishment of heparin-tau or tau-tau interactions and is indicative of ionic nature of aggregation.
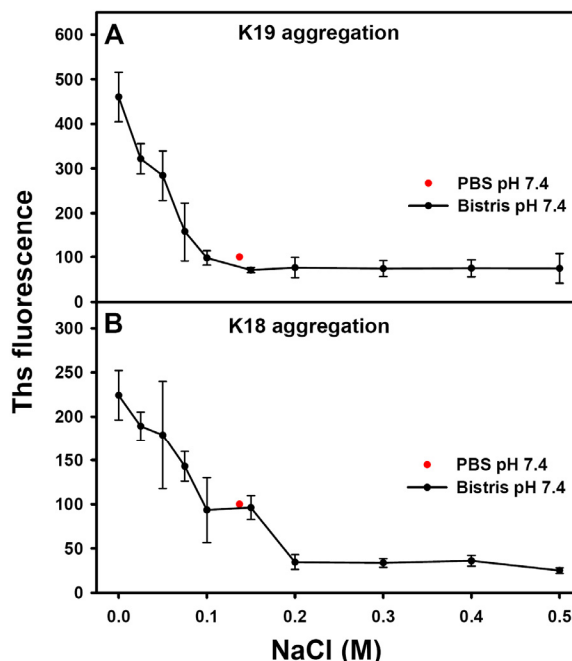
Figure 3.21: Aggregation efficiency of K19 and K18 at high salt concentration. Relative ThS fluorescence is shown from polymerization reactions of (A) K19 and (B) K18 at various salt concentrations. Aggregation was set up by taking 50 µM protein in 20 mM BisTris pH 7.4 buffer plus various salt concentration and added heparin 3000 (protein:heparin = 4:1), incubated at 37°C for 3 days. ThS fluorescence was measured as described in Fig. 3.17.

3.3.3 Effect of temperature on the aggregation of K19 and K18

As the temperature is increased, the interactions of a protein such as hydrogen bonding are weakened leading to increase of water around peptide bonds. The protein would now attempt to minimize its free energy by burying hydrophobic residues while exposing hydrophilic residues. To analyze the effect of increasing temperature on the aggregation of K19, polymerization reactions were set up with the equal concentration of K19 in the presence of heparin 3000 and incubated at various temperatures (25-80˚C). The degree of polymerization was analyzed by ThS fluorescence. The aggregation efficiency of K19 increased at 50˚C in comparison to 25˚C and 37˚C but decreased again at 70˚C and 80˚C (Fig. 3.22A). A similar behavior was found for the aggregation of K18 (Fig. 3.22B). This result is in good agreement with earlier result though the temperature range was only up to 50°C (Friedhoff et al., 1998).

Thus tau aggregation showed two phases upon temperature rise: (i) aggregation increase with temperature up to 50°C. This could be due to the strengthening of hydrophobic interactions particularly between hexapeptides (PHF6 and PHF6*). (ii) aggregation drop at temperatures above 50°C. This may be due to the decrease of tau-tau and tau-heparin interactions at these temperatures that do not allow the formation of hydrogen bonding.
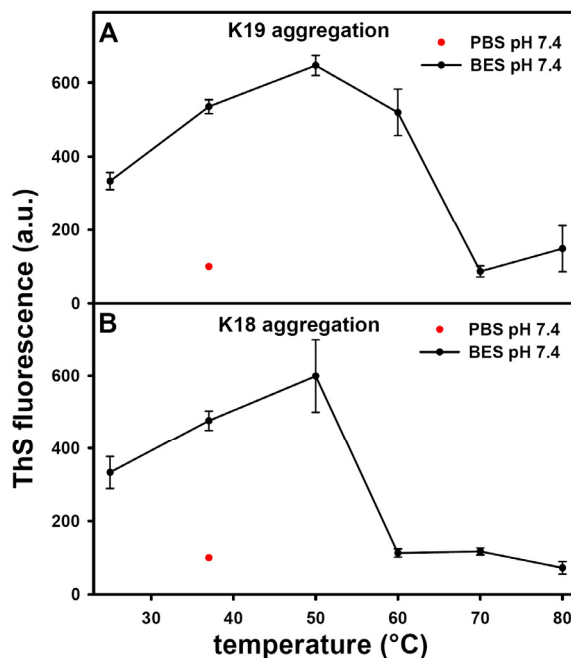
Figure 3.22: Aggregation efficiency of K19 and K18 against elevated temperatures. Relative ThS fluorescence is shown from polymerization reactions of (A) K19 and (B) K18 at various temperatures. Aggregation was set up by taking 50 µM protein in 20 mM BES pH 7.4 buffer in the presence of heparin 3000 (protein:heparin = 4:1), incubated at different temperatures for 3 days. ThS fluorescence was measured as described in Fig. 3.17.

3.3.4 ANS fluorescence measurement of aggregation

Hydrophobic patches are known to contribute to pathological aggregation of disease related proteins (Otzen et al., 2000; Chiti et al., 2002; Wurth et al., 2002) and usually form the core of the fibrils. To check whether there is an increased hydrophobicity upon aggregation of tau, 8-anilino-1-naphthalene sulfonic acid (ANS) was used to monitor aggregation. ANS binds to solvent-exposed hydrophobic clusters that are present in the intermediates of a protein fold and protein aggregates resulting in an increase in ANS fluorescence intensity (Slavik, 1982; Semisotnov et al., 1991; Kaylor et al., 2005). Monitoring the polymerization of tau constructs-K19 and K18 showed that the ANS fluorescence increased as polymerization proceeded (solid black and red line respectively, Fig. 3.23A). In fact, the ANS fluorescence of polymerizing K18 (containing two hydrophobic hexapeptides-PHF6 and PHF6*) showed higher values that of K19 aggregation (containing one hydrophobic hexapeptide-PHF6).

The primary sequence of tau has low hydrophobic content but contains two known hydrophobic stretches (PHF6 and PHF6*). Hence, the increase of hydrophobicity is mostly likely due to the

direct interaction of the hexapeptides during β-sheet formation upon aggregation. To control the reaction independently, ThS fluorescence was measured in parallel (dashed black and red line for K19 and K18 aggregation respectively, Fig. 3.23B) and later the presence of PHFs were confirmed by EM.
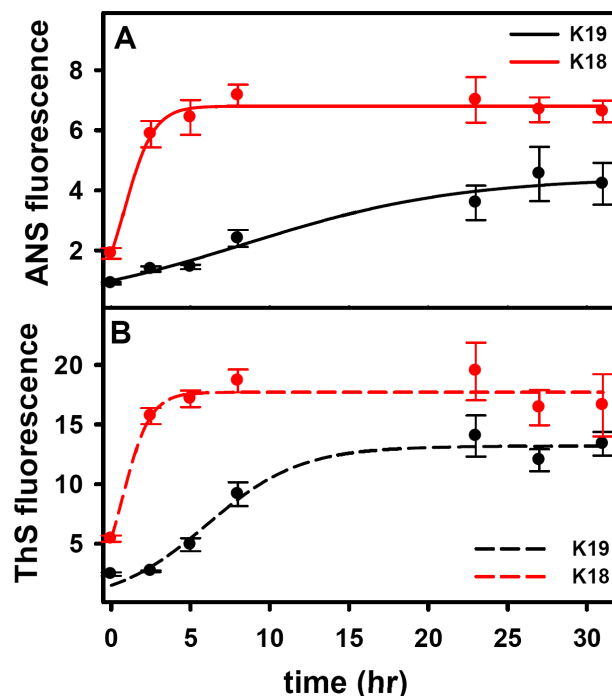
Figure 3.23: Monitoring aggregation of K19 and K18 by ANS fluorescence. Aggregation was started with 50 µM protein in the presence of heparin 6000 (protein:heparin = 4:1) and incubated at 37°C. A) The aggregation of K19 and K18 monitored by ANS fluorescence is shown (solid black and red lines respectively). 5 µl of reaction mixture was added with 100 µM ANS and incubated at 25°C to allow binding. The measurements were taken using excitation at 390 nm and emission 475 nm with slit bandwidths of 7.5 nm for both excitation and emission. B) The parallel measurement of aggregation K19 and K18 by ThS fluorescence (short dashed black and red lines respectively) is shown as well. ThS fluorescence was measured as described in Fig. 3.17.

3.4 Analysis of the structural properties of PHFs

PHF formation is thought to be similar to the aggregation of other amyloidogenic proteins. However, it is not clear what kinds of interactions are important for driving the aggregation, considering that tau is a natively unfolded. To understand the factors contributing the stability, PHFs were subjected to denaturation and various environments which could effect structure transition. For this analysis, PHFs derived from K19, K18 and K18ΔK280 were used. The mutation ΔK280 occurs in FTDP-17 and causes an increased tendency to form PHFs (Goedert et al., 1999; Barghorn et al., 2000).

3.4.1 Effect of GdnHCl on the stability of PHFs

Analysis of PHFs derived from tryptophan mutants of tau by intrinsic tryptophan fluorescence showed that PHFs can be dissolved at a half maximal concentration of about 1.0 M GdnHCl (Li et al., 2002). To validate the stability of PHFs by structural criteria, PHFs derived from K19, K18 and K18ΔK280 were measured by CD at increasing concentrations of denaturant.

With increasing concentration of GdnHCl, the negative ellipticity of K19 PHFs shifted from 217 nm to 200 nm indicating a change from β-structure to random coil (Fig. 3.24A). The plot of 205/217 nm ratio as function of GdnHCl concentration confirmed the structural transition from β-structure to random coil with the major transition point around 1.0 M GdnHCl for K19 PHFs as well as for K18 PHFs and 3.5 M GdnHCl for K18ΔK280 PHFs (Fig. 3.24B). Thus, PHFs from the FDTP mutant K18ΔK280 showed increased stability compared to PHFs from K19 and K18.

To validate the results obtained by CD, ANS fluorescence of PHFs was measured in the presence of GdnHCl. The decrease of the ANS fluorescence with increasing GdnHCl concentration supported the structural change of PHFs seen by CD and the dissociation of PHFs from K19, K18 and K18ΔK280 had midpoints around 0.5 M, 0.75 M and 2.0 M GdnHCl respectively (Fig. 3.24C). These values were lower than that were found in CD experiments. This may be explained by a model of dissolution of PHFs in which first the hydrophobic patches disappear before the secondary structure is diminished.
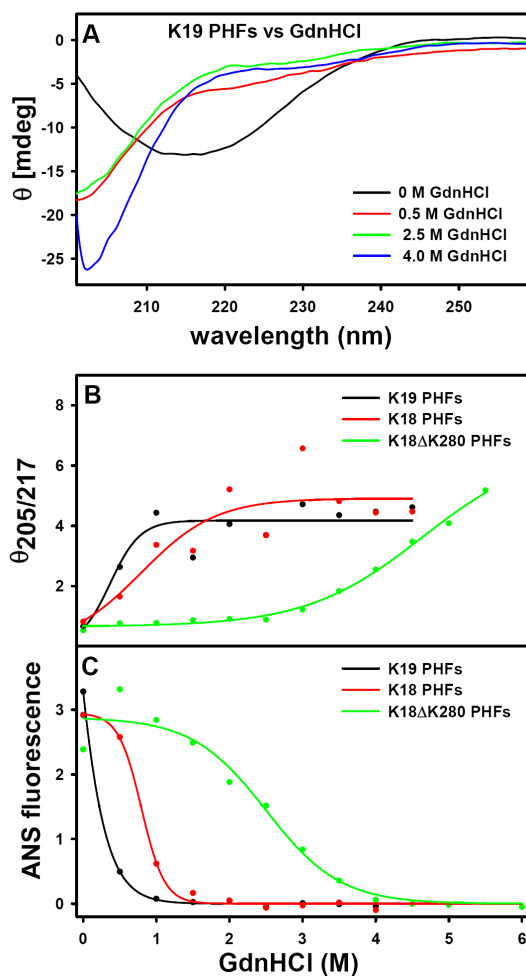
Figure 3.24: GdnHCl denaturation of PHFs. (A) CD spectra of K19 PHFs with increasing GdnHCl concentration. (B) 205/217 nm ratio from GdnHCl denaturation of PHFs measured by CD. (C) ANS fluorescence of PHFs against increasing GdnHCl. Spectra was taken with 0.01 cm cuvette at 20°C.

3.4.2 Structural transition of PHFs under varying pH

To check the contribution of salt bridges to the stability, PHFs were incubated at different pH values ranging from 2.0-12.0 and analyzed by CD. K19 PHFs showed partial β-structure at pH 7.0, but at pH 2.0 and 12.0 it showed a structural change towards a random coil structure (Fig. 3.25A). A plot of the ratio 200/217 against pH revealed that PHFs were disrupted from β-structure around pH 7.0 to random coil when incubated at pH < 5.0 and/or at pH > 10.0 (Fig. 3.25B). The same observation holds true for K18 PHFs with a slight change at higher pH (Fig. 3.25B).

Since the pKa for the negatively charged amino acids Glu and Asp lie around 4.0, it is likely that a change around pH 4.0 would result in a removal of ionic interactions. A similar explanation could be considered when PHFs were incubated at pH > 10.0, due to protonation of Arg and Lys. This observation leads to the hypothesis that the negatively charged amino acids (aspartic acid; note no glutamate acid in R2 and R3) and the positively charged amino acids (lysine and

arginine) may play an important role in stabilizing PHFs via their ability to form ionic interactions.
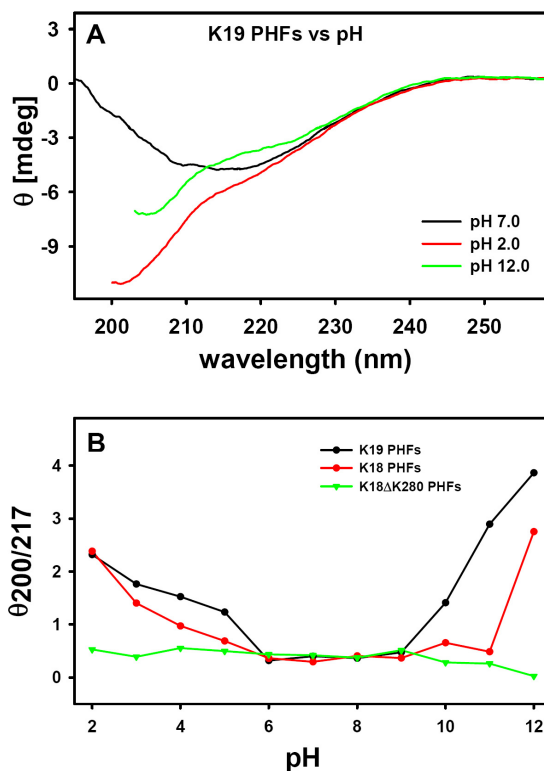
Figure 3.25: pH dependent structural transition of PHFs. (A) CD spectra of K19 PHFs with varying pH. (B) 200/217 ratio from pH dependent disaggregation of PHFs from K19 (black line), K18 (red line) and K18ΔK280 (green line) measured by CD. Experimental conditions as in Fig 3.1.

However, K18ΔK280 PHFs showed no structural variation at any pH (Fig. 3.25B). This could be due to a tight packing of the enlarged hydrophobic patch caused by a prolonged β-strand in this motif (von Bergen et al., 2001). Thus, changing the pH and subsequent disruption of ionic interactions is not sufficient to disrupt K18ΔK280 PHFs, which might be stabilized by hydrophobic interaction.

The change in the morphology of filaments incubated at different pH values was also analyzed by EM. We found that the filaments incubated at pH 2.0 and 12.0 were relatively shorter and thinner than characteristic PHFs incubated at pH 7.0 (Fig. 3.26). It is possible that the longer filaments are broken apart into shorter filaments at extreme pH values, but since EM analysis is only qualitative, this issue awaits further investigation.
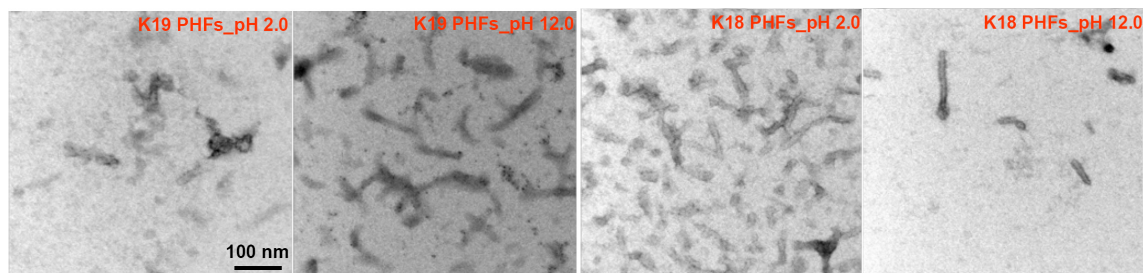
Figure 3.26: EM pictures of PHFs at different pH. EM pictures of K19 and K18 filaments after incubation in different pH are shown. The sample of filaments incubated was loaded on 600 mesh copper grid, washed twice with water and then stained with 2 % uranyl acetate. The grids were checked for the presence of filaments analyzed in Phillips CM transmission microscope. The scale bar represents 100 nm and is same for all the pictures.

3.4.3 Effect of temperature on the secondary structure of aggregated tau

To analyze the effect of the elevated temperature on the secondary structure, PHFs were investigated by CD at increasing temperature. K19 PHFs retained their partial β-structure over a wide range of temperatures (5-90°C) as measured by CD (Fig. 3.27A). Though CD spectra and the 200/217 nm ratio indicated a very slight structural variation above 70˚C, K19 PHFs were intact as checked by EM. K18 PHFs and K18ΔK280 PHFs did not show a significant change in the secondary structure at elevated temperature (Fig. 3.27B). The failure of elevated temperature to disturb the structure of PHFs suggests that stability arises from the contributions of directed salt bridges and hydrophobic interactions (Elcock, 1998; Lesk, 2003).
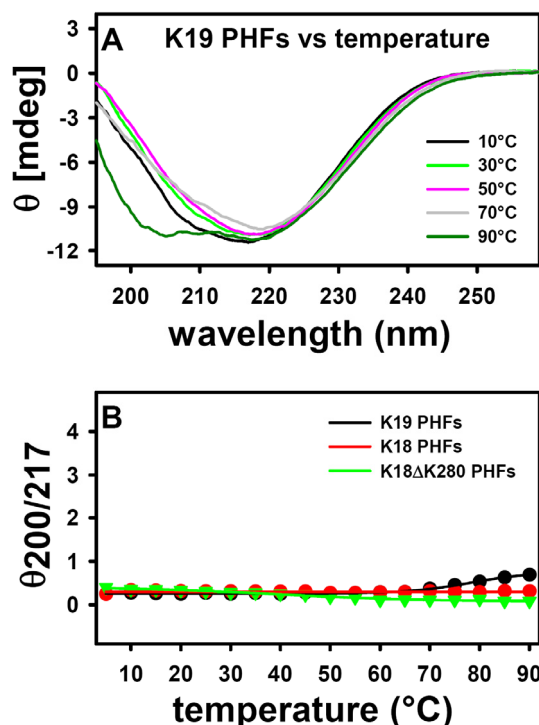
Figure 3.27: Influence of elevated temperature on the structure of PHFs. (A) CD spectra of K19 PHFs with varying temperature. (B) 200/217 nm ratio upon temperature variation measured by CD. Elevated temperature did not affect the structure of PHFs, probably due to the contribution of increased hydrophobic interactions and directed salt bridges. Experimental conditions were same as in Fig 3.1.

3.4.4 Effect of high salt and organic solvents on the structure of tau filaments

An attempt to perturb the structure of the tau filaments at high salt concentrations (0-750 mM Na_2SO_4) did not result in any change (Fig. 3.28A and 3.28B). The structure of the tau filaments remained the same at isopropanol concentration ranging from 5-25 % (Fig. 3.28C and 3.28D). These observations showed that neither higher salt concentration nor isopropanol affected the structure of the tau filaments once they are formed.
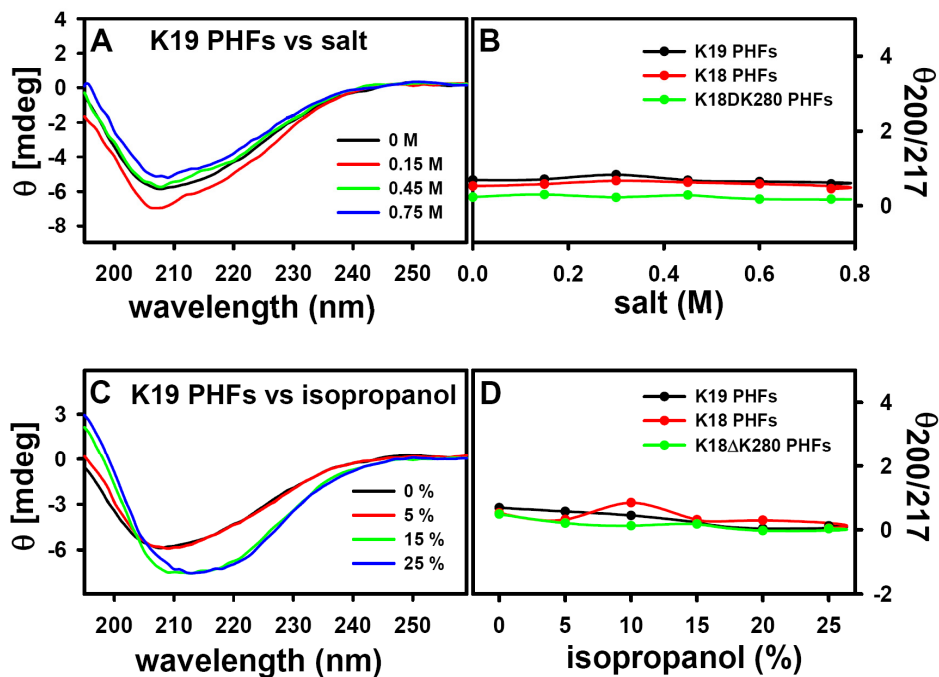
Figure 3.28: Structure of PHFs in high salt and alcohol. (A) CD spectra of K19 PHFs at various salt concentrations. (B) 200/217nm ratio upon salt variation measured by CD. (C) CD spectra of K19 PHFs with varying isopropanol concentration. (D) 200/217 ratio from isopropanol dependent transition of PHFs measured by CD. Note that the structure of PHFs is largely unaltered at high salt and isopropanol concentration. Experimental conditions as in Fig 3.1.

4 Discussion

Tau is an interesting protein from three perspectives:

1. It is important for the cell biology of the neurons because it stabilizes microtubules for their role in neurite outgrowth and axonal transport.

2. Its pathological aggregation in neurons constitutes one of the hallmarks of Alzheimer disease.

3. It belongs to the growing class of natively unfolded proteins which display novel features in protein chemistry.

Precise structural information on tau in solution has been difficult to obtain as it lacks defined structure which also precludes a crystallographic analysis. Spectroscopic evidences (CD, FTIR, intrinsic fluorescence), solution X-ray scattering and hydrodynamic evidence highlight the "natively unfolded" nature of tau, characterized by a lack of secondary structure, Gaussian coil-type character with persistence length around 2 nm and unusually large volume (Schweers et al., 1994; von Bergen et al., 2000; Li et al., 2002; Barghorn et al., 2004). Electron microscopy revealed that tau can be visualized as a rather extended rod-like form (Wille et al., 1992). When bound to microtubules, tau tends to align along the protofilament ridges but retains much of its disordered state (Al-Bassam et al., 2002; Santarella et al., 2004). NMR spectroscopy confirms the paucity of secondary structure, but in addition highlights certain sequence motifs in the repeat domain with an enhanced propensity for β-structure which are known to play a role in the abnormal aggregation into PHFs (von Bergen et al., 2000; Goux et al., 2004; Mukrasch et al., 2005).

The global folding of tau, the properties that govern the soluble and aggregate state and the conditions for aggregation are discussed below based on the study of tau under varying conditions. As a reference, the general effects of pH, temperature, salt etc are summarized in Table 4.1.

Conditions	Effect	On globular protein
pH	Intramolecular repulsion in areas of large charge density	Unfolding and/or aggregation
Temperature	Disturbs hydrogen bonding and changes the water structure around hydrophobic and hydrophilic side chains	Unfolding and/or aggregation
Salt	Shields charged amino acids and decreases water-protein interactions at high concentration	Solubility at low concentration and salting out (precipitation) at high concentration
Alcohol	Reduces water-protein interactions thus favoring intramolecular hydrogen bonding	Unfolding and formation of molten globular intermediates
GdnHCl	Increases the solubility of protein and decreases water-protein interactions	Unfolding

Table 4.1: Simplified overview of conditions affecting protein structure. The changes on the structure of globular proteins under the different condition such as pH variation, temperature etc are listed.

4.1 Low hydrophobicity defines unfolded nature of soluble tau

Based on evidence from several spectroscopic methods, the behavior of tau in solution was defined as natively unfolded (Wille et al., 1992; Schweers et al., 1994; Barghorn et al., 2004). Several attempts to explain the properties of such natively unfolded proteins are based on their primary sequences. It was argued that a high net charge at physiological pH and low hydrophobicity are the causes for the unfolded nature (Uversky et al., 2000; Uversky et al., 2001). The full length isoform htau40 has a very low hydrophobic content (mean hydrophobicity = 0.404) but a low net charge (only +2). However, this value of the net charge disguises the fact that tau is a multidomain protein with each domain carrying different net charges (Seitz et al., 2002). Particularly the repeat domain that forms the core of PHFs has a relatively high net charge (+9) with a mean hydrophobicity of 0.428.

The structure of soluble tau was investigated under varying conditions by CD to define the parameters governing the unfolded state of tau and the results are discussed below (Fig. 4.1):

(i) Soluble tau isoforms (htau40wt) and constructs (K19, K18 and K18ΔK280) do not show any conformational change upon pH variation. Tau constructs which possess net charges of ~ +9 compared to full length tau (net charge of +2) fail to get folded at pH values where their charge is neutralized. Besides accounting for the net charge, the charged residues also contribute for the overall low mean hydrophobicity of tau (see appendix for the hydropathy values of amino acids). Taken together, this observation leads to the conclusion that the low hydrophobicity might be the most important parameter defining the unfolded nature of tau.

The behavior of tau upon pH change can be compared to that of some other natively unfolded proteins such as α-synuclein and securin. α-synuclein is abundant in the neuronal cytoplasm and may have a role in synaptic plasticity, trafficking of cargoes between endoplasmic reticulum and Golgi apparatus. Aggregates of α-synuclein are associated mainly with Parkinson disease (Lee and Trojanowski, 2006). The 140 amino acid long α-synuclein has a mean hydrophobicity of 0.454 and a mean net charge of 0.055 with pI = 4.44 and has several similarities to tau in terms of biochemical properties of soluble and aggregated states. CD spectra of α-synuclein measured at different pH values showed a structural transition between pH 2.0 and 8.0 with a decrease of ellipticity at 196 nm and an increase of ellipticity at 222 nm. This transition of α-synuclein upon pH variation is believed to be a two-state transition between natively unfolded and a partially folded intermediate (Uversky et al., 2001). Securin, an estrogen-regulated proto-oncogene, is 202 amino acids long. It has a mean hydrophobicity and mean net charge of 0.45 and 0.05 respectively that are comparable to values of full length tau. CD spectra of securin showed that the structure does not alter as a function of pH (Sanchez-Puig et al., 2005).

(ii) With increasing temperature, tau isoforms and constructs showed a spectral shift with a decrease of the intensity at 200 nm and an increase of the intensity at 217 nm indicating a structural transition with an isodichroic point at ~ 210 nm. The temperature-dependent CD spectra of tau did not show major red shift from 200 nm as expected for a structural transition from random coil (~ 200 nm) to α-helix or β-structure (~ 217 nm). This temperature-dependent CD of tau is similar to that of the polyproline II helix for which the spectral change upon temperature rise is attributed to the transition to more disorder or flat β-structure (Makarov et al., 1992; Eker et al., 2003; Rath et al., 2005). PPII is a left-handed helix with three residues per turn and the rise per residue is ~ 3.1 Å. The mean residue ellipticity (MRE) of PPII observed by CD ranges from -60000 (collagen and poly-L-lysine) to -20000 deg cm^2 dmol^{-1} (model peptides) (Eker et al., 2003; Rath et al., 2005; Greenfield, 2006). In the case of tau, the MRE is ~ -16000 deg cm^2 dmol^{-1} which falls within range of -20000 to -5000 deg cm^2 dmol^{-1} that is observed for the denatured and natively unfolded proteins (Uversky et al., 2001; Barghorn et al., 2004; Greenfield, 2006). The discrepancies seen with MRE by CD could arise from the different source of model proteins and peptides and the exactitude to represent a unique conformational state.

As shown by NMR, tau constructs contain very little PPII conformation but stretches of amino acids with a tendency for β-structure (Mukrasch et al., 2005; Mukrasch et al., 2007). Based on this, it is reasonable to assume that the nascent β-structure elements are strengthened at high temperatures probably by increase of hydrophobic interactions. However, the 200/217 nm ratio of the spectra as a function of temperature suggests that structure induction may be a transient one and can not be propagated in a cooperative fashion pointing to lack of significant amount of hydrophobic amino acids. A similar pattern of spectral change upon temperature elevation was also observed for α-synuclein and interpreted as the formation of a partially folded intermediate due to increase of hydrophobic interactions (Uversky et al., 2001). In the case of securin, it was suggested that the presence of a small amount of a polyproline helix II (PPII) might be the reason for such a behavior (Sanchez-Puig et al., 2005).

(iii) The structure of tau at increasing salt concentrations remained unaltered. Since salt has ability to mask the charged residues, tau could get folded if there were enough hydrophobic content. The inability of salt to induce folding in tau again confirms that the unfolded nature of tau is due to low hydrophobicity.

(iv) Moderate concentrations of isopropanol show a slight effect on the structure of tau. In general, alcohols such as TFE or isopropanol decrease the water-protein interaction favoring the formation of intramolecular hydrogen bonding. This in turn leads to a preferred formation of

secondary structure, in particular α-helix chains (Shiraki et al., 1995; Povey et al., 2007). Tau derived peptides in the presence of alcohols such as TFE were shown to adopt α-helix (Minoura et al., 2002; Minoura et al., 2004). The aggregation of tau in the presence of a moderate concentration of TFE was also studied (Hiraoka et al., 2004; Kunjithapatham et al., 2005; Minoura et al., 2005; Mizushima et al., 2006). It may be mentioned that TFE was used to determine the low resistance of tau against the induction of structure, underlining its unfoldedness (von Bergen et al., 2001).

Figure 4.1: Charged and hydrophobic amino acids of tau. Amino acids sequence of full length isoform htau40 is shown with negatively charged amino acids colored in red, positively charged amino acids in blue and the hydrophobic amino acids in green. The known hexapeptide motifs are boxed. The results on the structure of tau under different conditions points to the low hydrophobic content of tau. The brown arrows in the amino acid sequence indicate the region of tau constructs-K19 (without V275-S305) and K18 that constitute part of microtubule binding domain and the core of PHFs.

The stable unfolded nature of tau under pH variation perhaps mimics the conformation of tau upon binding to microtubules. Charge neutralization of basic amino acids upon pH variation could be analogous to interaction of basic amino acids in the repeat domains of tau to the acidic glutamate rich C-terminus of tubulin subunits (EGEGEEEGEE in α-tubulin and EFEEEGEEDE in β-tubulin) (Paschal et al., 1989). Based on the recent NMR analysis of tau in the presence of SDS micelles, it was suggested that tau may form an α-helix on the surface of microtubules (Barre and Eliezer, 2006). Apart from this, the unaltered structure of tau over a wide range of pH supports the view that tau may retain much of its unfolded nature upon microtubule binding (Al-Bassam et al., 2002; Santarella et al., 2004). Further, tau-MT interactions may simply be charge based with the involvement of clusters of amino acids as shown by NMR (Mukrasch et al., 2005) and may not induce tau to any folding, e.g. formation of α-helix.

4.2 Global hairpin residual folding of tau in solution

Although tau is largely unfolded, several indirect observations suggest that tau cannot simply be a total random coil. Analysis of the hydrodynamic radii of tau isoforms show that tau could still get extended by chemical denaturation (Barghorn et al., 2004; von Bergen et al., 2005). Further strong hints for global conformational states of tau come from the reactivities of certain antibodies with discontinuous epitopes involving the sequences from both the N-terminus and the repeat domain (Carmel et al., 1996; Jicha et al., 1997a).

To obtain information on the global conformation of tau protein in solution, fluorescence resonance energy transfer (FRET) was used. FRET measurements have allowed an estimate of the distances between donor-acceptor in macromolecules and would provide some overall structural information about the macromolecule (Stryer, 1978). A series of tau constructs with tryptophan (donor; inserted by site directed mutagenesis) and IAEDANS (acceptor; attached to cysteine) at different positions enabled the use of FRET to probe the proximity of domains of tau. Energy transfer was determined by using steady-state measurements of tau constructs-labeled and unlabeled i.e. the donor emission in the presence or absence of acceptor.

The results of FRET analysis of tau mutants are summarized in Table 4.2 and are summarized as follows:

- In solution, the intrarepeat distances from residue 310 to 322 or from residue 310 to 291 are short (20 Å) and show pronounced FRET, consistent with some local compaction due to folding.

- The C-terminal domain (residues 432 and 435) is much closer (19-23 Å) to the center of the repeats (residues 291, 310, and 322) than expected based on a model of random coil structure, giving rise to substantial FRET and suggesting a hairpin like folding back of the tail onto the repeats.

- The N-terminal domain (residue 17) is not within FRET range of the repeat domain

- But the distance between the N-terminal end (residue 17) and the C-terminal end (residue 432) showed that two ends are close each other (21-24 Å).

In general, the native state of a folded protein has a sharply defined distance distribution between a given pair of residues whose FRET efficiency can be translated into a well-defined separation. This does not necessarily hold for a natively unfolded protein such as tau which exists in solution as a mixture of random coil, residual secondary structure elements and preferred conformational states which are moreover heterogeneous and mobile. In mostly unfolded proteins the distance

between a given FRET pair shows a wider distribution and the apparent FRET reflects this heterogeneity (Fig. 4.2) (Schuler et al., 2002).
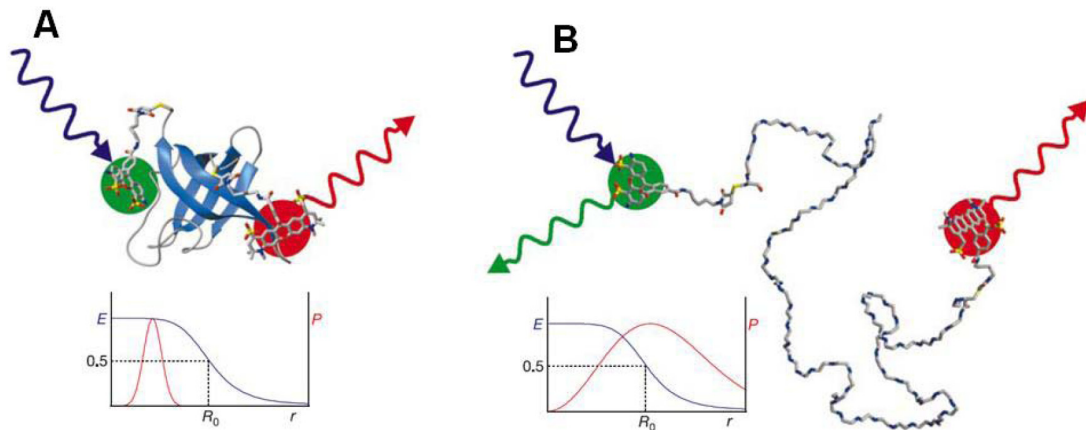
Figure 4.2: Schematic representation of distance distribution of a folded and an unfolded protein. A) A well folded protein has a sharply defined distance distribution (red line) for a given donor and acceptor (green and red circle in upper panel). B) An unfolded shows a wider distance distribution. Figure reproduced from Schuler et al., 2002.

A remarkable difference in the efficiency for the 435-310 pair (high) compared to the 433-310 pair (low) was observed. This is likely because the insertion of a bulky label in the C-terminal may cause either a disruption of the local conformation which might be a prerequisite for interaction with the repeat region or a direct effect on interaction while the assumed local helical structure remains intact. This region is predicted to be an amphipathic α-helix (Yanagawa et al., 1998; Esposito et al., 2000) and therefore, a change by two residues could easily convert an allowed label position into a forbidden one.

Denaturation can be expected to cause a considerable change of distances of the FRET pairs that are widely separated along the protein sequence. In general, GdnHCl is believed to increase the solubility of most parts of the protein compared to water thus allowing the stabilization of the more solvent exposed unfolded state relative to the native state (Nozaki and Tanford, 1970). Additionally GdnHCl is shown to weakly bind to the polypeptide chain and remove water molecules, thus disturbing backbone hydrogen bonding (Schellman, 1987; Timasheff, 2002).

The FRET distances observed did not show the full effect upon denaturation. In the case of the intra-repeat FRET pair (291-310) the distance increased from the native state of 21 Å to an apparent distance of 26 Å (Table 4.2) whereas the theoretical model expects 36 Å. This can be explained by noting that neither the initial state nor the chemically denatured state may comply with the assumptions about standard protein structure, which was found by denaturing well folded proteins (Navon et al., 2002; Krantz et al., 2004).

On the other hand, even the chemically denatured state may differ significantly from a pure random coil model (Fitzkee and Rose, 2004) especially in the presence of pronounced charge

asymmetries (as is the case with tau). A decrease in FRET efficiency was also observed upon GdnHCl treatment between the repeats and the C-terminus with efficiencies dropping from ~ 0.3 to ~ 0.1 upon denaturation. But the disturbance of interactions between N-terminus and repeats upon denaturation was difficult to estimate as the FRET efficiency of R-N$_{FRET}$ mutants was ~ 0.1 in native conditions, too low for reliable distance estimation.

Isoform	W (position)	IAEDANS (position)	E$_{FRET}$	R (Å)	L (Å)	E$_{DENAT}$	R$_{DENAT}$ (Å)
htau39	310	322	0.67	19.5	29.0		
htau40	310	322	0.67	19.5	29.0		
htau40	310	291	0.53	21.6	36.5	0.32	25.5
htau40	432	322	0.29	25.6	87.7		
htau40	432	291	0.37	24.0	99.3	0.08	32.7
htau40	310	435	0.73	18.4	93.5		
htau40	310	433	0.16	29.0	92.8		
htau39	432	322	0.45	22.8	87.7		
htau23	432	322	0.35	24.3	87.7		
htau40	18	322	0.14	30.1	138.1	0.09	32.3
htau40	18	291	0.08	33.5	145.9		
htau40	310	17	0.19	28.0	143.2		
htau39	18	322	0.18	28.8	138.1		
htau23	18	322	0.19	27.8	122.7		
htau40	432	17	0.59	20.8	170.4		
htau23	432	17	0.36	24.2	151.1		

Table 4.2: Summary of FRET efficiencies calculated and expected distances. FRET efficiencies (E$_{FRET}$), FRET distances (R) and theoretical distances (L) are listed for various mutants on the basis of htau40, htau39 and htau23. The observed distances for some mutants after chemical denaturation (R$_{DENAT}$) are also given.

Similarly if the polypeptide chain of tau is internally folded, it can be expected that the folding might cause partial immobilization of residues. But the EPR analysis of mutants with spin label TEMPO at positions 17, 431, 322 and 291 indicated a high flexibility, similar to that observed in flexible termini, flexible loop regions or unstructured proteins (Steinhoff, 2002). This agrees well with recent observations on the mobility of residues in the third repeat (Margittai and Langen, 2004). Taking into consideration that tau is a natively unfolded protein, these observations reinforce the view that the folding interactions are short lived and do not have the character of a firm docking of two binding sites that would cause substantial immobilization.

Initial clues to tau's conformation came from EM that showed tau as an elongated and flexible rod (Wille et al., 1992), as depicted in Figure 4.3A, with no long range interactions between any of the domains of tau. Recent studies show that the C-terminal residues (422-441) which may adopt α-helix interact with the repeat domain, causing an inhibition of the aggregation of tau (Gamblin et al., 2003a). This type of interaction can be depicted as in Figure 4.3B. A distinct conformational state represented in Figure 4.3C can be deduced from the reactivity of antibodies Alz50 and MC1 that recognize an epitope formed by residues near the N-terminus (residues 7-9)

and residues in the third repeat (313-322) (Carmel et al., 1996; Jicha et al., 1997a; Jicha et al., 1997b).
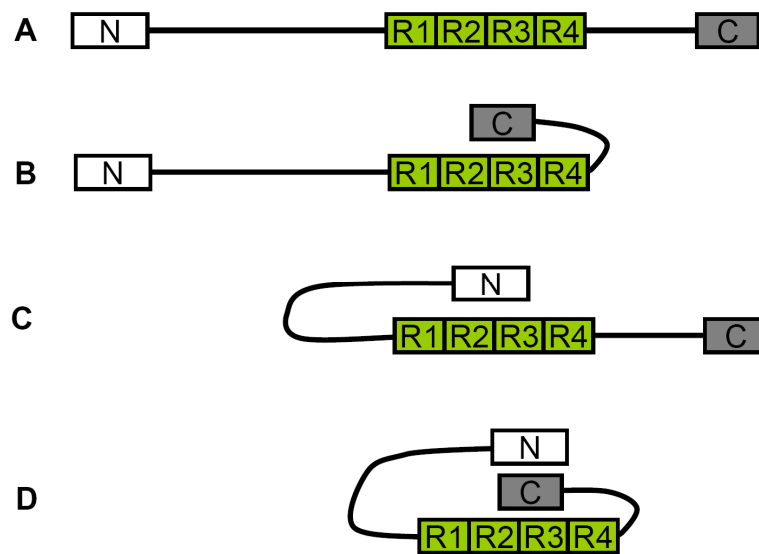
Figure 4.3: Possible conformations of tau in solution. (A) Tau as an extended structure. (B) The C-terminal tail folds over repeat domain ("C-hairpin"). (C) The N-terminal tail folds over repeat domain, which is detected by antibodies Alz-50 or MC1 ("N-hairpin"). (D) N-terminal and C-terminal tails are folded back to the repeat domain ("paperclip").

These observations are in good agreement with these results obtained by FRET and are suggestive of a global folding back of N- or C-terminal domains over the repeat domain which is transient in soluble tau but may become more stable (and thus detectable by antibodies) in pathologically folded tau. Similar conclusions are echoed by the distribution of tau mutations found in frontotemporal dementias (FTDP-17). Most of them occur in or near the repeat domain, consistent with the fact that this domain is responsible for microtubule binding and PHF assembly (Hutton, 2001). However, some mutations lie towards the ends of the tau molecule, e.g. R5L or R406W or T427M, compatible with the idea of a global hairpin folding of tau.
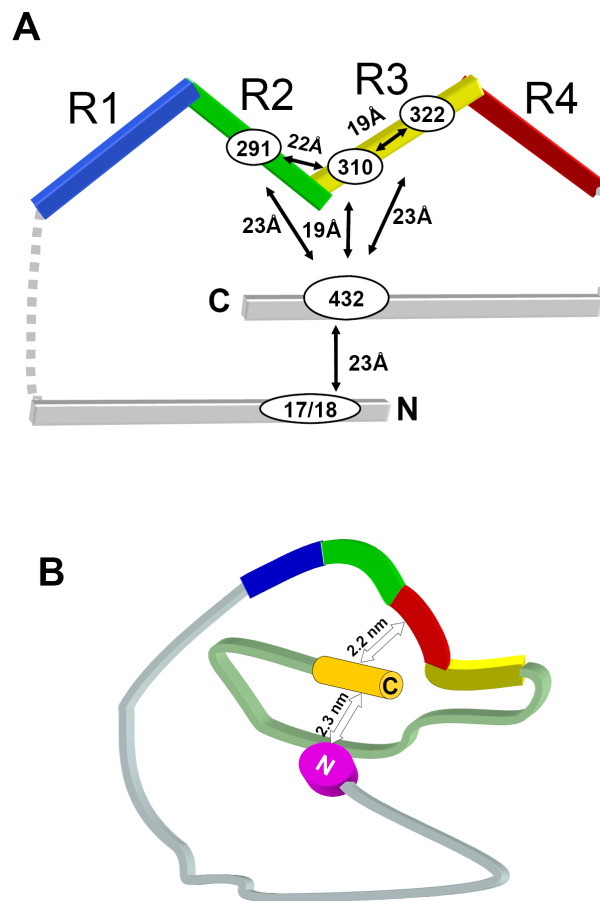
Figure 4.4: Paperclip conformation of tau in solution. (A) Distances between domains of tau deduced by FRET are shown. The molecule shows a paperclip-like fold which brings the N- and C-terminal ends into the vicinity of the repeat domain. Similar folded conformations are recognized by several antibodies specific for abnormal tau from Alzheimer's disease brain (e.g., Alz-50, MC1, and TG3). The approximate distances between labeled residues are indicated. (B) Representation of the paper clip model of tau depicted with full polypeptide chain.

A more quantitative basis of the long range interactions within tau is provided from the present study. The data suggest a complex of both termini and the repeats, mediated by the C-terminus of tau i.e. tau in solution is globally folded in a double sense, reminiscent of a 'paperclip'(Jeganathan et al., 2006). Both the C- and N-termini must be folded over to be near the center of the repeat domain (Fig. 4.3D and 4.4A, B). Further support for the long range interactions within tau comes from the reactivities of antibodies other than Alz50 and MC1 with discontinuous epitopes, which often recognize tau at an early stage of neurodegeneration. Examples are antibody Tau-66 that recognizes elements upstream of the repeat domain and residues in repeat R3 (Ghoshal et al., 2001; Garcia-Sierra et al., 2003), antibody MN423 that reacts against a truncation site downstream of the repeats (at E391) and residues within the repeat domain (Skrabana et al., 2004) and antibody SMI34 that reacts with an epitope that requires the repeat domain and one of the KSP motifs upstream or downstream from the repeats (Lichtenberg-Kraag et al., 1992).

4.3 Optimization of aggregation of tau

The experiments on soluble tau showed that the low hydrophobicity is dominant in defining the unfolded nature of tau. The aggregation of tau is induced *in vitro* by addition of polyanion-heparin (Goedert et al., 1996) which interacts mostly with positively charged amino acids (Mukrasch et al., 2005). Nevertheless, heparin does not get incorporated into the fibers (Necula et al., 2005; von Bergen et al., 2006b; Carlson et al., 2007). As heparin itself does not get incorporated into PHFs, the positively charged amino acids can probably be neutralized by the aspartic acids or other hydrogen acceptors like histidine.

The conditions for tau aggregation vary between different studies. In an extension of previous studies (Friedhoff et al., 1998), the aggregation of tau constructs K19 and K18 was done in the presence of heparin at a wide range of conditions and the results (Fig. 4.5) are summarized as follows:

- Charge neutralization of tau (at pH near but less than pI) is important for tau aggregation

- Optimal temperature (~ 50°C) enhances aggregation

- Low salt concentration enhances aggregation

- Aggregated tau shows increased hydrophobic patches

The pH dependence of tau aggregation in the presence of heparin points to the ionic nature of the tau-heparin interaction. Aggregation of tau constructs K19 and K18 show a low efficiency at pH < 5.0; moderate between pH 6.0 and 7.0 and high between pH 8.0-10.0 which is close to the isoelectric point of tau constructs (~ 10.4). At pH < 4.0, the protonation of the carboxyl side chain of aspartic and glutamic acid residues (pKa of the carboxyl side chain is ~ 4.0) would result in the inability of these residues to form salt bridges with basic amino acids (lysine and arginine). In addition, the net charge of tau increases with lowering pH causing repulsion between tau molecules due to the high positive charge. It is also likely that the lower pH would affect the charged sites of heparin (negatively charged at neutral pH) which might in turn influence the interaction with tau. In comparison to tau aggregation, α-synuclein (pI = 4.44) was shown to aggregate faster at low pH probably due to the induction of partially folded conformational state (Uversky et al., 2001). However, it should be noted the aggregation of α-synuclein was self-driven, whereas the aggregation of tau depends on its charge based interaction with heparin.

Increased aggregation at pH 8.0-10.0 can be largely due to the minimization of the net charge of tau constructs (pI = ~ 10.4). But aggregation at these pH values does not take place in absence of heparin and also at pH values > pI. This explains the fact that heparin may specifically act by

shielding certain basic amino acids to nucleate the aggregation. For example, lysine (pKa = 10.53) is still partially charged at pH 10.0 but not at pH 11.0 or 12.0. A few lysine residues of soluble tau (K312 in PHF6 and K331) are reported to interact with heparin (Mukrasch et al., 2005). Concomitant with the low net charge at high pH, the interaction of hydrophobic patches of tau (the hexapeptides PHF6 and PHF6*) could also increase whereas at neutral and acidic pH, the interaction of these motifs would be minimal due to the high repulsive charge of the protein.
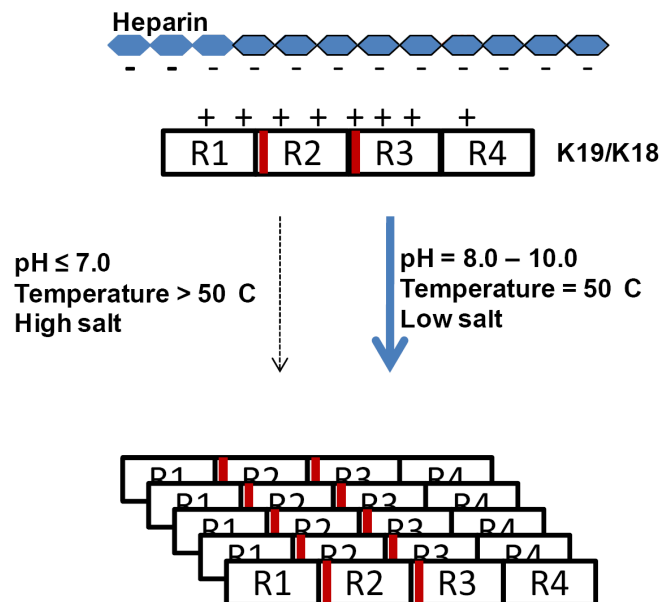
Figure 4.5: Aggregation conditions for tau constructs. Aggregation of K19 and K18 in the presence of heparin is greatly enhanced at pH values where the inherent charge of tau protein is minimized (pH 8.0-10.0). Temperature up to 50°C and low salt concentration in solution speeds up the aggregation. Upon aggregation, solvent exposed hydrophobic patches appear. Heparin in diamonds and tau constructs are shown with respective charges at physiological pH. Thicker arrow indicates strong aggregation tendency in the mentioned conditions while dotted arrow indicates less or nil aggregation. Red line in the tau constructs indicate known hydrophobic stretches (PHF6 and PHF6*).

Enhanced aggregation of the repeat domain in the presence of heparin upon charge neutralization can be correlated to: (i) hyperphophorylation of tau that may increase the aggregation (Avila, 2006). It can be assumed that phophosphate moieties present in the flanking regions could perhaps neutralize certain positive charged resides of the repeat domain making hyperphosphorylated tau more susceptible to aggregation. However, this assumption has to be verified because phosphorylation also modifies other properties of tau e.g. microtubule binding, proteolytic susceptibility (Mandelkow et al., 1995; Mandelkow and Mandelkow, 1998; Binder et al., 2005). (ii) Nonsaturable binding of tau to microtubules. Overloading of tau on the microtubule surface is reported to result in conformational changes of tau that are reminiscent to PHF formation (Ackmann et al., 2000). This can be explained by the neutralization of the basic repeat domains of tau by the acidic surface of microtubules which might make tau on the microtubule surface prone to aggregation. However, it should be noted that binding regions in

tau to heparin and microtubules overlap as analyzed by NMR, leading to the notion that binding of tau to microtubules would be a protective mechanism against aggregation.

The aggregation of tau showed an optimal temperature of 50˚C and decreased at higher temperatures (> 60˚C). This result was partly in agreement with the earlier result (Friedhoff et al., 1998). At elevated temperatures, hydrophobic residues tend to interact more in order to avoid increasing entropy changes caused by water structure. This may partially explain the increased aggregation of tau up to 50°C that is probably due to preferred formation of salt bridges and hydrophobic interactions. Given the highly charged nature of tau, the temperature dependence of aggregation may be dominated by ionic interactions more than hydrophobic interaction. At temperatures > 50°C, aggregation decreases probably due to the increase of conformational energy that seems to overcome the effect of directed salt bridges and hydrophobic interactions or decrease of unspecific salt bridges between tau and heparin. In comparison, the aggregation of α-synuclein was also shown to increase at high temperatures, probably due to the formation a partially folded intermediate which is more prone for aggregation than the native state (Uversky et al., 2001).

The aggregation efficiency of K19 and K18 in the presence of heparin was strongly attenuated with increasing salt concentration. This dependency can be explained because the interaction between heparin and tau must be of ionic nature that can be attenuated at high salt concentrations (Friedhoff et al., 1998).

Tau aggregation monitored by the environment sensitive fluorophore ANS showed a significant increase of hydrophobicity. ANS is widely used to detect the presence of hydrophobic clusters in proteins (Slavik, 1982; Semisotnov et al., 1991) and the solvent-exposed hydrophobic clusters upon specific and unspecific aggregations (Kaylor et al., 2005). The increased ANS fluorescence as tau polymerized is likely to arise from a direct interaction of PHF6 and PHF6* motifs of two tau molecules to form hydrophobic patches (Fig. 4.5). This view is supported by higher ANS fluorescence values for the aggregation of K18 than that for K19.

However, tryptophan quenching experiments showed that the core of tau filaments are rather inaccessible (Li et al., 2002). This observation opposes a view that ANS would bind to hexapaptides inside the core. In fact, the binding mechanism of fluorescent dyes such as ThS, ANS (Fig 4.6) to the amyloid aggregates lacks the detailed information. It may be worth noting that the crystal structure of MurA (UDPGlcNAc enolpyruvyltransferase, an enzyme involved in bacterial wall synthesis) bound to ANS revealed that the naphthalene ring of ANS is sandwiched between a Pro and the hydrophobic side chain of Arg with the sulfonate group is hydrogen-bonded to the main-chain amide of Gly and to the guanidinium group of Arg (Schonbrunn et al.,

2000). The distance between the centre of ANS molecule and carbon atoms of the protein is ~ 3.5 Å on both sides. This distance is very close to the distance between the side chains of two amino acids that are in the cross β-structure. Thus, it may also be assumed that ANS binds to the outer surface of the tau aggregates where it can intercalate between the side chains of amino acids that are facing outside. Thioflavin T which has a benzothiazole group similar to thioflavin S has been shown to bind along the fiber axis of insulin fibers between the protofilaments (Groenning et al., 2007)
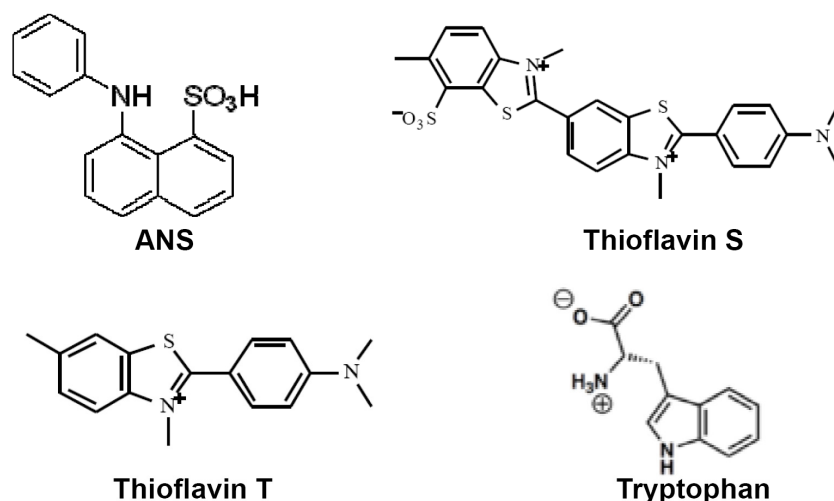
Figure 4.6: Structure of ANS, thioflavin S, thioflavin T and tryptophan. The structure of thioflavin S and thioflavin T which are believed to bind to cross β-structure of amyloid fibrils and the structure of ANS used to indentify the exposed hydrophobic patches are shown. For reference, the structure of tryptophan, an intrinsic fluorophore, is also shown.

4.4 Stability of PHFs is determined by salt bridges

Tau aggregation follows the principles of other amyloidogenic proteins in that tau filaments are built on cross-β-structure that is characteristic of amyloid aggregates. However, the contributing factors for the aggregation and the stability of aggregates differ depending on the primary structure of the region of the protein involved in the aggregation. Results of the analysis of factors that stabilize PHFs are as follows:

(i) K19 PHFs and K18 PHFs have transition points around 1.0 M GdnHCl but K18ΔK280 PHFs shows a transition around 3.5 M GdnHCl. These values were validated by ANS fluorescence. The disruption of PHFs from K18 and K19 was achieved at very mild concentrations of GdnHCl, compared to that of stably folded proteins like tubulin (4.5 M GdnHCl). This may point to a lesser contribution of the hydrophobic interactions for the stability. In contrast, PHFs made from the FDTP mutant K18ΔK280 show increased stability that is explained by the formation of a larger amphipathic patch (von Bergen et al., 2001).

(ii) Partial disruption of PHFs from K19 and K18 at pH values < 4.0 and/or >10.0 as judged by CD and EM. The protonation of the carboxyl side chain of aspartic and glutamatic acid residues

at pH < 4.0 and that of lysine and arginine at pH > 10.0 could disturb the ionic interaction between them. This reinforces the importance of salt bridges for the stability of PHFs. But pH variation shows no effect on the structure of K18ΔK280 PHFs and this might be explained by a tight packing of the enlarged hydrophobic patch caused by a long β-strand in this motif (von Bergen et al., 2001).

The result that ionic interactions mostly contribute to stability of PHFs (Fig. 4.7) is supported by some previous studies. The importance of certain charged amino acid for tau aggregation was recently shown (Li and Lee, 2006). In that study, a tau mutant with deletion of K311 failed to polymerize, leading to the speculation that this lysine residue is involved in the formation of salt bridge. Crystals obtained from the hexapeptide (VQIVYK) are in a cross β-spine structure, arranged in a zipper like fashion forming a dry interface (dominated by hydrophobic interactions) and a wet interface (dominated by ionic interactions) (Sawaya et al., 2007). With this model of tau filaments, it may be reasonable to expect the disturbance of a wet interface upon pH variation due to the loss of ionic interactions. In contrast, the β-helix model proposed based on EPR analysis of htau40 do not directly support the importance of ionic interactions (Margittai and Langen, 2004, 2006). However, it can not be ruled out that positively charged amino acids (especially lysine) that are aligned in register might be interacting with residual heparin along the fiber axis (Sibille et al., 2006). In this case, it is likely that at higher pH the lysine side chains get neutralized or at low pH perhaps heparin negative charges are compromised. Either way, the stability of tau filaments is affected.

(iii) Unaltered structure of PHFs upon temperature elevation. Elevated temperature is known to favor specific ionic interactions and hydrophobic interactions (Elcock, 1998; Lesk, 2003). The behavior of PHF upon elevated temperature could be due to the formation of specific salt bridges and increased hydrophobic interactions. Thermal stability of the amyloid fibrils may be related to the fundamental properties of fibril structure such as specific arrangement of the hydrophobic and hydrogen-bonding residues (Meersman and Dobson, 2006). In the amyloid fibrils, main chain interactions are dominant (hydrogen bonding between the β-strands) exposing polar residues and hydrophobic residues. Upon temperature rise, it may be assumed that there might be the formation of salt bridges and the strengthening of hydrophobic interactions within protofilaments as well as between the protofilaments.

(iv) Unaltered structure of PHFs at high salt and moderate isopropanol concentration. This reinforces the notion that once PHFs are formed, the molecular interactions are rather stable and that neither salt nor alcohol can force tau molecule in PHF to adopt any other structure.

Hypothetical directed salt bridges
and hydrophobic patches
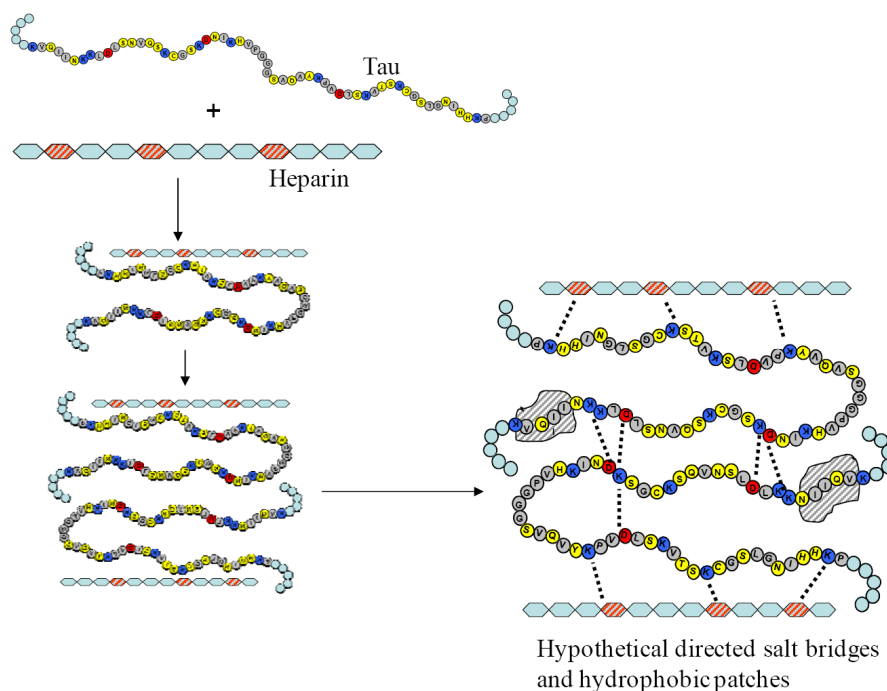
Figure 4.7: Scheme of PHFs stabilizing factors. Soluble tau upon incubation with heparin aggregates into PHFs due to neutralization of charge in the basic repeat region of tau caused by ionic interactions between heparin and tau. Upon aggregation, tau shows an increase of hydrophobic patches probably due to direct interaction of known β-structural elements of tau in R3 and R2 (PHF6 and PHF6* respectively). PHFs are stabilized by major salt bridges as evidenced by denaturation at mild GdnHCl concentration and pH dependent disruption of β-structure of PHFs.

The major results of this study are summarized in the Table 4.3.

	Conditions	Effect	Possible interpretation
Structure of soluble tau	pH	Unaltered	Lack of hydrophobicity
	Temperature	Spectra with a characteristic isobestic point	Transient strengthening of hydrophobic interactions
	Salt	Unaltered	Lack of hydrophobicity
	Alcohol	Induction of α-helix	Intramolecular hydrogen bonding
	FRET	Global hairpin folding	
Aggregation	pH	Better at pH values near pI	Charge neutralization
	Temperature	Optimal temperature 50°C	Strengthening of hydrophobic interaction at 50°C but loss of tau-tau or tau-heparin interaction at > 50°C
	Salt	Better aggregation at low salt concentration	Loss of tau-heparin interaction at high salt concentration
PHFs	GdnHCl	Denaturation points at low concentration	Hydrophobic interactions may contribute less to stability
	pH	Partial disaggregation	Dominated by ionic interactions
	Temperature	Unaltered	Contribution by ionic and hydrophobic interactions
	Salt	Unaltered	Contribution by ionic and hydrophobic interactions
	Alcohol	Unaltered	Contribution by ionic and hydrophobic interactions

Table 4.3: Summary of effect of varying conditions on the structure of tau in soluble state, upon aggregation and on PHFs.

5 Summary

Tau normally functions to bind and stabilize microtubules. Tau is classified as a natively unfolded protein. It has a very low content of secondary structural elements. Tau aggregates to insoluble fibers called paired helical filaments in Alzheimer disease. The residual folding and intramolecular interactions within tau are largely unknown, and the factors contributing to the formation and stability of PHFs are not well understood. The results from this present study are aimed at a better understanding of the structure of soluble tau and PHFS. These observations could form a basis for elucidating the molecular architecture of PHFs. The results are summarized as follows:

(i) Soluble tau repeat domain constructs (K19 and K18) and the longest isoform (htau40wt) remained as random coil at pH ranging 2.0-12.0 and at salt concentration (0-0.75 M). In contrast, elevated temperature induces β-structure and alcohol tends to slightly favor formation of α-helix. Overall, these results confirm that the low hydrophobic content of tau is the main cause for its unfolded nature.

(ii) The global folding of tau was examined by fluorescence resonance energy transfer (FRET). The observed FRET distances were significantly different from the theoretical distance expected for a random coil. Notably, the C-terminal end of tau folds over into vicinity of the repeat domain, the N-terminus remains outside the FRET distance of the repeat domain, yet both ends of the molecule approach one another similar to a paperclip-like suprastructure. The interactions between the domains are obliterated by denaturation in GdnHCl, pointing to fluctuating chain that otherwise is almost as flexible as a denatured protein. This folding agrees well with the reactivities of certain antibodies (Alz50, MC1, Tau66 and SMI34) that detect abnormal tau in early stages of Alzheimers disease, suggesting that a stabilization of the folded state could have pathological consequences.

(iii) The aggregation of tau constructs in the presence of heparin is more efficient at pH near the pI that minimizes net charge of tau. Temperature and salt dependence of tau aggregation suggest a strong influence of ionic interactions. Nevertheless, hydrophobic patches appear in tau aggregates as measured by ANS fluorescence.

(iv) The denaturation of PHFs at mild concentrations of GdnHCl as well as the partial dissolution of PHFs at pH 2.0 and 12.0 points to ionic nature of interactions within PHFs. In contrast, PHFs are stable at elevated temperature, at high salt concentrations and in alcohols like isopropanol showing that once PHFs are formed the interactions become stabilized.

6 References

Ackmann, M., Wiech, H., and Mandelkow, E. (2000). Nonsaturable binding indicates clustering of tau on the microtubule surface in a paired helical filament-like conformation. The Journal of biological chemistry *275*, 30335-30343.

Al-Bassam, J., Ozer, R.S., Safer, D., Halpain, S., and Milligan, R.A. (2002). MAP2 and tau bind longitudinally along the outer ridges of microtubule protofilaments. J Cell Biol *157*, 1187-1196.

Alonso, A., Zaidi, T., Novak, M., Grundke-Iqbal, I., and Iqbal, K. (2001). Hyperphosphorylation induces self-assembly of tau into tangles of paired helical filaments/straight filaments. Proceedings of the National Academy of Sciences of the United States of America *98*, 6923-6928.

Andreadis, A. (2005). Tau gene alternative splicing: expression patterns, regulation and modulation of function in normal brain and neurodegenerative diseases. Biochimica et biophysica acta *1739*, 91-103.

Avila, J. (2006). Tau phosphorylation and aggregation in Alzheimer's disease pathology. FEBS letters *580*, 2922-2927.

Baldwin, R.L. (1986). Temperature dependence of the hydrophobic interaction in protein folding. Proceedings of the National Academy of Sciences of the United States of America *83*, 8069-8072.

Barghorn, S., Zheng-Fischhofer, Q., Ackmann, M., Biernat, J., von Bergen, M., Mandelkow, E.M., and Mandelkow, E. (2000). Structure, microtubule interactions, and paired helical filament aggregation by tau mutants of frontotemporal dementias. Biochemistry *39*, 11714-11721.

Barghorn, S., and Mandelkow, E. (2002). Toward a unified scheme for the aggregation of tau into Alzheimer paired helical filaments. Biochemistry *41*, 14885-14896.

Barghorn, S., Davies, P., and Mandelkow, E. (2004). Tau paired helical filaments from Alzheimer's disease brain and assembled in vitro are based on beta-structure in the core domain. Biochemistry *43*, 1694-1703.

Barre, P., and Eliezer, D. (2006). Folding of the repeat domain of tau upon binding to lipid surfaces. Journal of molecular biology *362*, 312-326.

Baumann, K., Mandelkow, E.M., Biernat, J., Piwnica-Worms, H., and Mandelkow, E. (1993). Abnormal Alzheimer-like phosphorylation of tau-protein by cyclin-dependent kinases cdk2 and cdk5. FEBS letters *336*, 417-424.

Berriman, J., Serpell, L.C., Oberg, K.A., Fink, A.L., Goedert, M., and Crowther, R.A. (2003). Tau filaments from human brain and from in vitro assembly of recombinant protein show cross-beta structure. Proceedings of the National Academy of Sciences of the United States of America *100*, 9034-9038.

Biernat, J., Mandelkow, E.M., Schröter, C., Lichtenberg-Kraag, B., Steiner, B., Berling, B., Meyer, H.E., Mercken, M., Vandermeeren, A., Goedert, M.*, et al.* (1992). The switch of tau protein to an Alzheimer-like state includes the phosphorylation of two serine-proline motifs upstream of the microtubule binding region. EMBO J *11*, 1593-1597.

Biernat, J., and Mandelkow, E.M. (1999). The development of cell processes induced by tau protein requires phosphorylation of serine 262 and 356 in the repeat domain and is inhibited by phosphorylation in the proline-rich domains. Mol Biol Cell *10*, 727-740.

Binder, L.I., Guillozet-Bongaarts, A.L., Garcia-Sierra, F., and Berry, R.W. (2005). Tau, tangles, and Alzheimer's disease. Biochimica et biophysica acta *1739*, 216-223.

Braak, H., and Braak, E. (1995). Staging of Alzheimer's disease-related neurofibrillary changes. Neurobiol Aging *16*, 271-278; discussion 278-284.

Brandt, R., Lee, G., Teplow, D.B., Shalloway, D., and Abdel-Ghany, M. (1994). Differential effect of phosphorylation and substrate modulation on tau's ability to promote microtubule growth and nucleation. The Journal of biological chemistry *269*, 11776-11782.

Brandt, R., Leger, J., and Lee, G. (1995). Interaction of tau with the neural plasma membrane mediated by tau's amino-terminal projection domain. J Cell Biol *131*, 1327-1340.

Butner, K.A., and Kirschner, M.W. (1991). Tau protein binds to microtubules through a flexible array of distributed weak sites. J Cell Biol *115*, 717-730.

Carlson, S.W., Branden, M., Voss, K., Sun, Q., Rankin, C.A., and Gamblin, T.C. (2007). A complex mechanism for inducer mediated tau polymerization. Biochemistry *46*, 8838-8849.

Carmel, G., Mager, E.M., Binder, L.I., and Kuret, J. (1996). The structural basis of monoclonal-antibody Alz50s selectivity for Alzheimer's-disease pathology. Journal of Biological Chemistry *271*, 32789-32795.

Chen, J., Kanai, Y., Cowan, N.J., and Hirokawa, N. (1992). Projection domains of MAP2 and tau determine spacings between microtubules in dendrites and axons. Nature *360*, 674-677.

Chiti, F., Taddei, N., Baroni, F., Capanni, C., Stefani, M., Ramponi, G., and Dobson, C.M. (2002). Kinetic partitioning of protein folding and aggregation. Nat Struct Biol *9*, 137-143.

Chiti, F., and Dobson, C.M. (2006). Protein misfolding, functional amyloid, and human disease. Annual review of biochemistry *75*, 333-366.

Cleveland, D.W., Hwo, S.Y., and Kirschner, M.W. (1977). Physical and chemical properties of purified tau factor and the role of tau in microtubule assembly. Journal of molecular biology *116*, 227-247.

Crowther, R.A., and Wischik, C.M. (1985). Image reconstruction of the Alzheimer paired helical filament. Embo J *4*, 3661-3665.

Crowther, R.A. (1991). Straight and paired helical filaments in Alzheimer disease have a common structural unit. Proceedings of the National Academy of Sciences of the United States of America *88*, 2288-2292.

Cummings, J.L. (2004). Alzheimer's disease. The New England journal of medicine *351*, 56-67.

D'Souza, I., Poorkaj, P., Hong, M., Nochlin, D., Lee, V.M., Bird, T.D., and Schellenberg, G.D. (1999). Missense and silent tau gene mutations cause frontotemporal dementia with parkinsonism-chromosome 17 type, by affecting multiple alternative RNA splicing regulatory elements. Proceedings of the National Academy of Sciences of the United States of America *96*, 5598-5603.

Daggett, V., and Fersht, A. (2003a). The present view of the mechanism of protein folding. Nature reviews *4*, 497-502.

Daggett, V., and Fersht, A.R. (2003b). Is there a unifying mechanism for protein folding? Trends in biochemical sciences *28*, 18-25.

Delacourte, A., and Defossez, A. (1986). Alzheimer's disease: Tau proteins, the promoting factors of microtubule assembly, are major components of paired helical filaments. J Neurol Sci *76*, 173-186.

Derkinderen, P., Scales, T.M., Hanger, D.P., Leung, K.Y., Byers, H.L., Ward, M.A., Lenz, C., Price, C., Bird, I.N., Perera, T.*, et al.* (2005). Tyrosine 394 is phosphorylated in Alzheimer's paired helical filament tau and in fetal tau with c-Abl as the candidate tyrosine kinase. J Neurosci *25*, 6584-6593.

Drewes, G., Lichtenberg-Kraag, B., Doring, F., Mandelkow, E.M., Biernat, J., Goris, J., Doree, M., and Mandelkow, E. (1992). Mitogen activated protein (MAP) kinase transforms tau protein into an Alzheimer-like state. Embo J *11*, 2131-2138.

Drewes, G., Ebneth, A., Preuss, U., Mandelkow, E.M., and Mandelkow, E. (1997). MARK, a novel family of protein kinases that phosphorylate microtubule-associated proteins and trigger microtubule disruption. Cell *89*, 297-308.

Drewes, G., Ebneth, A., and Mandelkow, E.M. (1998). MAPs, MARKs and microtubule dynamics. Trends Biochem Sci *23*, 307-311.

Drubin, D.G., and Kirschner, M.W. (1986). Tau protein function in living cells. J Cell Biol *103*, 2739-2746.

Ebneth, A., Godemann, R., Stamer, K., Illenberger, S., Trinczek, B., and Mandelkow, E. (1998). Overexpression of tau protein inhibits kinesin-dependent trafficking of vesicles, mitochondria, and endoplasmic reticulum: implications for Alzheimer's disease. J Cell Biol *143*, 777-794.

Ebneth, A., Drewes, G., Mandelkow, E.M., and Mandelkow, E. (1999). Phosphorylation of MAP2c and MAP4 by MARK kinases leads to the destabilization of microtubules in cells. Cell Motil Cytoskeleton *44*, 209-224.

Eftink, M.R. (1991). Fluorescence techniques for studying protein structure. Methods Biochem Anal *35*, 127-205.

Eker, F., Griebenow, K., and Schweitzer-Stenner, R. (2003). Stable conformations of tripeptides in aqueous solution studied by UV circular dichroism spectroscopy. Journal of the American Chemical Society *125*, 8178-8185.

Elcock, A.H. (1998). The stability of salt bridges at high temperatures: implications for hyperthermophilic proteins. Journal of molecular biology *284*, 489-502.

Esposito, G., Viglino, P., Novak, M., and Cattaneo, A. (2000). The solution structure of the C-terminal segment of tau protein. J Pept Sci *6*, 550-559.

Fellous, A., Francon, J., Lennon, A.M., and Nunez, J. (1977). Microtubule assembly in vitro. Purification of assembly-promoting factors. Eur J Biochem *78*, 167-174.

Fernandez-Escamilla, A.M., Rousseau, F., Schymkowitz, J., and Serrano, L. (2004). Prediction of sequence-dependent and mutational effects on the aggregation of peptides and proteins. Nat Biotechnol *22*, 1302-1306.

Ferri, C.P., Prince, M., Brayne, C., Brodaty, H., Fratiglioni, L., Ganguli, M., Hall, K., Hasegawa, K., Hendrie, H., Huang, Y.*, et al.* (2005). Global prevalence of dementia: a Delphi consensus study. Lancet *366*, 2112-2117.

Fitzkee, N.C., and Rose, G.D. (2004). Reassessing random-coil statistics in unfolded proteins. Proceedings of the National Academy of Sciences of the United States of America *101*, 12497-12502.

Friedhoff, P., Schneider, A., Mandelkow, E.M., and Mandelkow, E. (1998). Rapid assembly of Alzheimer-like paired helical filaments from microtubule-associated protein tau monitored by fluorescence in solution. Biochemistry *37*, 10223-10230.

Gamblin, T.C., Berry, R.W., and Binder, L.I. (2003a). Modeling tau polymerization in vitro: a review and synthesis. Biochemistry *42*, 15009-15017.

Gamblin, T.C., Chen, F., Zambrano, A., Abraha, A., Lagalwar, S., Guillozet, A.L., Lu, M., Fu, Y., Garcia-Sierra, F., LaPointe, N.*, et al.* (2003b). Caspase cleavage of tau: linking amyloid and neurofibrillary tangles in Alzheimer's disease. Proceedings of the National Academy of Sciences of the United States of America *100*, 10032-10037.

Garcia-Sierra, F., Ghoshal, N., Quinn, B., Berry, R.W., and Binder, L.I. (2003). Conformational changes and truncation of tau protein during tangle evolution in Alzheimer's disease. J Alzheimers Dis *5*, 65-77.

Garcia, M.L., and Cleveland, D.W. (2001). Going new places using an old MAP: tau, microtubules and human neurodegenerative disease. Curr Opin Cell Biol *13*, 41-48.

Gasteiger E., Hoogland C., Gattiker A., Duvaud S., Wilkins M.R., Appel R.D., and A, B. (2005). Protein Identification and Analysis Tools on the ExPASy Server. John M Walker (ed): The Proteomics Protocols Handbook, Humana Press, 571-607.

Ghoshal, N., Garcia-Sierra, F., Fu, Y., Beckett, L.A., Mufson, E.J., Kuret, J., Berry, R.W., and Binder, L.I. (2001). Tau-66: evidence for a novel tau conformation in Alzheimer's disease. J Neurochem *77*, 1372-1385.

Goedert, M., Spillantini, M.G., Potier, M.C., Ulrich, J., and Crowther, R.A. (1989). Cloning and sequencing of the cDNA encoding an isoform of microtubule-associated protein tau containing four tandem repeats: differential expression of tau protein mRNAs in human brain. Embo J *8*, 393-399.

Goedert, M. (1996). Tau protein and the neurofibrillary pathology of Alzheimer's disease. Ann N Y Acad Sci *777*, 121-131.

Goedert, M., Jakes, R., Spillantini, M.G., Hasegawa, M., Smith, M.J., and Crowther, R.A. (1996). Assembly of microtubule-associated protein tau into Alzheimer-like filaments induced by sulphated glycosaminoglycans. Nature *383*, 550-553.

Goedert, M., Jakes, R., and Crowther, R.A. (1999). Effects of frontotemporal dementia FTDP-17 mutations on heparin-induced assembly of tau filaments. FEBS letters *450*, 306-311.

Gong, C.X., Liu, F., Wu, G., Rossie, S., Wegiel, J., Li, L., Grundke-Iqbal, I., and Iqbal, K. (2004). Dephosphorylation of microtubule-associated protein tau by protein phosphatase 5. J Neurochem *88*, 298-310.

Gong, C.X., Liu, F., Grundke-Iqbal, I., and Iqbal, K. (2005). Post-translational modifications of tau protein in Alzheimer's disease. J Neural Transm *112*, 813-838.

Goode, B.L., Denis, P.E., Panda, D., Radeke, M.J., Miller, H.P., Wilson, L., and Feinstein, S.C. (1997). Functional interactions between the proline-rich and repeat regions of tau enhance microtubule binding and assembly. Mol Biol Cell *8*, 353-365.

Goux, W.J., Kopplin, L., Nguyen, A.D., Leak, K., Rutkofsky, M., Shanmuganandam, V.D., Sharma, D., Inouye, H., and Kirschner, D.A. (2004). The formation of straight and twisted filaments from short tau peptides. The Journal of biological chemistry *279*, 26868-26875.

Greenfield, N., and Fasman, G.D. (1969). Computed circular dichroism spectra for the evaluation of protein conformation. Biochemistry *8*, 4108-4116.

Greenfield, N.J. (2006). Using circular dichroism spectra to estimate protein secondary structure. Nature protocols *1*, 2876-2890.

Groenning, M., Norrman, M., Flink, J.M., van de Weert, M., Bukrinsky, J.T., Schluckebier, G., and Frokjaer, S. (2007). Binding mode of Thioflavin T in insulin amyloid fibrils. Journal of structural biology.

Gustke, N., Steiner, B., Mandelkow, E.M., Biernat, J., Meyer, H.E., Goedert, M., and Mandelkow, E. (1992). The Alzheimer-like phosphorylation of tau protein reduces microtubule binding and involves Ser-Pro and Thr-Pro motifs. FEBS letters *307*, 199-205.

Gustke, N., Trinczek, B., Biernat, J., Mandelkow, E.M., and Mandelkow, E. (1994). Domains of tau protein and interactions with microtubules. Biochemistry *33*, 9511-9522.

Hardy, J., and Selkoe, D.J. (2002). The amyloid hypothesis of Alzheimer's disease: progress and problems on the road to therapeutics. Science *297*, 353-356.

Hasegawa, M., Smith, M.J., and Goedert, M. (1998). Tau proteins with FTDP-17 mutations have a reduced ability to promote microtubule assembly. FEBS letters *437*, 207-210.

Hiraoka, S., Yao, T.M., Minoura, K., Tomoo, K., Sumida, M., Taniguchi, T., and Ishida, T. (2004). Conformational transition state is responsible for assembly of microtubule-binding domain of tau protein. Biochem Biophys Res Commun *315*, 659-663.

Hirokawa, N. (1993). Axonal transport and the cytoskeleton. Current opinion in neurobiology *3*, 724-731.

Hirokawa, N. (1994). Microtubule organization and dynamics dependent on microtubule-associated proteins. Curr Opin Cell Biol *6*, 74-81.

Hong, M., Zhukareva, V., Vogelsberg-Ragaglia, V., Wszolek, Z., Reed, L., Miller, B.I., Geschwind, D.H., Bird, T.D., McKeel, D., Goate, A.*, et al.* (1998). Mutation-specific functional impairments in distinct tau isoforms of hereditary FTDP-17. Science (New York, NY *282*, 1914-1917.

Horiguchi, T., Uryu, K., Giasson, B.I., Ischiropoulos, H., LightFoot, R., Bellmann, C., Richter-Landsberg, C., Lee, V.M., and Trojanowski, J.Q. (2003). Nitration of tau protein is linked to neurodegeneration in tauopathies. Am J Pathol *163*, 1021-1031.

Hubbell, W.L., Cafiso, D.S., and Altenbach, C. (2000). Identifying conformational changes with site-directed spin labeling. Nat Struct Biol *7*, 735-739.

Hudson, E.N., and Weber, G. (1973). Synthesis and characterization of two fluorescent sulfhydryl reagents. Biochemistry *12*, 4154-4161.

Hutton, M., Lendon, C.L., Rizzu, P., Baker, M., Froelich, S., Houlden, H., Pickering-Brown, S., Chakraverty, S., Isaacs, A., Grover, A.*, et al.* (1998). Association of missense and 5'-splice-site mutations in tau with the inherited dementia FTDP-17. Nature *393*, 702-705.

Hutton, M. (2001). Missense and splice site mutations in tau associated with FTDP-17: multiple pathogenic mechanisms. Neurology *56*, S21-25.

Ihara, Y., Abraham, C., and Selkoe, D.J. (1983). Antibodies to paired helical filaments in Alzheimer's disease do not recognize normal brain proteins. Nature *304*, 727-730.

Illenberger, S., Drewes, G., Trinczek, B., Biernat, J., Meyer, H.E., Olmsted, J.B., Mandelkow, E.M., and Mandelkow, E. (1996). Phosphorylation of Microtubule Associated Proteins MAP2 and MAP4 by the Protein Kinase p110^{mark}: Phosphorylation Sites and Regulation of Microtubule Dynamics. J Biol Chem *271*, 10834-10843.

Ishiguro, K., Shiratsuchi, A., Sato, S., Omori, A., Arioka, M., Kobayashi, S., Uchida, T., and Imahori, K. (1993). Glycogen synthase kinase 3 beta is identical to tau protein kinase I generating several epitopes of paired helical filaments. FEBS letters *325*, 167-172.

Jeganathan, S., von Bergen, M., Brutlach, H., Steinhoff, H.J., and Mandelkow, E. (2006). Global hairpin folding of tau in solution. Biochemistry *45*, 2283-2293.

Jicha, G.A., Bowser, R., Kazam, I.G., and Davies, P. (1997a). Alz-50 and MC-1, a new monoclonal antibody raised to paired helical filaments, recognize conformational epitopes on recombinant tau. J Neurosci Res *48*, 128-132.

Jicha, G.A., Lane, E., Vincent, I., Otvos, L., Jr., Hoffmann, R., and Davies, P. (1997b). A conformation- and phosphorylation-dependent antibody recognizing the paired helical filaments of Alzheimer's disease. J Neurochem *69*, 2087-2095.

Johnson, G.V., and Stoothoff, W.H. (2004). Tau phosphorylation in neuronal cell function and dysfunction. J Cell Sci *117*, 5721-5729.

Kampers, T., Friedhoff, P., Biernat, J., Mandelkow, E.M., and Mandelkow, E. (1996). RNA stimulates aggregation of microtubule-associated protein tau into Alzheimer-like paired helical filaments. FEBS letters *399*, 344-349.

Kaylor, J., Bodner, N., Edridge, S., Yamin, G., Hong, D.P., and Fink, A.L. (2005). Characterization of oligomeric intermediates in alpha-synuclein fibrillation: FRET studies of Y125W/Y133F/Y136F alpha-synuclein. J Mol Biol *353*, 357-372.

Kidd, M. (1963). Paired helical filaments in electron microscopy of Alzheimer's disease. Nature (Lond) *197*, 192-193.

Kirschner, D.A., Abraham, C., and Selkoe, D.J. (1986). X-ray diffraction from intraneuronal paired helical filaments and extraneuronal amyloid fibers in Alzheimer disease indicates cross-beta conformation. Proceedings of the National Academy of Sciences of the United States of America *83*, 503-507.

Kishi, M., Pan, Y.A., Crump, J.G., and Sanes, J.R. (2005). Mammalian SAD kinases are required for neuronal polarization. Science (New York, NY *307*, 929-932.

Kosik, K.S., Joachim, C.L., and Selkoe, D.J. (1986). Microtubule-associated protein tau (tau) is a major antigenic component of paired helical filaments in Alzheimer disease. Proceedings of the National Academy of Sciences of the United States of America *83*, 4044-4048.

Kosik, K.S., and McConlogue, L. (1994). Microtubule-associated protein function: lessons from expression in Spodoptera frugiperda cells. Cell Motil Cytoskeleton *28*, 195-198.

Krantz, B.A., Trivedi, A.D., Cunningham, K., Christensen, K.A., and Collier, R.J. (2004). Acid-induced unfolding of the amino-terminal domains of the lethal and edema factors of anthrax toxin. Journal of molecular biology *344*, 739-756.

Kunjithapatham, R., Oliva, F.Y., Doshi, U., Perez, M., Avila, J., and Munoz, V. (2005). Role for the alpha-helix in aberrant protein aggregation. Biochemistry *44*, 149-156.

Kyte, J., and Doolittle, R.F. (1982). A simple method for displaying the hydropathic character of a protein. Journal of molecular biology *157*, 105-132.

Laemmli, U.K. (1970). Cleavage of structural proteins during the assembly of the head of bacteriophage T4. Nature *227*, 680-685.

Lakowicz., J. (1999). Energy transfer. Principles of fluorescence spectroscopy *Second edition; Kluwer academic/Plenum publishers*, 367-394.

Lee, G., Cowan, N., and Kirschner, M. (1988). The primary structure and heterogeneity of tau protein from mouse brain. Science (New York, NY *239*, 285-288.

Lee, G., Newman, S.T., Gard, D.L., Band, H., and Panchamoorthy, G. (1998). Tau interacts with src-family non-receptor tyrosine kinases. J Cell Sci *111 (Pt 21)*, 3167-3177.

Lee, G. (2005). Tau and src family tyrosine kinases. Biochimica et biophysica acta *1739*, 323-330.

Lee, V.M., Goedert, M., and Trojanowski, J.Q. (2001). Neurodegenerative tauopathies. Annual review of neuroscience *24*, 1121-1159.

Lee, V.M., and Trojanowski, J.Q. (2006). Mechanisms of Parkinson's disease linked to pathological alpha-synuclein: new targets for drug discovery. Neuron *52*, 33-38.

Lesk, A.M. (2003). Hydrophobicity--getting into hot water. Biophysical chemistry *105*, 179-182.

Li, G., Levitus, M., Bustamante, C., and Widom, J. (2005). Rapid spontaneous accessibility of nucleosomal DNA. Nature structural & molecular biology *12*, 46-53.

Li, L., von Bergen, M., Mandelkow, E.M., and Mandelkow, E. (2002). Structure, stability, and aggregation of paired helical filaments from tau protein and FTDP-17 mutants probed by tryptophan scanning mutagenesis. The Journal of biological chemistry *277*, 41390-41400.

Li, W., and Lee, V.M. (2006). Characterization of Two VQIXXK Motifs for Tau Fibrillization in Vitro. Biochemistry *45*, 15692-15701.

Lichtenberg-Kraag, B., Mandelkow, E.M., Biernat, J., Steiner, B., Schroter, C., Gustke, N., Meyer, H.E., and Mandelkow, E. (1992). Phosphorylation-dependent epitopes of neurofilament antibodies on tau protein and relationship with Alzheimer tau. Proceedings of the National Academy of Sciences of the United States of America *89*, 5384-5388.

Litersky, J.M., and Johnson, G.V. (1995). Phosphorylation of tau in situ: inhibition of calcium-dependent proteolysis. J Neurochem *65*, 903-911.

Litman, P., Barg, J., and Ginzburg, I. (1994). Microtubules are involved in the localization of tau mRNA in primary neuronal cell cultures. Neuron *13*, 1463-1474.

Liu, Y., and Bolen, D.W. (1995). The peptide backbone plays a dominant role in protein stabilization by naturally occurring osmolytes. Biochemistry *34*, 12884-12891.

Lu, Q., Soria, J.P., and Wood, J.G. (1993). p44mpk MAP kinase induces Alzheimer type alterations in tau function and in primary hippocampal neurons. J Neurosci Res *35*, 439-444.

Lund, J., and Dalton, H. (1985). Further characterisation of the FAD and Fe2S2 redox centres of component C, the NADH:acceptor reductase of the soluble methane monooxygenase of Methylococcus capsulatus (Bath). Eur J Biochem *147*, 291-296.

Makarov, A.A., Lobachov, V.M., Adzhubei, I.A., and Esipova, N.G. (1992). Natural polypeptides in left-handed helical conformation. A circular dichroism study of the linker histones' C-terminal fragments and beta-endorphin. FEBS letters *306*, 63-65.

Makrides, V., Massie, M.R., Feinstein, S.C., and Lew, J. (2004). Evidence for two distinct binding sites for tau on microtubules. Proceedings of the National Academy of Sciences of the United States of America *101*, 6746-6751.

Mandelkow, E., Song, Y.H., Schweers, O., Marx, A., and Mandelkow, E.M. (1995). On the structure of microtubules, tau, and paired helical filaments. Neurobiol Aging *16*, 347-354.

Mandelkow, E., von Bergen, M., Biernat, J., and Mandelkow, E.M. (2007). Structural principles of tau and the paired helical filaments of Alzheimer's disease. Brain pathology (Zurich, Switzerland) *17*, 83-90.

Mandelkow, E.M., and Mandelkow, E. (1998). Tau in Alzheimer's disease. Trends Cell Biol *8*, 425-427.

Margittai, M., and Langen, R. (2004). Template-assisted filament growth by parallel stacking of tau. Proceedings of the National Academy of Sciences of the United States of America *101*, 10278-10283.

Margittai, M., and Langen, R. (2006). Side Chain-dependent Stacking Modulates Tau Filament Structure. The Journal of biological chemistry *281*, 37820-37827.

Marx, A., Pless, J., Mandelkow, E.M., and Mandelkow, E. (2000). On the rigidity of the cytoskeleton: are MAPs crosslinkers or spacers of microtubules? Cell Mol Biol (Noisy-le-grand) *46*, 949-965.

Matsudaira, P.T., and Burgess, D.R. (1978). SDS microslab linear gradient polyacrylamide gel electrophoresis. Anal Biochem *87*, 386-396.

Matsumoto, S., and Hammes, G.G. (1975). Fluorescence energy transfer between ligand binding sites on aspartate transcarbamylase. Biochemistry *14*, 214-224.

Meersman, F., and Dobson, C.M. (2006). Probing the pressure-temperature stability of amyloid fibrils provides new insights into their molecular properties. Biochimica et biophysica acta *1764*, 452-460.

Minoura, K., Tomoo, K., Ishida, T., Hasegawa, H., Sasaki, M., and Taniguchi, T. (2002). Amphipathic helical behavior of the third repeat fragment in the tau microtubule-binding domain, studied by (1)H NMR spectroscopy. Biochem Biophys Res Commun *294*, 210-214.

Minoura, K., Yao, T.M., Tomoo, K., Sumida, M., Sasaki, M., Taniguchi, T., and Ishida, T. (2004). Different associational and conformational behaviors between the second and third repeat fragments in the tau microtubule-binding domain. Eur J Biochem *271*, 545-552.

Minoura, K., Mizushima, F., Tokimasa, M., Hiraoka, S., Tomoo, K., Sumida, M., Taniguchi, T., and Ishida, T. (2005). Structural evaluation of conformational transition state responsible for self-assembly of tau microtubule-binding domain. Biochem Biophys Res Commun *327*, 1100-1104.

Mizushima, F., Minoura, K., Tomoo, K., Sumida, M., Taniguchi, T., and Ishida, T. (2006). Fluorescence-coupled CD conformational monitoring of filament formation of tau microtubule-binding repeat domain. Biochem Biophys Res Commun *343*, 712-718.

Mukrasch, M.D., Biernat, J., von Bergen, M., Griesinger, C., Mandelkow, E., and Zweckstetter, M. (2005). Sites of TAU important for aggregation populate beta -structure and bind to microtubules and polyanions. J Biol Chem.

Mukrasch, M.D., von Bergen, M., Biernat, J., Fischer, D., Griesinger, C., Mandelkow, E., and Zweckstetter, M. (2007). The 'Jaws' of the Tau-microtubule interaction. The Journal of biological chemistry.

Navon, A., Ittah, V., Scheraga, H.A., and Haas, E. (2002). Formation of the hydrophobic core of ribonuclease A through sequential coordinated conformational transitions. Biochemistry *41*, 14225-14231.

Necula, M., Chirita, C.N., and Kuret, J. (2005). Cyanine dye N744 inhibits tau fibrillization by blocking filament extension: implications for the treatment of tauopathic neurodegenerative diseases. Biochemistry *44*, 10227-10237.

Novak, M., Kabat, J., and Wischik, C.M. (1993). Molecular characterization of the minimal protease resistant tau-unit of the Alzheimer's-disease paired helical filament. EMBO J *12*, 365-370.

Nozaki, Y., and Tanford, C. (1970). The solubility of amino acids, diglycine, and triglycine in aqueous guanidine hydrochloride solutions. The Journal of biological chemistry *245*, 1648-1652.

Nukina, N., and Ihara, Y. (1986). One of the antigenic determinants of paired helical filaments is related to tau protein. J Biochem (Tokyo) *99*, 1541-1544.

Otzen, D.E., Kristensen, O., and Oliveberg, M. (2000). Designed protein tetramer zipped together with a hydrophobic Alzheimer homology: a structural clue to amyloid assembly. Proceedings of the National Academy of Sciences of the United States of America *97*, 9907-9912.

Paschal, B.M., Obar, R.A., and Vallee, R.B. (1989). Interaction of brain cytoplasmic dynein and MAP2 with a common sequence at the C terminus of tubulin. Nature *342*, 569-572.

Pawar, A.P., Dubay, K.F., Zurdo, J., Chiti, F., Vendruscolo, M., and Dobson, C.M. (2005). Prediction of "aggregation-prone" and "aggregation-susceptible" regions in proteins associated with neurodegenerative diseases. J Mol Biol *350*, 379-392.

Poorkaj, P., Bird, T.D., Wijsman, E., Nemens, E., Garruto, R.M., Anderson, L., Andreadis, A., Wiederholt, W.C., Raskind, M., and Schellenberg, G.D. (1998). Tau is a candidate gene for chromosome 17 frontotemporal dementia. Ann Neurol *43*, 815-825.

Povey, J.F., Smales, C.M., Hassard, S.J., and Howard, M.J. (2007). Comparison of the effects of 2,2,2-trifluoroethanol on peptide and protein structure and function. Journal of structural biology *157*, 329-338.

Rath, A., Davidson, A.R., and Deber, C.M. (2005). The structure of "unstructured" regions in peptides and proteins: role of the polyproline II helix in protein folding and recognition. Biopolymers *80*, 179-185.

Reynolds, M.R., Berry, R.W., and Binder, L.I. (2005). Site-specific nitration and oxidative dityrosine bridging of the tau protein by peroxynitrite: implications for Alzheimer's disease. Biochemistry *44*, 1690-1700.

Rice, P., Longden, I., and Bleasby, A. (2000). EMBOSS: the European Molecular Biology Open Software Suite. Trends Genet *16*, 276-277.

Rissman, R.A., Poon, W.W., Blurton-Jones, M., Oddo, S., Torp, R., Vitek, M.P., LaFerla, F.M., Rohn, T.T., and Cotman, C.W. (2004). Caspase-cleavage of tau is an early event in Alzheimer disease tangle pathology. J Clin Invest *114*, 121-130.

Sambrook, J., and Maniatis, T. (1989). Gel Electrophoresis of DNA. Molecular Cloning: A Laboratory Manual *Second Edition*, 6.5.

Sanchez-Puig, N., Veprintsev, D.B., and Fersht, A.R. (2005). Human full-length Securin is a natively unfolded protein. Protein Sci *14*, 1410-1418.

Sanger, F., Nicklen, S., and Coulson, A.R. (1977). DNA sequencing with chain-terminating inhibitors. Proceedings of the National Academy of Sciences of the United States of America *74*, 5463-5467.

Santarella, R.A., Skiniotis, G., Goldie, K.N., Tittmann, P., Gross, H., Mandelkow, E.M., Mandelkow, E., and Hoenger, A. (2004). Surface-decoration of microtubules by human tau. Journal of molecular biology *339*, 539-553.

Sawaya, M.R., Sambashivan, S., Nelson, R., Ivanova, M.I., Sievers, S.A., Apostol, M.I., Thompson, M.J., Balbirnie, M., Wiltzius, J.J., McFarlane, H.T.*, et al.* (2007). Atomic structures of amyloid cross-beta spines reveal varied steric zippers. Nature *447*, 453-457.

Schellman, J.A. (1987). Selective binding and solvent denaturation. Biopolymers *26*, 549-559.

Schonbrunn, E., Eschenburg, S., Luger, K., Kabsch, W., and Amrhein, N. (2000). Structural basis for the interaction of the fluorescence probe 8-anilino-1-naphthalene sulfonate (ANS) with the antibiotic target MurA. Proceedings of the National Academy of Sciences of the United States of America *97*, 6345-6349.

Schuler, B., Lipman, E.A., and Eaton, W.A. (2002). Probing the free-energy surface for protein folding with single-molecule fluorescence spectroscopy. Nature *419*, 743-747.

Schweers, O., Schonbrunn-Hanebeck, E., Marx, A., and Mandelkow, E. (1994). Structural studies of tau protein and Alzheimer paired helical filaments show no evidence for beta-structure. The Journal of biological chemistry *269*, 24290-24297.

Schweers, O., Mandelkow, E.M., Biernat, J., and Mandelkow, E. (1995). Oxidation of cysteine-322 in the repeat domain of microtubule-associated protein tau controls the in vitro assembly of paired helical filaments. Proceedings of the National Academy of Sciences of the United States of America *92*, 8463-8467.

Seitz, A., Kojima, H., Oiwa, K., Mandelkow, E.M., Song, Y.H., and Mandelkow, E. (2002). Single-molecule investigation of the interference between kinesin, tau and MAP2c. Embo J *21*, 4896-4905.

Semisotnov, G.V., Rodionova, N.A., Razgulyaev, O.I., Uversky, V.N., Gripas, A.F., and Gilmanshin, R.I. (1991). Study of the "molten globule" intermediate state in protein folding by a hydrophobic fluorescent probe. Biopolymers *31*, 119-128.

Shiraki, K., Nishikawa, K., and Goto, Y. (1995). Trifluoroethanol-induced stabilization of the alpha-helical structure of beta-lactoglobulin: implication for non-hierarchical protein folding. Journal of molecular biology *245*, 180-194.

Shirazi, S.K., and Wood, J.G. (1993). The protein tyrosine kinase, fyn, in Alzheimer's disease pathology. Neuroreport *4*, 435-437.

Sibille, N., Sillen, A., Leroy, A., Wieruszeski, J.M., Mulloy, B., Landrieu, I., and Lippens, G. (2006). Structural impact of heparin binding to full-length Tau as studied by NMR spectroscopy. Biochemistry *45*, 12560-12572.

Skrabana, R., Kontsek, P., Mederlyova, A., Iqbal, K., and Novak, M. (2004). Folding of Alzheimer's core PHF subunit revealed by monoclonal antibody 423. FEBS letters *568*, 178-182.

Slavik, J. (1982). Anilinonaphthalene sulfonate as a probe of membrane composition and function. Biochimica et biophysica acta *694*, 1-25.

Sontag, E., Nunbhakdi-Craig, V., Lee, G., Brandt, R., Kamibayashi, C., Kuret, J., White, C.L., 3rd, Mumby, M.C., and Bloom, G.S. (1999). Molecular interactions among protein phosphatase 2A, tau, and microtubules. Implications for the regulation of tau phosphorylation and the development of tauopathies. The Journal of biological chemistry *274*, 25490-25498.

Spillantini, M.G., Murrell, J.R., Goedert, M., Farlow, M.R., Klug, A., and Ghetti, B. (1998). Mutation in the tau gene in familial multiple system tauopathy with presenile dementia. Proceedings of the National Academy of Sciences of the United States of America *95*, 7737-7741.

Steinhoff, H.J. (1990). Residual motion of hemoglobin-bound spin labels and protein dynamics: viscosity dependence of the rotational correlation times. Eur Biophys J *18*, 57-62.

Steinhoff, H.J. (2002). Methods for study of protein dynamics and protein-protein interaction in protein-ubiquitination by electron paramagnetic resonance spectroscopy. Front Biosci *7*, c97-110.

Stryer, L. (1978). Fluorescence energy transfer as a spectroscopic ruler. Annu Rev Biochem *47*, 819-846.

Sunde, M., Serpell, L.C., Bartlam, M., Fraser, P.E., Pepys, M.B., and Blake, C.C. (1997). Common core structure of amyloid fibrils by synchrotron X-ray diffraction. J Mol Biol *273*, 729-739.

Tcherkasskaya, O., and Uversky, V.N. (2003). Polymeric aspects of protein folding: a brief overview. Protein Pept Lett *10*, 239-245.

Terry, R.D. (1963). The Fine Structure of Neurofibrillary Tangles in Alzheimer's Disease. J Neuropathol Exp Neurol *22*, 629-642.

Thies, E., and Mandelkow, E.M. (2007). Missorting of tau in neurons causes degeneration of synapses that can be rescued by the kinase MARK2/Par-1. J Neurosci *27*, 2896-2907.

Thomas, P.D., and Dill, K.A. (1993). Local and nonlocal interactions in globular proteins and mechanisms of alcohol denaturation. Protein Sci *2*, 2050-2065.

Tian, Q., and Wang, J. (2002). Role of serine/threonine protein phosphatase in Alzheimer's disease. Neurosignals *11*, 262-269.

Timasheff, S.N. (2002). Thermodynamic binding and site occupancy in the light of the Schellman exchange concept. Biophysical chemistry *101-102*, 99-111.

Trojanowski, J.Q., and Lee, V.M. (1995). Phosphorylation of paired helical filament tau in Alzheimer's disease neurofibrillary lesions: focusing on phosphatases. Faseb J *9*, 1570-1576.

Uversky, V.N., Gillespie, J.R., and Fink, A.L. (2000). Why are "natively unfolded" proteins unstructured under physiologic conditions? Proteins *41*, 415-427.

Uversky, V.N., Li, J., and Fink, A.L. (2001). Evidence for a partially folded intermediate in alpha-synuclein fibril formation. The Journal of biological chemistry *276*, 10737-10744.

Uversky, V.N. (2002a). What does it mean to be natively unfolded? Eur J Biochem *269*, 2-12.

Uversky, V.N. (2002b). Natively unfolded proteins: a point where biology waits for physics. Protein Sci *11*, 739-756.

van Swieten, J., and Spillantini, M.G. (2007). Hereditary frontotemporal dementia caused by Tau gene mutations. Brain pathology (Zurich, Switzerland) *17*, 63-73.

Vigo-Pelfrey, C., Seubert, P., Barbour, R., Blomquist, C., Lee, M., Lee, D., Coria, F., Chang, L., Miller, B., Lieberburg, I.*, et al.* (1995). Elevation of microtubule-associated protein tau in the cerebrospinal fluid of patients with Alzheimer's disease. Neurology *45*, 788-793.

von Bergen, M., Friedhoff, P., Biernat, J., Heberle, J., Mandelkow, E.M., and Mandelkow, E. (2000). Assembly of tau protein into Alzheimer paired helical filaments depends on a local sequence motif ((306)VQIVYK(311)) forming beta structure. Proceedings of the National Academy of Sciences of the United States of America *97*, 5129-5134.

von Bergen, M., Barghorn, S., Li, L., Marx, A., Biernat, J., Mandelkow, E.M., and Mandelkow, E. (2001). Mutations of tau protein in frontotemporal dementia promote aggregation of paired helical filaments by enhancing local beta-structure. The Journal of biological chemistry *276*, 48165-48174.

von Bergen, M., Barghorn, S., Biernat, J., Mandelkow, E.M., and Mandelkow, E. (2005). Tau aggregation is driven by a transition from random coil to beta sheet structure. Biochimica et biophysica acta *1739*, 158-166.

von Bergen, M., Barghorn, S., Jeganathan, S., Mandelkow, E.M., and Mandelkow, E. (2006a). Spectroscopic approaches to the conformation of tau protein in solution and in paired helical filaments. Neurodegener Dis *3*, 197-206.

von Bergen, M., Barghorn, S., Muller, S.A., Pickhardt, M., Biernat, J., Mandelkow, E.M., Davies, P., Aebi, U., and Mandelkow, E. (2006b). The core of tau-paired helical filaments studied by scanning transmission electron microscopy and limited proteolysis. Biochemistry *45*, 6446-6457.

Weingarten, M.D., Lockwood, A.H., Hwo, S.Y., and Kirschner, M.W. (1975). A protein factor essential for microtubule assembly. Proceedings of the National Academy of Sciences of the United States of America *72*, 1858-1862.

Wilhelmsen, K.C., Lynch, T., Pavlou, E., Higgins, M., and Nygaard, T.G. (1994). Localization of disinhibition-dementia-parkinsonism-amyotrophy complex to 17q21-22. Am J Hum Genet *55*, 1159-1165.

Wille, H., Drewes, G., Biernat, J., Mandelkow, E.M., and Mandelkow, E. (1992). Alzheimer-like paired helical filaments and antiparallel dimers formed from microtubule-associated protein tau in vitro. J Cell Biol *118*, 573-584.

Williamson, R., Scales, T., Clark, B.R., Gibb, G., Reynolds, C.H., Kellie, S., Bird, I.N., Varndell, I.M., Sheppard, P.W., Everall, I.*, et al.* (2002). Rapid tyrosine phosphorylation of neuronal proteins including tau and focal adhesion kinase in response to amyloid-beta peptide exposure: involvement of Src family protein kinases. J Neurosci *22*, 10-20.

Wilson, D.M., and Binder, L.I. (1995). Polymerization of microtubule-associated protein tau under near-physiological conditions. The Journal of biological chemistry *270*, 24306-24314.

Wilson, D.M., and Binder, L.I. (1997). Free fatty acids stimulate the polymerization of tau and amyloid beta peptides. In vitro evidence for a common effector of pathogenesis in Alzheimer's disease. Am J Pathol *150*, 2181-2195.

Wischik, C.M., Novak, M., Edwards, P.C., Klug, A., Tichelaar, W., and Crowther, R.A. (1988a). Structural characterization of the core of the paired helical filament of Alzheimer disease. Proceedings of the National Academy of Sciences of the United States of America *85*, 4884-4888.

Wischik, C.M., Novak, M., Thogersen, H.C., Edwards, P.C., Runswick, M.J., Jakes, R., Walker, J.E., Milstein, C., Roth, M., and Klug, A. (1988b). Isolation of a fragment of tau derived from the core of the paired helical filament of Alzheimer disease. Proceedings of the National Academy of Sciences of the United States of America *85*, 4506-4510.

Wisniewski, H.M., Merz, P.A., and Iqbal, K. (1984). Ultrastructure of paired helical filaments of Alzheimer's neurofibrillary tangle. J Neuropathol Exp Neurol *43*, 643-656.

Wood, J.G., Mirra, S.S., Pollock, N.J., and Binder, L.I. (1986). Neurofibrillary tangles of Alzheimer disease share antigenic determinants with the axonal microtubule-associated protein tau (tau). Proceedings of the National Academy of Sciences of the United States of America *83*, 4040-4043.

Woody, R.W., Clark, D.C., Roberts, G.C., Martin, S.R., and Bayley, P.M. (1983). Molecular flexibility in microtubule proteins: proton nuclear magnetic resonance characterization. Biochemistry *22*, 2186-2192.

Wu, P., and Brand, L. (1994). Conformational flexibility in a staphylococcal nuclease mutant K45C from time-resolved resonance energy transfer measurements. Biochemistry *33*, 10457-10462.

Wurth, C., Guimard, N.K., and Hecht, M.H. (2002). Mutations that reduce aggregation of the Alzheimer's Abeta42 peptide: an unbiased search for the sequence determinants of Abeta amyloidogenesis. Journal of molecular biology *319*, 1279-1290.

Yan, S.D., Chen, X., Schmidt, A.M., Brett, J., Godman, G., Zou, Y.S., Scott, C.W., Caputo, C., Frappier, T., Smith, M.A.*, et al.* (1994). Glycated tau protein in Alzheimer disease: a mechanism for induction of oxidant stress. Proceedings of the National Academy of Sciences of the United States of America *91*, 7787-7791.

Yanagawa, H., Chung, S.H., Ogawa, Y., Sato, K., Shibata-Seki, T., Masai, J., and Ishiguro, K. (1998). Protein anatomy: C-tail region of human tau protein as a crucial structural element in Alzheimer's paired helical filament formation in vitro. Biochemistry *37*, 1979-1988.

Yoshida, H., Crowther, R.A., and Goedert, M. (2002). Functional effects of tau gene mutations deltaN296 and N296H. J Neurochem *80*, 548-551.

Zingsheim, H.P., Herzog, W., and Weber, K. (1979). Differences in surface morphology of microtubules reconstituted from pure brain tubulin using two different microtubule-associated proteins: the high molecular weight MAP 2 proteins and tau proteins. Eur J Cell Biol *19*, 175-183.

7 Appendix

A.1. Abbreviations

(v/v)	Volume per volume
(w/v)	Weight per volume
~	Approximately
Å	Angstrom (0.1 nm)
AD	Alzheimer disease
ANS	8-anilino-1-naphthalene sulfonic acid
Aβ	β-amyloid peptide
BES	N, N-bis (2-hydoxyethyl)-2-aminoethanosulfonic acid
Bis Tris	Bis-(2-Hydroxylmethyl)-imino (hydroxymethyl)-methane
BSA	Bovine serum albumin
CAPS	2-(N-cyclohexylamino)-1-propanesulfonic acid
CCD	Charge coupled device
CD	Circular dichroism
CHES	2-(N-cyclohexylamino) ethanesulfonic acid
DMF	N, N-dimethyl formamide
DTT	Dithiothreitol
EDTA	Ethylendiaminetetraacetate
EGTA	Ethylenglycol-bis-(2-aminoethylether)-N, N, N', N'-tetra acetic acid
EM	Electron microscope
FPLC	Fast performance liquid chromatography
FRET	Fluorescence resonance energy transfer
FTDP-17	Frontotemporal dementia and parkinsonism linked to chromosome 17
FTIR	Fourier transform infrared
GdnHCl	Guanidine hydrochloride
H_2O	Water
HCl	Hydrochloric acid
HEPES	N-2-Hydroxyethyl-piperazine-N-2-ethanesulfonic acid
HFIP	3,3,3,3',3',3'-hexafluoro-2-propanol
HPLC	High pressure liquid chromatography
IAEDANS	5-((((2-iodoacetyl) amino) ethyl) amino) naphthalene-1-sulfonic acid
IPTG	Isopropyl-D-β-galactopyranoside
kDa	Kilodalton(s)
krpm	1000 revolutions per minute

LB	Luria-Bertani
MAPs	Microtubule-associated proteins
MARK	MAP/microtubule affinity regulating kinase
MES	2-(N-morpholino) ethanesulfonic acid
$MgCl_2$	Magnesium chloride
$MgSO_4$	Magnesium sulphate
MOPS	2-(N-morpholino) propanesulfonic acid
MT	Microtubules
MTSL	(1-Oxyl-2,2,5,5-tetramethyl-Δ^3-pyrroline-3-methyl)methanothiosulfonate
NaAc	Sodium acetate
NaCl	Sodium chloride
NaP	Sodium phosphate
NFT	Neurofibrillary tangles
NH_4Ac	Ammonium Acetate
NMR	Nuclear magnetic resonance spectroscopy
PAGE	Polyacrylamide gel electrophoresis
PBS	Phosphate buffered saline
PCR	Polymerization chain reaction
PHFs	Paired helical filaments
pI	Isoelectric point
PIPES	Piperazine-N,N'- bis- (2-ethanesulfonic) acid
PKA	Protein kinase A
PMSF	Phenylmethylsulfonylfluoride
PPII	Polyproline II helix
SDS	Sodium dodecyl sulfate
STEM	Scanning transmission electron microscopy
TE	Tris-EDTA
TEMPO	2,2,6,6-tetramethylpiperidine-1-oxyl radical
TFE	2,2-Trifluoroethanol,
ThS	Thioflavin S
Tris	Tris-(Hydroxylmethyl)-aminomethane

A.2. List of figures

A.3. List of tables

A.4. Oligonucleotides

A291C.for gcaacgtccagtccaagtgtggctcaaaggataatatcaaacacg

A291C.rev cgtgtttgatattatcctttgagccacacttggactggacgttgc

G322A.for gcaaggtaacctccaaggctggatccttaggcaacatcc

G322A.rev ggatgttgcctaaggatccagccttggaggttaccttgc

G322C.for gcaaggtaacctccaagtgtggatccttaggcaacatcc

G322C.rev ggatgttgcctaaggatccacacttggaggttaccttgc

S433C.for gctagctgacgaggtgtgtgcctccctggccaagcaggg

S433C.rev ccctgcttggccagggaggcacacacctcgtcagctagcg

S435C.for gctgacgaggtgtctgcctgcctggccaagcaggg

S435C.rev ccctgcttggccaggcaggcagacacctcgtcagc

T17C.for cctgtcccccaacccgtaacacccagcgtggtcttcc

T17C.rev ggaagaccacgctgggtgttacgggttggggggacagg

V432W.for   gccacactagctgacgagtggtctgcctccctggcc

V432W.rev   ggccagggaggcagaccactcgtcagctagtgtggc

Y18W.for   cgccaggaattcgaagtgatggaagatcacgctgggacgtgggggttggg

Y18W.rev   cccaaccccacgtcccagcgtgatcttccatcacttcgaattcctggcg

Y310W.for   gtgcaaatagtctggaaaccagtcgacctgagcaaggtg

Y310W.rev   caccttgctcaggtcgactggtttccagactatttgcac

A.5. Properties associated with standard amino acids

Amino acid	Abbreviated names		pKa of side chain	Hydropathy index[¥]
Nonpolar, aliphatic side chains				
Glycine	Gly	G		-0.4
Alanine	Ala	A		1.8
Valine	Val	V		4.2
Leucine	Leu	L		3.8
Isoleucine	Ile	I		4.5
Methionine	Met	M		1.9
Aromatic side chains				
Phenylalanine	Phe	F		2.8
Tyrosine	Tyr	Y	10.07	-1.3
Tyrptophan	Trp	W		-0.9
Polar, uncharged side chains				
Serine	Ser	S		-0.8
Proline	Pro	P		1.6
Threonine	Thr	T		-0.7
Cysteine	Cys	C		2.5
Asparagine	Asn	N	8.18	-3.5
Glutamine	Gln	Q		-3.5
Positively charged side chains				
Lysine	Lys	K	10.53	-3.9
Histidine	His	H	6.00	-3.2
Arginine	Arg	R	12.48	-4.5
Negatively charged side chains				
Aspartate	Asp	D	3.65	-3.5
Glutamate	Glu	E	4.25	-3.5

¥ - A scale combining hydrophobicity and hydrophilicity of side chains that used to measure the tendency of an amino acid to seek an aqueous environment (negative values) or a hydrophobic environment (positive values) (Kyte and Doolittle, 1982).

8 Acknowledgement

I sincerely thank Prof. Eckhard Mandelkow for the opportunity to carry out this work and providing all the necessary facilities. His guidance was immensely important to this project. I also thank Dr. Eva Maria Mandelkow for her constant encouragement and fruitful discussions throughout this work.

I thank Dr. Martin von Bergen who introduced me to many techniques, for his constant help throughout this project.

I also thank Dr. Jacek Biernat, Dr. Alexander Marx and Dr. Marcus Pickhardt for their generous support, technical advice and help during this work.

I thank Prof. Heinz-Jürgen Steinhoff and Henrik Brutlach, University of Osnabrück for their collaboration on the spin labeling study of soluble tau and PHFs.

I thank Dr. Li Li for providing the starting materials and Dr. Saravavan Panneerselvam for his generous help.

I thank Bianca Scharnweber for her excellent technical assistance and all the lab members for providing a nice environment.

I thank Dr. Beena Krishnan, Dr. Manikandan Karuppasamy and Venkatraman Parthasarathy, IISc, India for their help.

A note of thanks is due for my friends and family members.

Sadasivam Jeganathan

Curriculum Vitae

Name	:	Sadasivam Jeganathan
Home address	:	4/24B, Nadu Street, Valarpuram, Arakkonam, India, 631 603.
Date of Birth	:	30.05.1979
Nationality	:	Indian

University studies

1996-1999	:	Bachelor of Science in Biochemistry, Sri Sankara Arts and Science College, Kanchipuram, India.
2000-2002	:	Master of Science (Biochemistry), Department of Medical Biochemistry, University of Madras, Chennai, India.
2002-2003	:	Junior research fellow in Prof. Raghavan Varadarajan's lab, Indian Institute of Science, Bangalore, India.

Doctoral study

09.2003-10.2007	:	Max-Planck-Unit for Structural Molecular Biology c/o DESY Hamburg, Germany
Advisor	:	Prof. Eckhard Mandelkow
Thesis title	:	**Conformation of Human Microtubule Associated Protein-Tau**

Publications

Sadasivam Jeganathan, Martin von Bergen, Henrik Brutlach, Heinz-Jürgen Steinhoff, Eckhard Mandelkow; Global hairpin folding of tau in solution (2006); Biochemistry; 45(7):2283-93.

Declaration (Erklärung)

I declare that I have carried out this thesis by myself and have not used external help except where explicitly indicated. This thesis was not submitted to any other university. I did not make any earlier attempt to submit this work as a doctoral thesis.

Sadasivam Jeganathan

September, 2007

Hamburg

Hiermit erkläre ich, dass ich die vorliegende Arbeit selbständig und ohne fremde Hilfe verfasst, andere als die angegebenen Quellen und Hilfsmittel nicht benutzt und die den verwendeten Werken wörtlich oder inhaltlich entnommenen Stellen als solche kenntlich gemacht habe.

Ferner versichere ich, dass ich diese Dissertation noch an keiner anderen Universität eingereicht habe, um ein Promotionsverfahren eröffnen zu lassen. Hiermit erkläre ich auch, dass ich keine anderen früheren Versuche gemacht habe, die Arbeit zur Promotion einzureichen.

Sadasivam Jeganathan

September, 2007

Hamburg

European Molecular Biology Laboratory
Europäisches Laboratorium für Molekularbiologie
Laboratoire Européen de Biologie Moléculaire

Dr. Simon Holton

Hamburg, 6. September 2007

To whom it may concern,

This letter is to certify that as a native English speaker I have read the Ph.D. thesis entitled **'Conformation of Human Microtubule Associated Protein-Tau'**. This thesis is to be submitted to the University of Hamburg by Sadasivam Jeganathan.

Yours sincerely,

Dr. Simon Holton